New insights in the oxidative conversion of alkanes:

Exploring Li-promoted MgO catalysts and plasma micro-reactors

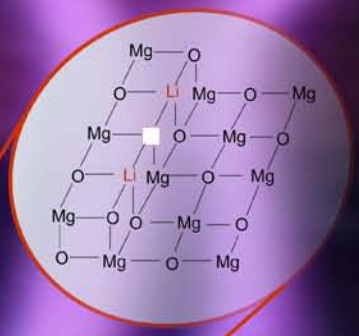

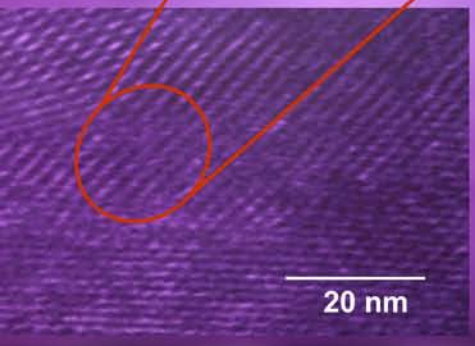

Cristiano Trionfetti

University of Twente
Enschede - The Netherlands

NEW INSIGHT IN OXIDATIVE CONVERSION OF ALKANES

Exploring Li- promoted MgO catalysts and plasma micro-reactors

Cristiano Trionfetti

The research described in this thesis was performed under the auspices of the NIOK, Netherlands Institute for Catalysis Research.

Cover design: Ing. Bert Geerdink, Catalytic Processes and Materials (CPM), University of Twente, Enschede, The Netherlands.

Cover Illustrations: The micro-discharges produced under plasma condition in a microreactor are here illustrated as background.

Publisher: Gildeprint B.V., Enschede
Enschede,
The Netherlands.

ISBN: 978-90-365-2679-1

NEW INSIGHT IN OXIDATIVE CONVERSION OF ALKANES

EXPLORING Li- PROMOTED MgO CATALYSTS AND PLASMA MICRO-REACTORS

Proefschrift

ter verkrijging van
de graad van doctor aan de Universiteit Twente,
op gezag van de rector magnificus,
prof. dr. W. H. M. Zijm,
volgens besluit van het College van Promoties
in het openbaar te verdedigen
op donderdag 29 May 2008 om 15.00 uur

door

Cristiano Trionfetti
geboren op 25 februari 1976
te Roma, Italie

This dissertation is approved by the promoter:

prof. dr. ir. L. Lefferts

And the assistant-promoter

dr. K. Seshan

Doctoral Supervisory Committee:

prof. dr. W.P.M. Van Swaaij (chairman): University of Twente, Enschede, The Netherlands

prof. dr. ir. L. Lefferts (promoter): University of Twente, Enschede, The Netherlands

dr. K. Seshan (assistant-promoter): University of Twente, Enschede, The Netherlands

prof. dr. ir. J.G.E. Gardeniers: University of Twente, Enschede, The Netherlands

prof. dr. ir. M.J. Groenefeld: University of Twente, Enschede, The Netherlands

prof. dr. ir. M.T. Kreutzer: University of Delft, The Netherlands

prof. dr. ir. H. Kuipers: University of Twente, Enschede, The Netherlands

prof. dr. J.A. Lercher: Technical University of Munich, Germany

dr. M. Ruitenbeek: Sabic Europe Research, Geleen, The Netherlands

"There is no reason to become alarmed, and we hope you
enjoy the rest of the flight.
By the way, is there anyone on board who
knows how to fly a plane?"

From ***Airplane*** (1980)

*To everyone who loved me, supported and
trusted in me.*

CONTENTS

CHAPTER III

Presence of Lithium Ions in MgO Lattice: Surface Characterization by Infra Red Spectroscopy and Reactivity towards Oxidative Conversion of Propane

CHAPTER IV

Lithium ions incorporation in MgO for oxidative dehydrogenation/cracking of propane: active site characterization and mechanism of regeneration

CHAPTER V

Oxidative conversion of propane in a microreactor in the presence of plasma over MgO based catalysts – An experimental study

CHAPTER VI

Alkane activation at ambient temperatures – Unusual selectivities, C-C, C-H bond scission vs C-C bond coupling

Summary

In this study the preparation of Li-promoted MgO catalysts is described using, respectively, (i) wet impregnation and (ii) sol-gel method. In the case of Li-promoted MgO catalysts, defects sites, due to the surface substitution of Mg^{2+} ions by a Li^{+} ion in the MgO matrix, are reported to play a significant role in processes involving oxidation reactions. More specifically, the impregnation of MgO supports with aqueous solutions of Li salts (i.e., $LiNO_3$), as route to prepare Li-promoted MgO catalysts, allows a homogeneous distribution of lithium on the catalyst surface. However, in this specific case, high temperature treatments are required. In fact, incorporation of lithium ions in MgO (forming a substitutional solid solution) takes place only at ≥700°C causing drastic sintering effect that result in materials with low surface area and thus low catalytic activity. Sol-gel preparation is here presented as an alternative and promising route for the preparation of Li-promoted MgO catalysts. In this study, Li-promoted MgO catalysts were prepared *via* co-gelling $Mg(OCH_3)_2$ and $LiNO_3$. Our observations during gel studies suggested that the presence of lithium ions in the sol-gel system drastically influenced the extent of hydrolysis and condensation. In particular lithium ions can be incorporated already in magnesia at the Li-Mg-gel stage facilitating formation of a substitutional solid solution. Furthermore, the results showed that high temperature treatments are not required and very active materials are formed after calcination at temperatures below 600°C. In addition, the enhanced lithium incorporation minimizes the amount of free lithium phases present. Our observations suggest that in the case of Li-promoted MgO catalysts both those effects are responsible for the high thermal stability and high surface area obtained after calcination.

In this work, IR spectroscopic characterization of Lewis acid sites (Mg^{2+}_{LC}) using carbon monoxide is also extensively reported and presented as a tool to investigate the effect of the incorporation of lithium ions in MgO. Our results suggest that sol-gel catalysts possess a higher amount of incorporated lithium ions in MgO. These findings are in agreement with the results obtained from active site titration using CO_2 sorption experiments and oxidation reduction cycles with H_2. Interestingly, the results showed that incorporated lithium ions efficiently provide the stabilization of active oxygen species [O^{-}] in MgO forming [$Li^{+}O^{-}$] sites. Therefore, the activity and selectivity improvements during the oxidative conversion of

propane can be explained by the promoting effect of lithium to enhance the creation of active oxygen species [O^-] in MgO.

Accordingly, during the oxidative dehydrogenation/cracking of propane over Li-promoted MgO catalysts prepared using sol-gel route, a higher number of active [Li^+O^-] sites per cm^3 of reactor volume was achieved compared to conventionally prepared materials and superior yields were recorded (same amounts of catalyst in the reactor).

The presence of gas phase oxygen during the oxidative dehydrogenation/cracking of propane over Li-promoted MgO catalysts is also crucial. In fact, oxygen reacts with radicals present in the gas phase and as result more reactive radicals are formed. More importantly, the second function of gas phase oxygen molecules is the regeneration of the active sites. In this respect, our observations suggest that the reaction mechanism for the deactivation/regeneration of active surface sites strongly depends on the operation temperatures. In this thesis, we demonstrated using mass spectrometry that at 550°C the catalyst deactivation implies the formation of stable [OH^-] groups and the regeneration of the active site does not require oxygen removal from the lattice structure of MgO. In fact, as described by Sinev, a sort of ‘’oxidative dehydrogenation’’ of hydroxyl groups occurs. In contrast, at 700°C the interaction of propane molecules with [Li^+O^-] sites produces unstable surface [OH^-] groups which implies a de-hydroxylation step involving evolution of water accompanied by the formation of oxygen vacancies. Thus, at the higher temperatures, the catalyst deactivation/regeneration goes *via* the traditional scheme of re-oxidation according to Ito and Lunsford mechanism.

The different operating conditions during oxidative dehydrogenation/cracking of propane and the different olefin selectivity observed are also here discussed. In particular, in the case of oxidative cracking of propane, our observations showed that the temperature can be a tool to control the ratio ethylene to propylene.

For this purpose, the oxidative conversion of alkanes (C_1-C_3 range) was performed in a plasma micro-reactor. In this case, due to a cold plasma, hydrocarbon activation *via* homolytic C-H and C-C bond rupture (forming radicals) occurred exclusively in the gas phase at near ambient temperatures (<50°C). In contrast to the results obtained at higher temperatures (≥550°C), in all the experiments performed in a plasma micro-reactor, mainly products that require the formation of C-C bonds were observed. Indeed, C-C bond formation is an exothermic process and therefore favored at lower temperatures.

Furthermore, the oxidative conversion of propane in a plasma micro-reactor was also performed in presence of a thin layer of Li-promoted MgO catalyst deposited in the micro-

channel where the cold plasma was ignited. Interestingly, alkyl radicals, exclusively formed by the cold plasma, can either initiate radical chain reactions in the gas phase or intensively interact with the catalyst surface due to the high surface to volume ratio typical of micro scale reactors. Based on our results, selective interaction between catalyst surface and radical species could be recorded under our conditions and further investigation performed changing catalyst composition showed that secondary H-atom abstraction from propyl radicals takes place.

Samenvatting

In dit proefschrift is de preparatie van Li-gestimuleerde MgO katalysatoren beschreven, gebruikmakend van respectievelijk (i) natte impregnatie en (ii) een sol-gel methode. In het geval van Li-gestimuleerde MgO katalysatoren is bekend dat defecte posities, die het gevolg zijn van het aan het oppervlak verwisselen van Mg^{2+} ionen door een Li^{+} ion in de MgO matrix, een belangrijke rol spelen in processen zoals oxidatie reacties. Meer specifiek, de methode om Li-gestimuleerde MgO katalysatoren te maken middels het impregneren van MgO supports met waterige oplossingen van Li zouten (i.e. $LiNO_3$) leidt tot een homogene verdeling van lithium aan het oppervlak van de katalysator. Echter, deze methode vereist hoge temperatuurstappen: de opname van lithium ionen in MgO geschiedt alleen op 700ºC, welke een ingrijpende sintering tot gevolg heeft hetgeen resulteert in materialen met een laag oppervlak en derhalve een lage katalytische activiteit. Sol-gel preparatie is een veel belovend alternatief voor de preparatie van Li-gestimuleerde MgO katalysatoren. In dit proefschrift is beschreven hoe dergelijke katalysatoren gemaakt kunnen worden middels het co-gellen van $Mg(OCH_3)_2$ en $LiNO_3$. Waarnemingen tijdens de gel experimenten tonen dat de aanwezigheid van lithium ionen in het sol-gel systeem de mate van hydrolyse en condensatie sterk beïnvloedt. Lithium ionen kunnen reeds worden opgenomen in magnesia in de Li-Mg-gel fase, en vergemakkelijken de vorming van een vervangbare vaste oplossing. Tevens zijn geen hoge temperatuurstappen nodig, en sterk actieve materialen worden verkregen na calcinatie op temperaturen onder 600ºC. Daarnaast minimaliseert het aantal aanwezige vrije lithium fases vanwege de toename in opgenomen lithium. Waarnemingen suggereren dat voor Li-gestimuleerde MgO katalysatoren deze beide effecten verantwoordelijk zijn voor de goede thermische stabiliteit en het hoge oppervlakte-gebied na calcineren.

In dit werk wordt uitgelegd dat IR spectroscopische karakterisatie van Lewis zuur posities (Mg^{2+}_{LC}) met koolstofmonoxide gebruikt kan worden om het effect van het opnemen van lithium ionen in MgO te onderzoeken. De resultaten tonen aan dat sol-gel katalysatoren een grotere hoeveelheid opgenomen lithium ionen in MgO bevatten. Dit is in overeenstemming met resultaten verkregen uit actieve positie tritratie middels CO_2-opname experimenten en oxidatie-reductie kringen met H_2. Interessant feit is dat de resultaten aantonen dat opgenomen lithium ionen zorgen voor efficiënte stabilisatie van actieve zuurstof 'species' $[O^-]$ in MgO, waarbij $[Li^+O^-]$ posities gevormd worden. Gevolg is dat de verbeterde activiteit en selectiviteit

tijdens de oxidatieve omzetting van propaan verklaard kan worden door het stimulerende effect van lithium, welke de vorming van actieve zuurstof 'species' [O^-] in MgO versterkt.

Dit alles heeft tot gevolg dat voor de oxidatieve dehydrogenatie/kraak van propaan over Li-gestimuleerde MgO katalysatoren die gemaakt zijn met de sol-gel methode, een toename in het aantal actieve [Li^+O^-] posities per cm^3 reactor volume behaald is ten opzicht van conventioneel gemaakte materialen en dientengevolge een superieure opbrengst (zelfde hoeveelheid katalysator in de reactor).

De aanwezigheid van gas fase zuurstof tijdens de oxidatieve dehydrogenatie/kraak van propaan over Li-gestimuleerde MgO katalysatoren is eveneens belangrijk. Zuurstof reageert met radicalen die aanwezig zijn in de gas fase, wat leidt tot de vorming van meer reactive radicalen. Belangrijker is de tweede functie van gas fase zuurstof moleculen: het regenereren van actieve posities. Met betrekking tot dit punt tonen waarnemingen aan dat het reactie mechanisme voor de deactivatie/regeneratie van actieve oppervlakte posities sterk afhangt van de werktemperatuur. In dit proefschrift is met massa spectrometrie aangetoond dat rond 550ºC deactivatie van de katalysator plaats vindt vanwege de vorming van stabiele [OH^-] groepen en voor het regeneren van de actieve positie is het niet noodzakelijk zuurstof te verwijderen van de raster-structuur van MgO. Feitelijk vindt een "oxidatieve dehydrogenatie" van hydroxyl groepen plaats, zoals beschreven door Sinev. Dit in tegenstelling tot 700ºC, want voor deze temperatuur leidt de interactie tussen propaan moleculen met [Li^+O^-] posities tot de vorming van instabiele oppervlakte [OH^-] groepen, welke een de-hydroxylatie stap tot gevolg heeft waarbij water gevormd wordt in combinatie met vacante zuurstof posities. Dus voor hoge temperaturen geschiedt het deactiveren/regenereren van de katalysator middels het klassieke schema van her-oxideren volgens het Ito en Lunsford mechanisme.

Tevens zijn de verschillende 'olefin' selectiviteiten die gevonden zijn voor verschillende uitvoeringscondities gedurende het oxidatief dehydrogeneren/kraken van propaan bediscussieerd. In het specifieke geval van het oxidatief kraken van propaan is aangetoond dat de temperatuur een 'tool' kan zijn voor het beheersen van de verhouding ethyleen-propyleen.

Voor dit doel is de oxidatieve omzetting van alkanen (C_1-C_3 reeks) uitgevoerd in een plasma micro-reactor. Als gevolg van een koud plasma vind in dit geval de hydrokoolstof activatie plaats via het homolytisch verbreken van C-H en C-C bindingen (vorming van radicalen) in uitsluitend de gas fase rond kamertemperatuur (<50ºC). In tegenstelling tot de resultaten verkregen voor hogere temperaturen (≥550ºC), zijn voor de experimenten uitgevoerd in de plasma micro-reactor met name produkten gevonden waarvoor de vorming van C-C bindingen nodig is. Daar het vormen van C-C bindingen een exotherm proces is, vind dit vooral op lagere temperaturen plaats.

De oxidatieve omzetting van propaan is tevens bestudeerd in een plasma micro-reactor waarin in het microkanaal een dunne laag Li-gestimuleerde MgO katalysator is aangebracht op de plaats waar het koude plasma ontstoken wordt. Interessant gegeven is dat alkyl radicalen, die uitsluitend gevormd worden door het koude plasma, zowel gas fase radicaal ketting reacties opstarten alsmede een zeer hoge interactie hebben met het katalytisch oppervlak, vanwege de hoge karakteristieke oppervlakte-volume verhouding van micro-schaal reactoren. Op basis van de verkregen data kan gesteld worden dat inzicht verkregen is in de selectieve interactie tussen het katalytisch oppervlak en radicaal 'species' voor de huidige experimentele condities. Uit vervolg-onderzoek, waarbij de samenstelling van de katalysator is veranderd, kan gesteld worden dat secundaire H-atoom afkoppeling van propyl radicalen plaats vindt.

Chapter 1

Introduction

1.1 General introduction: oxidative dehydrogenation cracking of propane

The motivation for developing active and selective catalysts to convert propane to propylene is the ability to convert an inexpensive and abundant alkane feedstock to considerably more valuable olefin [1-3].

At the moment, commercial conversion of propane to propylene is based on an endothermic and non oxidative process using heterogeneous catalysts, resulting in H_2 as by-product (catalytic dehydrogenation) [4-6]. Because this reaction is endothermic, high temperatures are needed to obtain reasonable propylene yields, though coking causes rapid catalyst deactivation [7]. Commercial catalytic technologies such as (i) OLEFLEX (UOP, Pt/Al_2O_3 catalyst) [8], (ii) CATOFIN (ABB Lummus / Air Products, Cr catalyst) [9], (iii) STAR (Philips Petroleum Pt based catalysts) [10] and (iv) FBD (Snamprogetti, Chromium oxide catalyst) [11] appeared in 1980's but have not made much commercial impact.

Alternatively, the production of propylene from propane by means of oxidative processes (ODH) takes place in the presence of hydrogen acceptors such as molecular oxygen [12-14]. In fact, the process relies on the oxidation of hydrogen to water and thus utilizes the heat of formation of water, turning an otherwise endothermic process into an exothermic one [15-17].

$$C_3H_8 + O_2 \rightarrow C_3H_6 + H_2O \qquad \Delta H = -86 \text{ kJ/mol} \qquad (1)$$

In this way, oxidative dehydrogenation process overcomes thermodynamic limitations and in principle can be run at lower temperatures. This allows for improvement in selectivity and/or olefins yield as well as catalyst stability [18]. However, the addition of oxygen unfortunately also allows for competing combustion reactions of the starting propane and/or desired products to carbon oxides [19, 20]. In particular, susceptibility of olefins towards consecutive unselective combustion makes the design of an efficient catalyst a challenging task [21, 22].

Efforts in the last years were concentrated on redox-type oxide catalysts (mostly V_2O_5 based). In the case of ODH of propane, the best catalysts showed olefins yields lower than 30% and maximum propane conversion lower than 40% [17]. In contrast, the best performance was obtained with non-reducible alkali or alkaline earth metal oxides. The most successful of these catalysts is Li-promoted MgO [23, 24]. Remarkably, the oxidative conversion of propane over non-redox type of catalysts such as Li/MgO does not exclusively lead to propylene since ethylene is also produced in large amounts [25, 26]. Thus, oxidative cracking reactions represent additional competing routes, lowering the propylene yield. Though no distinction is being made in literature between oxidative dehydrogenation and oxidative cracking, these types of reactions differ indeed substantially. In fact, oxidative dehydrogenation should be used for reactions that operate at temperatures below 500°C without significant C-C breaking. On the contrary, oxidative dehydrogenation/cracking takes place *via* ignition and subsequent gas phase reactions at temperature higher than 500°C, producing alkenes also with carbon number lower than the starting feedstock. Thus, the term oxidative dehydrogenation/cracking reactions will be used in the case of propane conversion over Li-promoted MgO catalysts.

It is well established that $[O^-]$ centers on oxide surfaces (i.e., Li/MgO) possess the ability to cleave C-H bonds [27, 28]. More specifically, Lunsford *et al.* suggested that surface $[O^-]$ centers in Li/MgO catalysts, stabilized by lithium ions present in MgO lattice, can abstract $H^\cdot$ from CH_4 molecules to generate $CH_3^\cdot$ radicals [29, 30]. A detailed kinetic study of propane oxidation over Li/MgO catalysts was performed by Leveles and coworkers [25, 26]. In agreement with Lunsford *et al.*, Leveles reported that the activation of propane takes place on the catalysts surface *via* the formation of propyl radicals (eq. 2).

$$C_3H_8 + [O^-] \rightarrow C_3H_7^\cdot + [OH^-] \qquad (2)$$

Moreover, desorption of propyl radicals to the gas phase initiates radical chain reactions which determine the homogeneous contribution to ODH (especially at high temperatures). Although, propane conversion to olefins without the use of catalyst is feasible and results in olefins [31, 32], Burch and Crabb demonstrated that a combination of homogeneous and heterogeneous routes, contributing to ODH reaction, offer the best opportunity to obtain commercially accepted yields of propylene [33].

In general, the oxidative conversion of ethane and propane to commodity chemical intermediates may represent an alternative to steam cracking and may have the potential to

radically transform the chemical industry. More specifically, the effectiveness of the catalysts (activity and selectivity) will eventually determine the economic attractiveness of an alkane-based chemical processes [34].

1.2 Catalyst preparation using sol-gel method

Magnesium oxide powders, alumina and silica are mainly used as catalysts or supports and in the synthesis of refractory ceramics. For all of those applications, particle size, porosity and surface area are of major importance and are strongly dependent on the preparation methods [35, 36].

A colloid is defined as a suspension in which particle size of the dispersed phase is extremely small (1-1000 nm in size) and therefore gravitational forces are negligible and the only dominating interactions are typically short-range forces such as Van der Waals attraction and hydrogen bonds [37]. Interestingly, colloidal suspensions of solid particles in liquids are called sols. Furthermore, particles interaction leading to the formation of a continuous three-dimensional network is generally indicated as gel. Thus, sol-gel preparation that involves, respectively, the formation of a sol followed by formation of a gel can be used to generate polymers or solid particles from which ceramics can be obtained [38].

Starting materials (precursors) for sol-gel preparations consist of metals surrounded by ligands, including inorganic salts i.e., $Al(NO_3)_3$, $Mg(NO_3)_2$ etc. and organic compounds such as $Al(OC_4H_9)$, $Mg(OCH_3)_2$, etc. However, most of the literature results are based on the latter approach. With an alkoxide as precursor, generally indicated as $M(OR)_n$, sol-gel chemistry can be described in terms of 2 classes of reactions [39, 40]:

Hydrolysis: $\text{-MOR} + H_2O \rightarrow \text{-MOH} + \text{ROH}$ (3)

Condensation: $\text{-MOH} + \text{ROM-} \rightarrow \text{-MOM-} + \text{ROH}$ (4)

or $\text{-MOH} + \text{HOM-} \rightarrow \text{-MOM-} + H_2O$ (5)

Using this description we can highlight two key points of the sol-gel method. First, a gel can be formed because of the condensation of partially hydrolyzed species into a three-dimensional polymeric network. Second, any factor that can affect either one of both of the reactions (i.e., temperature, solvent, pH, types of precursors and their concentration) may likely have an impact on the gel properties. In particular, the type of precursor is an important

parameter because the size of the alkoxy ligands changes the rates of both hydrolysis and condensation. Another parameter that influences a sol-gel product is the drying conditions (*via* solvent removal). In fact, a gel is a solid encapsulating a solvent and the time between the formation of a gel and its drying, known as aging, can affect the morphology of a gel. Scherer [41] pointed out that a gel is not static and during aging can continue to undergo hydrolysis and condensation.

The ability to control the composition and the textural properties of the gels at the molecular level is relevant for the preparation of catalytic materials. In particular, high purity can be achieved because of the quality of available precursors and moreover the surface area and pore size distribution can be tailored controlling the rate of condensation and particle growth [42]. However, it is here appropriate to stress that calcination of a gel results in materials with lower surface area and pore volume. In general, a sol-gel preparation characterized by a rapid condensation leads to small network and significant particle growth. The collapse of this network during calcinations drastically decreases the surface area and pore volume. On the contrary, the possibility of slowing down the condensation step may offer the possibility to allow branching to occur before particle growth can take place. In the latter case, the products upon calcination possess larger surface area and pore volume.

A one step sol-gel preparation can also be used to introduce dopants into oxides and prepare catalytic materials. In this respect, Ward and Ko recently prepared zirconia-sulfate gels by mixing sulfuric acid directly with the zirconium alkoxide in the sol-gel step [43]. Using X-ray diffraction and IR spectroscopy the authors found that sulfate ions are initially trapped in the bulk of the gel. Remarkably, upon calcination, the crystallization of zirconia support resulted in high surface materials and moreover was accompanied by the presence of surface active species containing sulfur that promote n-butane isomerization. Similarly, high surface area Li-promoted MgO may be prepared by the homogenous hydrolysis of magnesium alkoxide and inorganic lithium salts [44].

1.3 Surface generated gas phase radicals: the homogeneous contribution

The idea of homogeneous reactions accompanying heterogeneous catalytic processes was considered not feasible until the early 1980s when oxidative coupling of methane was discovered [45-47]. In this way, it was shown that products such as ethane can be formed *via* the recombination of free methyl species which escape to the gas phase upon interaction of methane molecules with catalytically active surface sites. More specifically, it was shown that the formation of free radicals is feasible on the catalyst surface and their further

transformation in the gas phase may represent the major and essential reaction pathway determining the overall products distribution. In addition, the homolytic cleavage of C-H bonds to radicals, as reported by Sinev (based on thermo-chemical considerations), seems to be the most energetically feasible process [48-50].

In this respect, the participation of surface generated gas-phase radicals in catalytic reactions has supported the concept of heterogeneous-homogeneous reactions [51-55]. An early example was proposed by Keulks *et al.* (1972) during their studies on the partial oxidation of propylene over bismuth molybdate and several other metal oxides [56]. However, Nguyen and Kung successfully elucidated the role of homogeneous radical reactions in oxidative dehydrogenation of propane over V-Mg-O catalysts, revealing the contribution of each component (homogeneous and heterogeneous) in the overall process [57]. The technique used in this study involved the addition of a post-catalytic volume, downstream the catalyst bed (Fig.1). The same post catalytic volume was then packed with quartz chips, *i.e.* an effective radical quencher, to diminish the contribution of gas phase reactions. In fact, if the reaction was entirely heterogeneously catalyzed, intermediates would remain adsorbed on the surface and react further to yield products before desorption. Thus, the presence of a void volume (post-catalytic volume) should not affect the conversion or product selectivity [25]. If the reaction involved a heterogeneous-homogeneous pathway some surface reaction intermediates would desorb into the post-catalytic volume and react further in the gas phase. Thus, the presence of a large void volume would increase yields and most likely change the product distribution. Therefore, by determining conversion and selectivity, in both the presence and absence of quartz chips in the post catalytic volume, the importance of homogeneous-heterogeneous pathway could be evaluated.

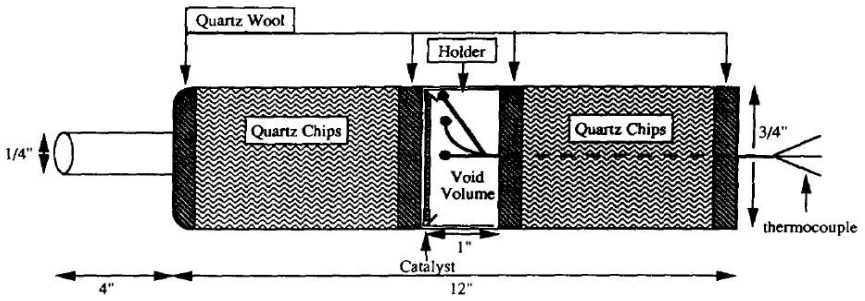

Fig. 1. Schematic diagram of the reactor used by Nguyen and Kung [56].

Radicals are characterized by a short life time and undergo a complex network of chemical reactions. Indeed, to determine the importance of surface-generated gas phase radicals in catalyzed reactions their detection is essential. Although, conventional mass

spectrometry has been employed very early (ca 1948) as a direct detection method [58] it was only at the beginning of 1980 that newer and more advanced spectroscopic techniques for detection of surface generated radicals were developed i.e., MIER [59, 60] and MIESR [61, 62].

Matrix isolation infra red spectroscopy (MIER) was especially used by McCain and Godin to study the partial oxidation of propylene to propylene oxide [63]. The effluent gas mixture was collected in an inert argon matrix maintained at a temperature of 8 K and the spectra were obtained by a standard IR spectroscopy. In addition, the use of electron paramagnetic resonance, coupled with cryogenic trapping techniques (MIESR) for the detection of surface generated gas phase radicals during catalytic processes, has proven extremely valuable. The pioneering work of Martir demonstrated, by means of this technique, that gas phase radicals were produced during the reaction at T=300-600°C of methane over Al_2O_3, SiO_2 and MgO (this was by far the most active) [60]. Moreover, doping studies of MgO demonstrated that lithium greatly increased the concentration of gas phase methyl radicals, suggesting that lithium promotes the formation of active surface centers [64]. In particular, Lunsford and coworkers proposed that the increased activity was due to the formation of stabilized [Li^+O^-] active centers in the MgO lattice [65]. Furthermore, based on matrix isolation EPR studies (MIESR), it was proposed that C_2 products (during oxidative coupling of methane) were produced *via* a mechanism involving surface generated gas phase methyl radicals at high temperature (600°C) as presented below [66]:

$$2CH_3^{\cdot} \rightarrow C_2H_6 \quad (6)$$

$$C_2H_6 + O^- \rightarrow C_2H_5^{\cdot} + OH^- \quad (7)$$

$$C_2H_5^{\cdot} + O^{2-} \rightarrow O\,C_2H_5^- + e^- \quad (8)$$

$$O\,C_2H_5^- \rightarrow C_2H_4 + OH^- \quad (9)$$

1.4 C-H bond activation at low temperature: micro-plasma reactors

The direct conversion of alkanes is a challenging problem due to the strong C-H (e.g., 415 kJ/mol, for methane) and C-C bonds (350 KJ/mol for ethane) present. Despite the use of oxygen and/or selective catalysts for efficient conversion, high temperatures are required to get appreciable alkane conversions (T≥600ºC) [67, 68]. However, as we discussed, the activation of C-C and C-H bonds at higher temperatures, even in the presence of

heterogeneous catalyst systems, tend to be initiated by homogeneous splitting of the bond, creation of radicals and radical chain reactions leading to products.

It is generally accepted that active species (i.e., electrons, ions and radicals) can be generated at lower operation temperature by using a plasma as compared to thermal catalytic processes [69, 70]. Remarkably, hydrocarbon activation using plasmas generated between two parallel electrodes by dielectric barrier discharge (DBD), as a result of electron impact collisions, is reported to take place at ambient temperatures (<50°C) [71, 72]. Moreover, the use of a micro-reactor implies a small and confined reactor space that may determine a more uniform and dense plasma followed by a better control of the residence time. In addition, the use of a micro-reactor facilitates the generation of non-thermal plasma at pressures higher than 1 atmosphere, unlike conventional plasma systems which need low pressure.

1.4.1 Micro-reactors: definition and general advantages

An accepted definition of micro-reactors is ‘’miniaturized reaction systems fabricated using methods of micro technology’’ [73]. In fact, in the case of micro-reactors, the typical internal dimensions of channels are in between sub–micrometer and the sub-millimeter range. For example, the majority of today’s micro-reactors/heat exchanger devices contain micro-channels with typical widths of 50 μm to 500 μm and separating walls between 20 and 50 μm thick.

The origins of micro chemical systems are rooted in microanalysis which deals with the development of methods for handling small quantities of materials. However, the miniaturization techniques available for fabrication of micro chemical systems were limited and the efforts were mainly concentrated on the development of microscopic and micro analytical techniques. However, this has changed in the last 20 years since the rapid advances in the micro electronic industry facilitate novel applications of miniaturization to all aspects of engineering [74].

In the chemical industry in the early 1990s, a reduction in scale of traditional pilot plants was suggested to decrease the environmental impact and lowering costs (as part of process development) [75]. Reactors are integral component of any process and therefore the concept of reactor miniaturization was proposed a few years later [76]. Drivers for miniaturizing are (i) the production of fine chemicals and drugs (pharmaceutical industry) and (ii) on-site and on-demand production of hazardous chemicals [77].

Due to the small size, micro-reactors imply also small internal volumes (generally a few µl) and high surface to volume ratios. The benefit of that is intensified mass and heat transport. As a result, in the case of micro-exchangers/mixers devices, respectively, the measured heat transfer coefficient exceeds those typical for conventional heat exchangers with one order of magnitude (ca. 25.000 W/m^2 K) and the mixing times are in between millisecond and nanoseconds (hardly achievable using conventional stirrer) [78]. Additionally, the possibility of making micro-reactors of proper materials (i.e., silicon and stainless steel) helps to better control highly exothermic and endothermic reactions as compared to conventional macro systems. Moreover, utilizing small quantities of chemicals is advantageous in those apllications [79].

Metal multichannel micro-reactors are widely used because of favorable heat transfer characteristics [73]. Generally, choice of the metal depends on the application taking into account factors such as, (i) corrosion, (ii) thermal properties, (iii) mechanical stress, and (iv) catalytic inertness [80]. Glass micro reactors are also widely used but the temperature is limited to about 600°C [81]. Micro-reactors employed to withstand much higher temperatures are made of silicon and ceramics [82]. In particular, a ceramic like Al_2O_3 turns out to be an interesting support for catalytic application. However, micro reactors made of silicon are considered being extremely interesting for their high mechanical strength and thermal conductivity. In fact, silicon micromachining processes are reliable and have high standard regarding precision [80].

The specific advantages, using micro-reactors, are to provide (i) a well-defined set of operating conditions, and (ii) the minimal time demand to equilibriate while fast changes of conditions are performed. These factors induced important applications in high-throughput experimentation, enabling parallel testing of large numbers of catalysts in separate micro-reactors.

However, most of the common solutions used to introduce catalysts in conventional systems *i.e.*, the use of pellets as tube fillings (fixed bed reactor) or dispersed fine powder (fluidized bed reactor) can not be easily applied when using micro-reactors. In fact, irregular packing of powder would abolish the advantages above mentioned, causing non uniform temperature and concentration profiles. Thus, deposition of layers of catalyst with defined thickness on the wall of microreactors is a promising approach. Several preparation methods have been explored for that, *i.e.*, physical vapor deposition [83], chemical vapor deposition [84] and sol-gel coating processes [85].

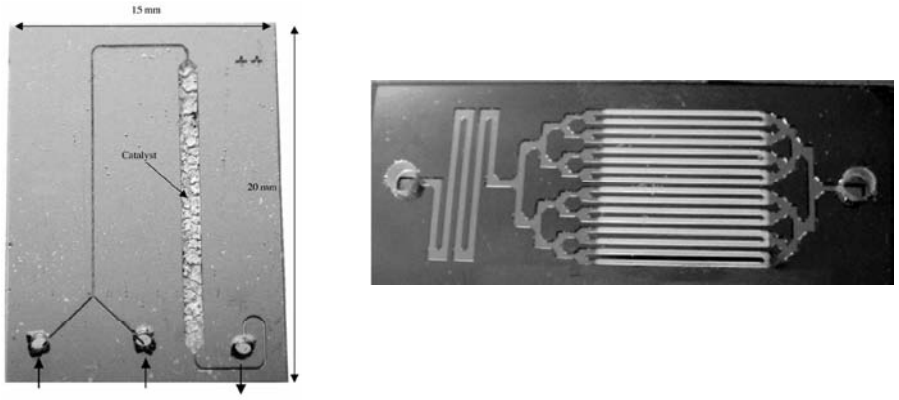

Fig. 2. Micro-reactors with deposited catalysts: (left hand) Pd/Al_2O_3 catalyst prepared by sol-gel infiltration, (right hand) with sputter deposited Ag catalyst [83-85].

1.4.2 Dielectric barrier discharge

Discharges can be generated using DC and AC voltages applied between two electrodes [86]. Electrons present in the discharge area are accelerated by the applied electric field towards the anode and ionize the gas present by collision. At the same time the positively charged ions generated by collision will be accelerated toward the cathode. Thus, the plasma is ignited and discharges are present in the gap area between the electrodes. In fact, plasma state is conventionally described as an ionized gas (where one or more free electrons are present). Furthermore, the breakdown voltage is the minimal potential needed for achieving self-sustaining discharges.

The dielectric barrier discharge (DBD) configuration (see Figure 3) can be used to generate a non thermal (cold) plasma in a gas volume between two planar plates, for a wide range of pressure [87]. The earliest and still common application of a DBD is ozone generation [88]. Industrial ozone generators consist of discharge tubes with a length of 1 to 3 m and diameter of 20 to 50 mm made of glass. Moreover, lamps and displays (based on DBD) are recently of high interest as applications. More interestingly, removal of pollutants in waste gas streams with DBD is promising technology for destruction of H_2S (already carried out in 1876 by Berthelot *et al.* [89]) and NH_3 [90].

The development of micro-machining, as discussed before, enabled shrinking of chemical devices. Plasma devices followed the same trend and in the last decade scientists focused on miniaturization of discharges, especially using dielectric barrier discharge configurations.

Longwitz *et al.*, in their pioneer work, developed a micro-glow discharge as an ion source for ion mobility spectrometry [91]. The device was micro-structured on fused silica chips or

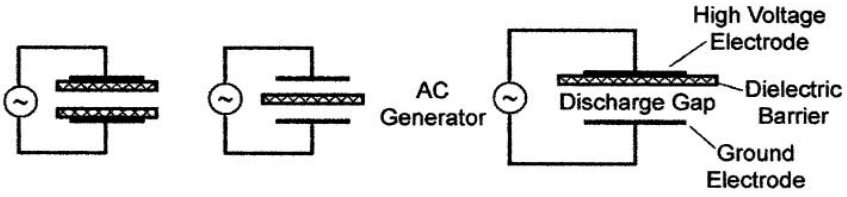

Fig. 3. Basic dielectric barrier discharge configuration [88].

Pyrex wafers. The micro-channel, also named plasma chamber, was made by HF-etching and the electrodes were formed by deposition of Cr and gold. The device was placed in a vacuum system in which gas type and pressure were adjusted. Breakdwon was studied for electrode gaps varying from 1 to 50 µm using Ar or N_2 at atmospheric pressure and stable dischrges were obtained. However, the life time of the structure was limited to a few hours.

Interestingly, similar plasma chamber were used to determine the limit of detection of methane in a helium gas flow by measuring molecular spectral emission of CH bands. In that respect, it was found that the detection limit is in the range of parts per billion (ppb). During these experiments, the micro-device was also connected to a gas chromatograph. Surprisingly, higher hydrocarbons then methane were detected, showing the capability of plasma to effectively activate methane *via* formation of radicals which can react and lead to ethane and ethylene [92-95].

1.5 Objectives and outline of this thesis

The first target of this study focuses on how to prepare high surface area Li-promoted MgO catalysts for oxidative dehydrogenation/cracking of propane. In fact, it is generally accepted that Li-promoted MgO materials prepared by conventional method i.e., impregnation of MgO with lithium salts are characterized by low surface areas. This is mainly caused by (i) high calcination temperatures needed to build lithium ions into the MgO lattice to create [Li^+O^-] active sites, and (ii) formation of alkali compounds (*i.e.*, LiOH, Li_2O and Li_2CO_3) which facilitate sintering processes. In contrast, sol-gel techniques allow significant incorporation of doping elements *i.e.*, lithium ions into MgO lattice during gel formation and therefore under milder conditions (lower temperatures). Thus, high temperature treatments are not required, preventing drastic decrease of catalyst surface area. In particular, the mechanism of incorporation of lithium ions in the magnesia gel structure is investigated. Moreover, the effect of such incorporation on the final properties on Li-promoted MgO catalysts (after

calcination) is addressed. These aspects are discussed in chapter 2 based on the following publications:

C. Trionfetti, I.V. Babich, K. Seshan and L. Lefferts, Appl. Catal. A: Gen. 310 (2006) 105-113
C. Trionfetti, I.V. Babich, K. Seshan and L. Lefferts, Top. Catal. 39(3-4) (2006) 191-198

The second goal of this thesis is to characterize the surface chemistry of Li-promoted MgO catalysts, describing the effect of lithium incorporation in altering the concentration of the catalytically active step, edge and corner sites. A detailed investigation using low temperature IR spectroscopy of adsorbed CO molecules is reported. Moreover, we aim to study the influence of catalyst surface properties *i.e.*, composition and morphology due to lithium incorporation on the catalytic performance of Li-promoted MgO samples in oxidative dehydrogenation/cracking of propane. In this respect, we compared two sets of Li-promoted MgO catalysts, prepared using, respectively, sol-gel technique and the conventional wet impregnation method. New findings in the reaction mechanism are also given. In particular, the role of surface quenching reactions and suppression of cracking reactions pathway is elucidated. In addition, the elementary reaction steps taking place on the catalyst surface during the regeneration of $[Li^{+}OH^{-}]$ sites are investigated and also better elucidated. These aspects are discussed in chapters 3 and 4, based on the following manuscripts:

C. Trionfetti, I.V. Babich, K. Seshan and L. Lefferts, Langmuir (submitted 2008)
C. Trionfetti, I.V. Babich, K. Seshan and L. Lefferts, Catal. Today (Submitted 2008)

The final part of this dissertation consists of an investigation on the feasibility of employing plasma micro-reactors for low temperatures activation of hydrocarbons. Specifically, (i) conversion of alkanes (range C_1-C_3) in empty micro-reactors in the presence of plasma generated by dielectric barrier discharge (DBD), and (ii) the activation of C-C and C-H bonds to form radicals at room temperature, are reported. Moreover, attempts to deposit crystalline layers of Li-promoted MgO catalysts (with controlled thickness) in micro-channels are also shown. Furthermore, the interaction between radical species formed in the gas phase by DBD and catalyst surface is also investigated and discussed. The effect of low temperature activation on the products selectivity is elucidated. These aspects are discussed in the chapters 5 and 6, based on the following published papers:

C. Trionfetti, A. Agiral, Han Gardeniers, L. Lefferts, K. Seshan, J. Phys. Chem. C 112 (2008)
C. Trionfetti, A. Agiral, Han Gardeniers, L. Lefferts, K. Seshan, ChemPhysChem 9(4) (2008)

References

[1] J.F. Brazdil, Top. Catal. 38 (2006) 289.

[2] http://pubs.acs.org/cen/coverstory/83/8312petrochemicals.html

[3] http://www.petrochemistry.net/?HID=99.

[4] A. Syganok, R. Green, J. Giorgi, A. Sayari, Catal. Comm. 8(12) (2007) 2186.

[5] F. Cavani, F. Trifiro, Catal. Today 24(3) (1995) 307.

[6] S.T. Korhonen, T.A. S.M.K. Airaksinen; M.A. Banares, A. Outi I. Krause, Appl. Catal. A: General 333(1) (2007) 30.

[7] J. Gascon, C. Tellez, J. Herguido, M. Menendez, Appl. Catal. A: Gen. 282(1-2) (2005) 343.

[8] B.V. Vora, R.C. Berg, P.R. Pujado, CEER, Chemical Economy & Engineering Review 15(4) (1983) 27.

[9] F. Cavani, F. Trifiro, Chimica e l'Industria (Milan) 76(11) (1994) 708-13.

[10] G.F. Schuette, F. M. Brinkmeyer, R. O. Dunn, Chimica Oggi 12(1-2) (1994) 39.

[11] R.P. Badoni, Y. Kumar, U. Shanker, T.S.R. Rao, CEW, Chemical Engineering World 31(12) (1996) 105.

[12] F. Cavani, N. Ballarini, A. Cericola, Catal. Today 127 (2007) 113.

[13] E.A. Mamedov, V. Cortes Corberan, Appl. Catal. A 127 (1995) 1.

[14] M. Baerns, O. Buyevskaya, Catal. Today 45 (1998) 13.

[15] R.K. Grasselli, Catal. Today 49 (1999) 141.

[16] M.A. Banares, Catal. Today 51 (1999) 319.

[17] F. Cavani, F. Trifiro, Catal. Today 51 (1999) 561.

[18] L. Levels, S. Fuchs, K. Seshan, J.A. Lercher, L. Lefferts, Appl. Catal. A: Gen. 227 (2002) 287.

[19] S. Gaab, J. Find, T. Muller, J.A. Lercher, Top. Catal. 46 (1-2) (2007) 101.

[20] H.H. Kung, Adv. Catal. 401 (1994) 401.

[21] H.H. Kung, M.C. Kung, Appl. Catal. A: Gen. 157(1-2) (1997) 105.

[22] H. Dai, A.T. Bell, E. Iglesia, J. Catal. 221(2) (2004) 491.

[23] S.J. Conway, D.J. Wang, J.H. Lunsford, Appl. Catal. A: Gen. 79(1) (1991) L1-L5.

[24] S.J. Conway, J.H. Lunsford, J. Catal. 131(2) (1991) 513.

[25] L. Leveles, K. Seshan, J. A. Lercher, L. Lefferts, J. Catal. 218 (2003) 296.

[26] L. Leveles, K. Seshan, J. A. Lercher, L. Lefferts, J. Catal. 218 (2003) 307.

[27] J.X. Wang, J.H. Lunsford, J. Phys. Chem. 90 (1986) 5883.

[28] I. Balint, Ken-Ichi Aika, J. Chem. Soc. Faraday Transactions 91(12) (1995) 1805.

[29] J.H. Lunsford, Langmuir 5(1) (1989) 12.

[30] J.H. Lunsford, Adv. Catal. 35 (1987) 139.

[31] S.A.R. Mulla, O.V. Buyevskaya, M. Baerns, Appl. Catal. A: Gen. 226 (2002) 73.

[32] A.A. Lemonidou, A.E. Stambouli, Appl. Catal. A: Gen. 171(2) (1998) 325.

[33] R. Burch, E.M. Grabb, Appl. Catal. A: Gen. 100(1) (1993) 111.

[34] J.P. Lange, R.J. Schoonebeek, P.D.L. Mercera, F.W. van Breukelen, Appl. Catal. A: Gen. 283 (2005) 243.

[35] Y. Diao, W.P. Walawender, C.M. Sorensen, K.J. Klabunde, T. Ricker, Chem. Mater. 14 (2002) 362.

[36] R. Portillo, T. Lopez, R. Gomez, A. Bokhimi, A. Morales, O. Novaro, Langmuir 12 (1996) 40.

[37] C.J. Brinker, Sol Gel Science, Academic Press, New York, 1990, p. 108 (Chapter 3).

[38] J.L. Boldu´, E. Munoz, X. Bokhimi, O. Novaro, Langmuir 15 (1999) 32.

[39] T. Lopez, R. Gomez, A. Ramirez-Solis, E. Poulain, O. Novaro, J. Mol. Catal. 88 (1994) 71.

[40] G. W. Scherer, J. Non-Cryst. Solids 100 (1988) 77.

[41] H. Schmidt, J. Non-Cryst. Solids 100 (1988) 51.

[42] V.G. Kessler, G.I. Spijksma, G.A. Seisenbaeva, S. Hakansson, Dave H. A. Blank, H.J.M. Bouwmeester, J Sol-Gel Sci. Techn. 40 (2006) 163.

[43] D.A. Ward, E.I. Ko, Ind. Eng. Chem. Res. 34 (1995) 421.

[44] C. Trionfetti, I.V. Babich, K. Seshan, L. Lefferts, Appl. Catal. A: Gen. 310 (2006) 105.

[45] G.E. Keller, M.M. Bhasin, J. Catal. 73 (1982) 9.

[46] R. Pitchai, K. Klier, Catal. Rev. Sci. Eng. 28 (1986) 13.

[47] J.S. Lee, S.T. Oyama, Catal. Rev. Sci. Eng. 30 (1988) 249.

[48] M.Y. Sinev, Catal. Today 24 (1995) 389.

[49] M.Y. Sinev, J. Catal. 216 (2003) 468.

[50] M.Y. Sinev, Res. Chem. Intermed. 32 (2006) 205.

[51] J.H. Lunsford, Langmuir, 5 (1989) 12.

[52] K.D. Campbell, J.H. Lunsford, J. Phys. Chem. 92 (1988) 5792.

[53] D.J. Driscoll, K.D. Campbell, J.H. Lunsford, Adv. Catal. 35 (1987) 139.

[54] D.J. Campbell, J.H. Lunsford, 89 (1985) 4415.

[55] S.P. Mehandru, A.B. Anderson, J.F. Brazdil, J. Am. Chem. Soc. 110 (1988) 1715.

[56] G.W. Keulks, L.D. Krenzbe, T.M. Notermann, J. Catal. 24 (1972) 529.

[57] K.T. Nguyen, H.H. Kung, J. Catal. 122 (1990) 415.

[58] V.T. Amorebieta, A. Colussi, J. Phys. Chem. 86 (1982) 2760.

[59] D.E. Tevault, M.C. Lin, M.E. Umstead, R.R. Smardzeqski, Int. J. Chem. Kinet. 11 (1979) 445.

[60] W. Martir, J.H. Lunsford, J. Am. Chem. Soc. 103 (1981) 3728.

[61] J.C. Schultz, J.L. Beauchamp, J. Phys. Chem. 87 (1983) 3587.

[62] D.W. Squire, C.S. Dulcey, M.C. Lin, Chem Phys. Lett. 116 (1985) 525.

[63] C.C. McCain, G.W. Godin, Nature 202 (1964) 692.

[64] D.J. Driscoll, W. Martir, J.X. Wang, J.H. Lunsford, J. Am. Chem. Soc. 107 (1985) 58.

[65] J.X. Wang, J.H. Lunsford, J. Phys. Chem. 90 (1986) 5883.

[66] Y. Tong, J.H. Lunsford, J. Am. Chem. Soc. 113 (1991) 4741.

[67] T.V. Choudary, E. Aksoylu, D. Wayne Goodman, Catal. Rev. 45(1) (2003) 151.

[68] V.P. Vislovskiy, T.E. Suleimanov, M.Y. Sinev, Y.P. Tulenin, L.Y. Margolis, V. Cortes Corberan, Catal. Today 61 (2000) 287.

[69] F.M. Aghamir, N.S. Matin, A.H. Jalili, M.H. Esfarayeni, M.A. Khodagholi, R. Ahmadi, Plasma Sources Sci. Technol. 13 (2004) 707.

[70] A. Huang, G. Xia, J. Wang, S.L. Suib, Y. Hayashi, H. Matsumoto, J. Catal. 189 (2000) 349.

[71] A. Marafee, C. Liu, G. Xu, R. Mallinson, L. Lobban, Ind. Eng. Chem. Res. 36 (1997) 632.

[72] S.Y. Savinov, H. Lee, H.K. Song, B.K. Na, Ind. Eng. Chem. Res. 38(7) (1999) 2540.

[73] W. Ehrfeld, V. Hessel, H. Lowe, Microreactors: new technology of modern chemistry; Wiley/VCH Verlag, Weinheim, Germany (200).

[74] M.V. Kothare, Comput. Chem. Eng. 30 (2006) 1725.

[75] J. Sneddon, The Microchemical Journal, Ed. 2007 Dordrecht.

[76] J.J. Lerou, M.P Harold, J.F Riley, J.W. Ashmead, T.C. O'Brien, M. Johnson, J. Perrotto, C.T. Blaisdell, T.A. Rensi, J. Nyquist, Microfabricated minichemical systems: technical feasibility. Microsystem Technology for Chemical and Biological Microreactor, Ed. 1996, Mainz, Germany, DECHEMA.

[77] P.L. Millis, D.J. Quiram, J.F. Riley, Chem. Eng. Sci. 62 (2007) 6992.

[78] J. Branebjerg, P. Gravesen, J.P. Krog, C.R. Nielsen, fat mixing in lamination, 1996, pp 441, San Diego, CA.

[79] J.B. Knight, A. Vishwanath, J.P. Brody, R.H. Austin, Phys. Rev. Lett. 80 (1998) 3863.

[80] R. Tiggelaar, PhD thesis, University of Twente, Enschede, The Netherlands, 2004.

[81] M. Brivio, R.E. Oosterbroek, W. Verboom, M.H. Goedbloed, A. van den Berg, D.N. Reinhoudt, Chem. Comm. 15 (2003) 1924.

[82] N.H. Menzler, M. Bram, H.P. Buchkremer, D. Stover, J. Eur. Ceram. 23(3) (2003) 445.

[83] O. Younes-Metzler, J. Svagin, S. Jensen, C.H. Christensen, O. Hansen, U. Quaade, Appl. Cat. A 284 (2005) 5.

[84] E. Cao, A. Gavriilidis, W.B. Motherwell, Chem. Eng. Sci. 59 (2004) 4803.

[85] H. Chen, L. Bednarova, R.S. Besser, W.Y. Lee, Appl. Catal. A: Gen. 286 (2005) 186.

[86] H. Margenau, Phys. Rev. 73(4) (1948) 326.

[87] K.H. Becker, K.H. Schoenbach, J.G. Eden, J. Phys. D: Appl. Phys. 39 (2006) R55.

[88] U. Kogelschatz, Plasma Chem. Plasma Process. 23(1) (2003) 1.

[89] K. Kunze, PhD Thesis, University of Dortmund, Dortmund, Germany, 2004.

[90] M.B. Chang, T.D. Tseng, J. Environm. Eng. 122 (1996) 41.

[91] R. Longwitz, H. Van Lintel, P. Renaud, J. Vac. Sci. Technol. B 21(4) (2003) 1570.

[92] U. Kogelschatz, Contrib. Plasma Phys. 47 (2007) 80.

[93] U. Kogelschatz, Plasma Process. Polym. 4 (2007) 678.

[94] T. Nozaki, A. Hattori, K. Okazaki, Catal. Today 98 (2004) 607.

[95] B. Eliasson, U. Kogelschatz, J. Phys. B: At. Mol. Phys. 19 (1986) 1241.

Chapter 2

Formation of high surface area Li/MgO – Efficient catalyst for the oxidative dehydrogenation / cracking of propane

Abstract

In this study nano scale clusters of Li/MgO oxide with varying lithium contents are prepared via the sol gel method. The preparation routine consists of co-gelation of $LiNO_3$ and $Mg(OCH_3)_2$ in methanol/water solution followed by drying at 50°C under vacuum and calcination at 500°C in air. The structural and textural transformations that take place during oxide formation are studied with TGA-DSC-MS and FTIR spectroscopy. The obtained materials are characterized with TEM, N_2 physisorption and XRD. Presence of increasing amounts of lithium precursor causes extensive hydrolysis of the alkoxide sol. Appreciable amounts of lithium ions can be incorporated in the magnesia gel even under the mild conditions during sol-gel transformation. Non-incorporated lithium ions form a separate carbonate phase, which has a detrimental effect on the surface area due to enhanced sintering. The Li/MgO oxide materials thus prepared possess high surface area (50 -190 m^2/g) depending on Li content. Small amounts of lithium ions, when present as a dispersed phase, do not seem to influence the structural and textural characteristics of the magnesia gel and, in these cases, nanoscale Li/MgO oxide clusters with high surface areas similar to pure MgO can be prepared. Sol-gel derived Li/MgO is significantly more active and selective in ODH of propane in comparison with conventional Li/MgO catalyst, especially at low temperature.

***Keywords**: Sol-gel Li/MgO; Nanoscale oxide; Oxidative dehydrogenation/ cracking.*

2.1 Introduction

Oxides, in which defects act as catalytic sites, attract considerable attention as catalysts in processes involving oxidation reactions [1-3]. Oxidative dehydrogenation (ODH) is an example. ODH is an exothermic reaction, converts alkanes such as ethane or propane to olefins (ethylene, propylene) from which a variety of polymers and chemicals are made. The process has definite advantages over conventional dehydrogenation basically due to the presence of oxygen which prevents coking and overcomes thermodynamic equilibrium limitation [4].

Despite being an attractive possibility, the efforts focused on the redox-type ODH catalyst systems gave low yields (e.g., <30% propene yield from propane) due to total combustion to carbon oxides [5]. On the other hand non-redox* catalysts, such as Li/MgO mixed oxides, are reported in literature as promising catalytic systems for oxidative dehydrogenation and cracking of LPG, $C_2 - C_4$ range alkanes, due to their high activity and selectivity towards olefins formation (>50% yields) [6-8]. This study focuses on oxidative dehydrogenation / cracking of propane; the term ODH is used though for convenience.

Defect sites are reported to play a key role in Li/MgO catalyst and $[Li^+O^-]$ type defect sites are considered to be responsible for the catalytic activity [9-10]. Li/MgO materials prepared conventionally, for e.g., by impregnation of MgO with aqueous solution of Li salts followed by drying and calcination, are generally characterized by low surface areas [11]. It was shown that for MgO (90 m^2/g), incorporation of Li caused substantial loss of surface area of Li/MgO (2 m^2/g) after heat treatment at 650ºC [11]. This is mainly caused by (i) high temperature treatments necessary to build Li into the MgO lattice to create active sites [12] and (ii) alkali compounds facilitating sintering. As a result these catalysts have low activity. Enhancement of the surface area and defect site ($[Li^+O^-]$) concentration can help to improve activity of the Li/MgO catalysts and operate at lower temperatures. In order to achieve this, preparation of small oxide clusters in the nanometer range would be needed; spherical nanoparticles of 3 nm contain 50% of atoms or ions in the surface [13]. Such high surface area Li/MgO materials could be appropriate for ODH reactions, in contrast to oxidative coupling of methane, since the temperature of operation is much lower (< 600°C) than for the latter (> 750ºC) [14, 15].

* - Non-redox catalysts are defined here as catalysts that do not allow change in the valence of the metal ions; consequently oxygen ions are not removed under reaction.

Sol-gel method is suitable for preparing MgO oxides, as extensively discussed by K. Klabunde *et al.* [16], and homogeneous Li/MgO mixed oxides [17]. Typically MgO oxides thus obtained possess high surface area. The mild conditions during the formation of the hydroxide/oxide networks in gel result in porous and well dispersed systems. In the case of Li/MgO the doping is done by co-gelling a lithium salt and the magnesia precursor [18]. In this study attempts are made to prepare oxide clusters of Li/MgO *via* the sol gel method and to understand the structural and textural transformations that take place during oxide formation. Simultaneously we aim at achieving high incorporation of Li in the MgO lattice under mild temperatures. The catalytic performance of sol-gel derived catalysts is compared with conventionally prepared Li/MgO.

2.2 Experimental

2.2.1 Materials

Commercially available $Mg(OCH_3)_2$ solution (Aldrich, 8.7 wt%, in methanol), methanol (Merck) and $LiNO_3$ (Merck) were used. Water added to the solution was double de-ionized.

2.2.2 Catalysts preparation

A solution of $Mg(OCH_3)_2$ in methanol (0.4 M) containing $LiNO_3$ (in appropriate amounts to obtain 0, 1, 3 and 5 wt% Li in MgO) was mixed with water in methanol (0.8 M) at room temperature and allowed to stand for 24 h for gelation (wet gels). After drying at 50°C in vacuum for 7 hours the dried gels were calcined at 500°C in air for 1h.

2.2.3 Characterization of gel/oxide

The composition of the samples was determined by chemical analysis (AAS). X-ray diffraction patterns were recorded by a Philips PW1830 diffractometer using Cu K_α radiation, λ=0.1544 nm. XRD patterns were measured in reflection geometry in the 2θ range between 20° and 50°. N_2 adsorption measurements were carried out using a Micrometrics Tristar instrument. The samples were out-gassed in vacuum at 200°C for 24 hours prior to the analysis.

FTIR measurements were conducted using a Fourier transform spectrometer, Nicolet 20 XSB. In all experiments 10 mg of dried gel or oxide was mixed with KBr (catalyst : KBr ratio

1 to 4) and pressed into a disk. The disk was placed in a cell, heated up to 100°C and purged with air, before recording IR spectra at the desired temperatures.

The thermal analysis of the gels was done using a Setaram TGA-DSC 111, heating rate 5°C/min in air. Gases evolved during these measurements were analysed with mass spectrometry (QMS-Omnistar). Transmission electron microscopy (Philips CM30) was used to determine the size and shape of the particles.

2.2.4 Catalytic test

Sol-gel Li/MgO samples were calcined at 500°C for 1 hour, pressed, crushed and sieved to 0.3-0.35 mm particles. Catalytic tests were carried out in a fix-bed reactor (quartz tube, internal diameter 4 mm) in the range of temperature between 500 and 650°C. The catalyst bed (50 mg) was packed between two quartz-wool plugs. Before each catalytic test the catalysts had been pretreated in O_2/He flow (30 ml/min, 1 hour) at temperature 50°C higher than the reaction temperature. The feed consisted of 10% propane, 10% oxygen, 2% carbon dioxide and balance helium. Carbon dioxide has been added to the feed in order to achieve a constant CO_2 concentration over the whole catalyst bed, as CO_2 has an inhibiting effect upon the reaction. The total flow rate was 100 ml/min. A Varian 3800 GC was used to analyze all the gases. Impregnated Li/MgO catalysts have been tested under the same conditions.

2.3 Results

2.3.1 Characterization of the gels

2.3.1.1 Magnesia gel

Fig. 1a shows the result of TGA in air for a sample of magnesia gel (*Mg-gel*) obtained from hydrolysis of $Mg(OCH_3)_2$. The small weight loss of 3 % observed below 100°C is associated to residual methanol and water still present in the dried gel. This was typical for TGA profiles of all the gels recorded and will not be discussed further. The experimental weight loss of 34 %, between 300-350°C, corresponds to the decomposition of *Mg-gel*. Fig. 1b shows the analysis of gases evolved during the above TGA experiment as followed by mass spectrometry. Evolution of CO_2 in the temperature range corresponding to the weight loss in TGA indicates combustion of the organic species. Fig. 1c shows the DSC signal in air recorded during the gel decomposition. Two exothermic transitions are observed in the temperature ranges 200-250°C and 300-350°C respectively. For the first peak there is no corresponding weight loss in TGA (see Fig.1a) and it should represent an isomorphic

transformation. The second exothermic peak at 350°C corresponds to the combustion of the alkoxide gel.

Fig. 2 shows infra red spectra of gels treated at different temperatures. Fig. 2a represents the spectrum obtained from the *Mg-gel* at 100°C. In this case, peaks characteristic for –OH stretching (3600-3700 cm^{-1}) and -CH_3 stretching (2700-2900 cm^{-1}, methoxy groups) as well as a broad band between 3600 and 3400 cm^{-1} due to hydrogen bond formation are detected. As expected from the TGA/DSC data above, the methoxy groups should decompose below 350°C and thus were not observed in FTIR spectrum of the sample calcined at 500°C (Fig. 2b).

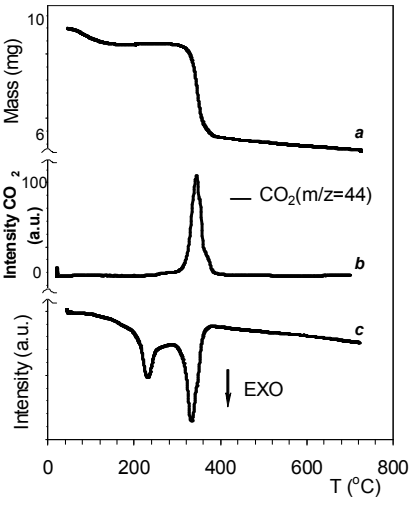

Fig. 1. TGA analysis of magnesium gel (a); analysis of gases produced followed by mass spectrometer (b); DSC data during the TGA experiments. Flow air 30 ml/min, temperature ramp 5°C/min.

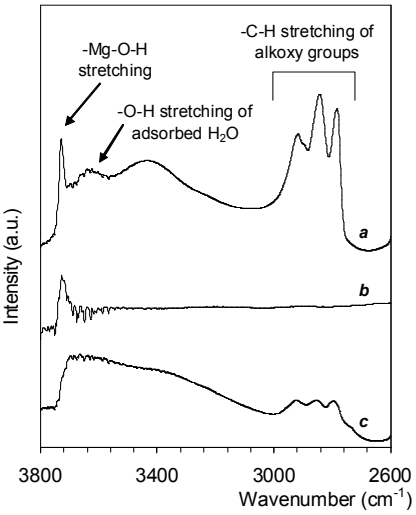

Fig. 2. IR spectra of Mg-gel heated to 100°C in air (a), Mg-gel heated to 500°C (b) and 5 wt% Li-Mg-gel heated to 100°C (c).

2.3.1.2 Li containing magnesia gel

Figure 3 & 4 shows the details of thermal analyses of two Li containing magnesia gels (*Li-Mg-gel*), i.e., 1 wt% and 5 wt% Li, respectively. The TGA profile for 1 wt% *Li-Mg-gel* was similar to that obtained for *Mg-gel*; the weight loss corresponded to 33% (Fig. 3a) and occurred in a single step between 300-350°C. In the case of 5 wt% *Li-Mg-gel* (Fig. 4a) two regions of weight losses were recorded: the first weight loss (27%) was observed around 300°C and the second (24%) at 650°C. Figs. 3b and 4b show MS analyses of evolved gases for 1 wt% and 5 wt% *Li-Mg-gel* during the TG experiments. The CO_2 signal corresponding to

the gel combustion was observed in both cases (300-350°C). However, it has to be noted that both the temperature of CO_2 evolution and the peak shape are different in the case of 5 wt% *Li-Mg-gel*, indicating that the nature of gel was different.

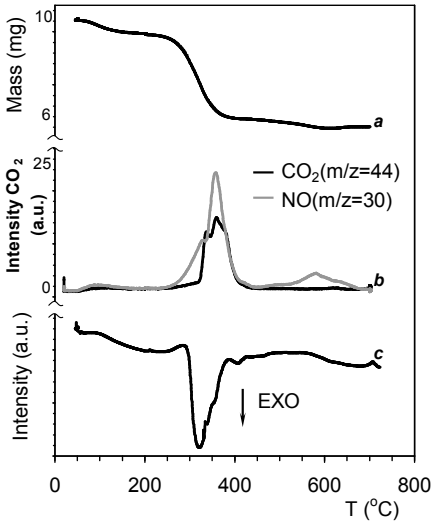

Fig. 3. Thermogravimetric analysis of 1 wt% *Li-Mg-gel* (a), analysis of gases produced followed by mass spectrometer (b) and differential scanning calorimetry during the TGA experiment (c). Flow air 30 ml/min, temperature ramp 5°C/min.

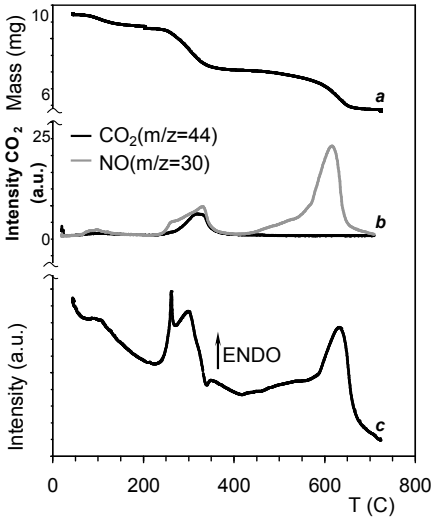

Fig. 4. Thermogravimetric analysis of 5 wt% *Li-Mg-gel* (a); analysis of gases produced followed by mass spectrometer (b) and differential scanning calorimetry during the TGA experiment (c). Flow air 30 ml/min, temperature ramp 5°C/min.

Additionally, two NO peaks around 350°C and 650°C (originating from decomposition of nitrate species present in gel) were observed with MS. The NO peak at 350°C is typical for $Mg(NO_3)_2$ decomposition [19]. Since the starting precursors for *Li-Mg-gel* were $Mg(OCH_3)_2$ and $LiNO_3$, some magnesium nitrate is apparently formed during gelation. Decomposition of bulk $LiNO_3$ was found around 650°C and, hence, the second NO peak observed is assigned to decomposition of unreacted $LiNO_3$ present in the gel. For the 5 wt% *Li-Mg-gel*, the intensity of the NO peak at 650°C is much higher. The corresponding TGA weight loss at 650°C (24 %, Fig. 4a,) indicates that about 60% of Li added was present as free $LiNO_3$ in the gel.

Figs. 3c and 4c show the DSC in air for the two lithium containing magnesia gels. In both Li containing gels, the isomorphic transition, observed for pure magnesia gel T<250°C, was absent. For the 1 wt% *Li-Mg-gel*, one exothermic peak (320°C) corresponding to gel combustion was recorded (Fig. 3c). In contrast, for the 5 wt% *Li-Mg-gel* two endothermic peaks were seen between 250-320°C and at 630°C (Fig. 4c). The first DSC signal between

250-320°C is typical for bulk $Mg(NO_3)_2$ decomposition. These two endothermic transitions therefore correspond to decomposition of Mg and Li nitrates, respectively.

For the 5 wt% *Li-Mg-gel* sample, the exothermic peak corresponding to alkoxide gel combustion (Fig. 1c) was not observable for two reasons: (i) the endothermic $Mg(NO_3)_2$ decomposition occurs in the same temperature range and overlaps with the exothermic signal (ii) the alkoxide content of the gel was low. In agreement, the infra red spectra of the 5 wt% *Li-Mg-gel* (Fig. 2c) showed much less intense $-CH_3$ stretching vibration. This also implies that the extent of hydrolysis in this sample is much higher.

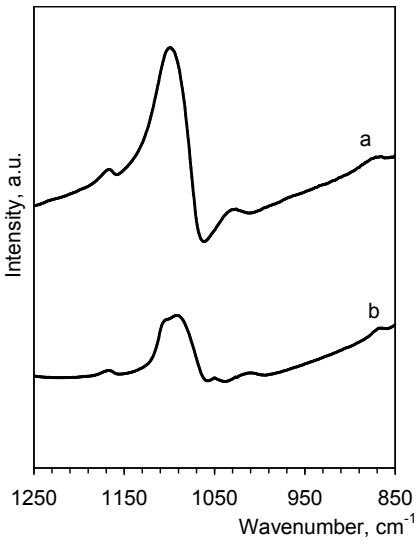

Fig. 5. FTIR of dried gels: *Mg-gel* (a) and 5 wt% *Li-Mg-gel* (b). Spectra have been taken at T=100°C. The signal at 1100 cm^{-1} is related to the bending of Mg-O-Mg bond.

Fig. 5 shows the IR spectra of the gels in the range 850 - 1250 cm^{-1}, i.e. the region typical for Mg-O-Mg bending vibrations [17]. The band at 1100 cm^{-1} is related to the presence of Mg-O-Mg bonds. The signal decreases when lithium is present in the *Mg-gel* (see Fig.5b).

2.3.2 Characterization of oxide materials

Table 1 shows the BET surface areas of oxide powders obtained after calcination of the gels at 500°C. Two important conclusions could be drawn (i) high surface area materials could be made by the sol-gel method and (ii) even in the presence of Li, for sol-gel Li/MgO oxide samples, high surface area (190 m^2/g) could be maintained in comparison to materials prepared conventionally (<10 m^2/g). However, at higher lithium concentration (5 wt%) the resulting surface area is less spectacular.

Table 1
BET surface areas for samples obtained using the sol-gel method, after calcination at 500ºC for 1h.

Samples	BET (m^2/g)
MgO	250
1 wt% Li/MgO	190
3wt % Li/MgO	70
5 wt% Li/MgO	50

XRD patterns of the oxide samples are

shown in Fig. 6. The peaks corresponding to MgO phase became narrower for samples with higher lithium loading. From the X-ray Line Broadening Analysis (XLBA) we estimated particle size of 5 nm in the case of MgO and this increased up to 10 nm for 5 wt% Li/MgO sample. In the case of samples containing higher amounts of lithium, peaks of Li_2CO_3 could also be observed. No other phases of Li, including $LiNO_3$, were detected by XRD.

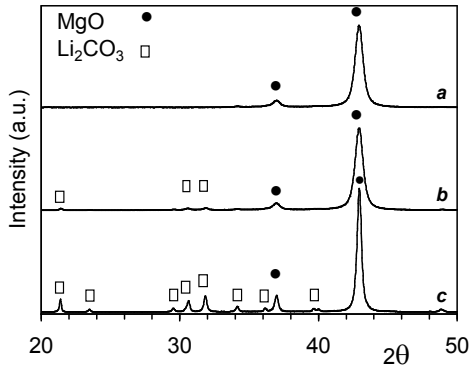

Fig. 6. XRD pattern for pure MgO (a), 1 wt% Li/MgO (b) and 5 wt% Li/MgO(c).

Semi-quantitative experiments were carried out with X-ray powder diffraction in order to estimate the amount of lithium present as a separate phase (Li_2CO_3) and thus to evaluate the amount of lithium incorporated into the lattice of MgO (solid solution). In Fig. 7, the relative intensity of the strongest line [002] of Li_2CO_3 and [200] of MgO is plotted for mechanical mixtures of Li_2CO_3 – MgO* and for sol gel Li/MgO samples. The differences between the data for mechanical mixtures and for the synthesized sol-gel samples with the same composition correspond to the amounts of lithium incorporated into MgO lattice. Based on these observations we can estimate the amount of Li incorporated into MgO lattice - 40% for 1 wt% Li, 25% for 3 wt% and 16% for 5 wt% Li in MgO.

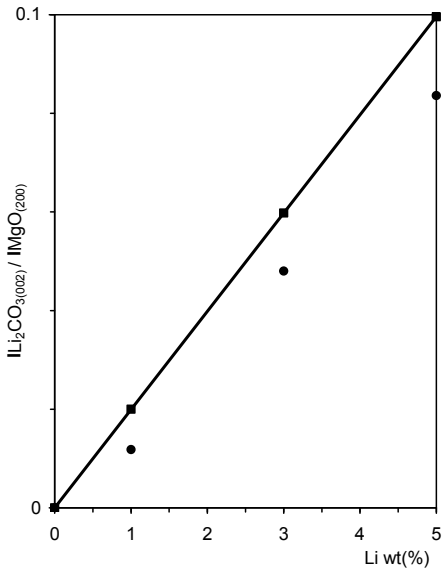

Fig. 7. Ratio between peak area of Li_2CO_3 and MgO in standard mechanical mixtures (■) and for Li/MgO samples obtained by sol gel method (●).

This means that solid solution in sol gel Li/MgO samples is already formed under mild conditions, *i.e.* by co-gelling $Mg(OCH_3)_2$ and $LiNO_3$ and calcination at 500°C.

* - XRD detection limit for bulk Li_2CO_3 in mechanical mixture with MgO is below 0,1 wt% Li.

Fig. 8a shows the influence of calcinations temperature on the surface areas. For the 1 wt% Li/MgO sample, high surface area could be maintained even after the thermal treatment at 700°C. Pore size distribution for 1 and 5 wt% Li/MgO samples does not change even after treatment at 700°C. TEM data (not presented here) show only a slight increase in the particle size in line with BET results.

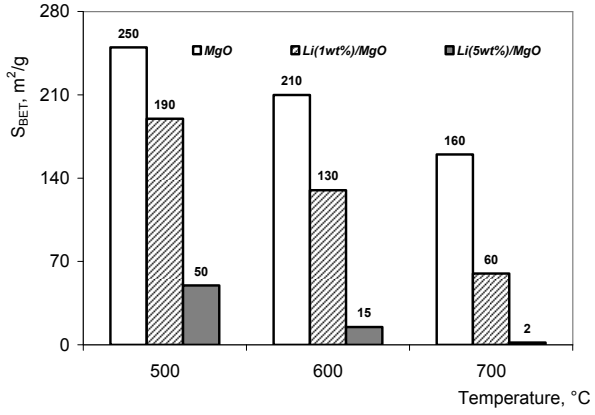

Fig. 8a. Surface areas of MgO and Li/MgO samples obtained by sol-gel method after calcination at different temperature.

For the sample with 5 wt% Li, thermal treatment had a drastic influence on the surface area; this may be due to the fact that the sample contained a considerable amount of free Li_2CO_3. In order to check this, samples of 1 wt% Li prepared by sol gel method and wet impregnation of MgO (Li present as $LiNO_3$) were subjected to similar thermal treatments.

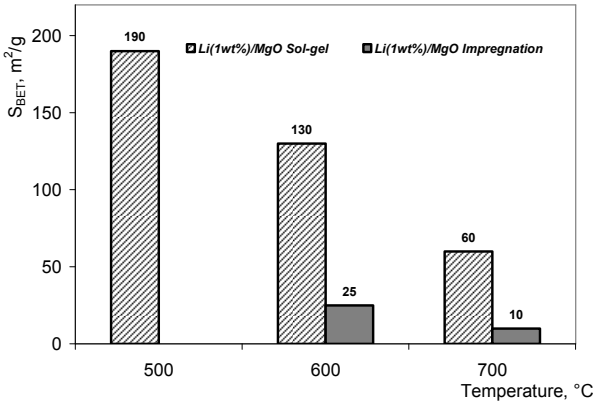

Fig. 8b. Surface area of 1 wt% Li/MgO obtained by sol-gel method and by conventional impregnation of high surface area MgO after calcinations at different temperature.

MgO used for impregnating $LiNO_3$ was the same high surface material prepared with the sol gel route. It can be seen from the Fig 8b that indeed: (i) Li when present as a free phase before calcinations affects surface area drastically with increase in temperature, and (ii) this influence is minimized when most of Li is built into the MgO lattice, *i.e.,* in the case of sol gel method samples.

2.3.3 Textural properties of gel and oxide samples

N_2 sorption isotherms were recorded for the dried gels and oxides to study the influence of lithium incorporation on the textural properties of the gel and oxide phases. For *Mg-gel* and 1 wt% *Li-Mg-gel* (Fig. 9) the isotherms are similar and typical for particles possessing mesoporosity (av. pore size 3.5 nm, surface area 300 m^2/g). For the 5 wt% *Li-Mg-gel*, the surface area was lower (25 m^2/g) and average pore size was much higher (20 nm). The results indicate that the texture of *Mg-gel* can be retained in the presence of small amounts of Li. At higher Li concentrations the texture is already changed at the gel stage.

Fig. 10 shows nitrogen adsorption isotherms for samples calcined at 500°C. In the case of MgO and 1 wt% Li/MgO, the hysteresis loop is typical for agglomerates of spherical particles, Type H1 [20]. For the 5 wt% Li/MgO sample, hysteresis loop was typical for pore structure made by aggregates of platelets, Type H3 [20]. This sample showed an appreciable loss in surface area as described earlier. TEM photographs for MgO and 5 wt% Li/MgO are presented in Scheme 1, (a) and (b), respectively. It can be seen from the photographs that lithium influences the shape of the oxide aggregates. For MgO a spherical particle shape was observed. 5 wt% Li/MgO showed typical cubic particle shape. Cubic particles are usually observed for sintered, crystalline MgO [21].

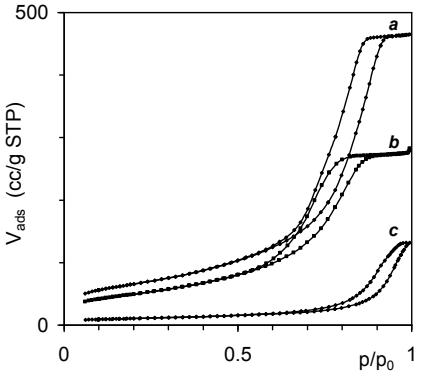

Fig. 9. Nitrogen adsorption isotherms of *Mg-gel* (a), 1 wt% *Li-Mg-gel* (b) and 5 wt% *Li-Mg-gel* (c).

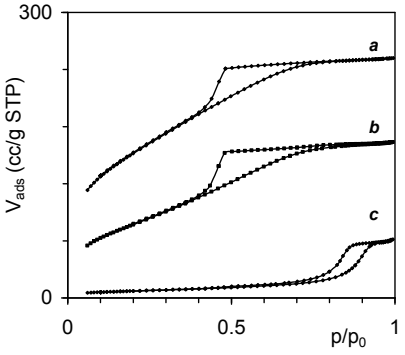

Fig. 10. Nitrogen adsorption isotherms MgO (a), 1 wt% Li/MgO (b) and 5 wt% Li/MgO (c) after calcinations at 500°C.

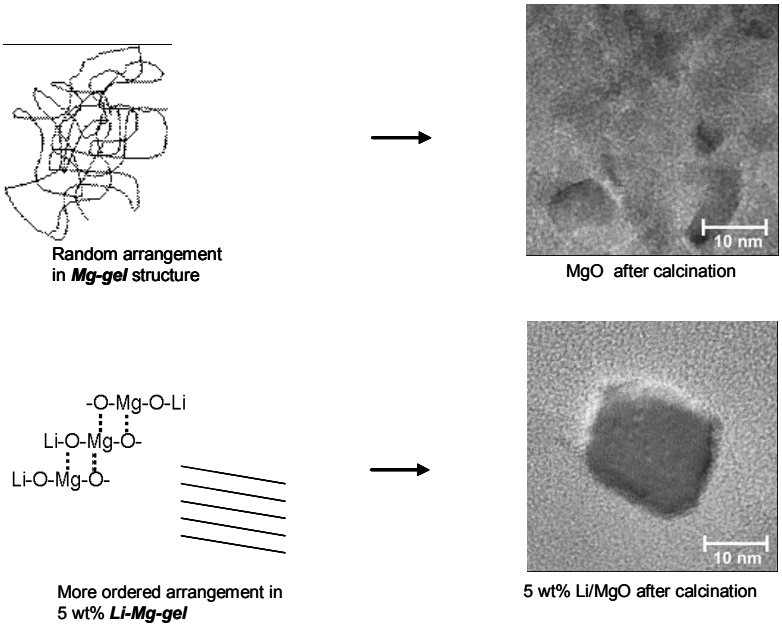

Scheme 1: Different chain length and arrangement at the gel stage: *Mg-gel* (a), 5 wt% *Li-Mg-gel* (b) and resulting oxide material, respectively.

2.3.4 Catalytic properties

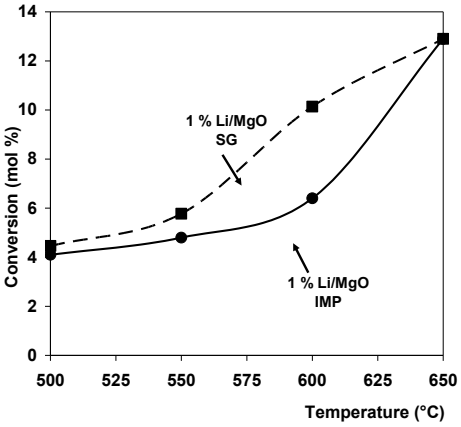

(a)

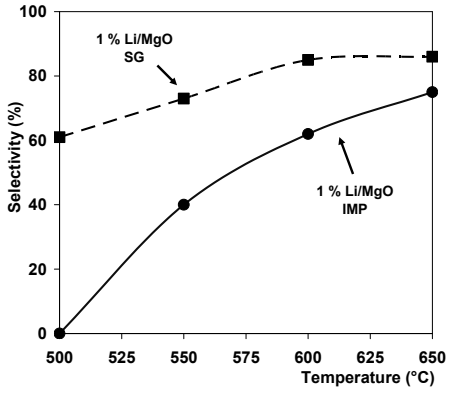

(b)

Fig. 11. Oxidative dehydrogenation of propane. Conversion (a) and selectivity to olefins (b) over 1 wt% Li/MgO catalyst obtained by sol-gel method (SG, square symbols) and conventional impregnation (IMP, round symbols) as function of temperature. Conditions: 10% propane, 10% oxygen, 2% CO2 and 78% He; GHSV= 120000 h-1.

Catalytic performance in oxidative dehydrogenation of propane in the range of temperature between 500 and 650°C is compared for 1 wt% Li/MgO catalysts prepared by sol-gel and conventional wet impregnation (Fig. 11a, b). In the reported experiments propane conversion is below 13% (using high space velocity) in order to avoid heat and mass transfer. The sol-gel catalyst gave appreciable higher propane conversion especially at 600°C. Olefins selectivity in the explored range of temperature is also higher for sol-gel Li/MgO than for conventionally prepared catalyst. Remarkably, at 500°C sol gel Li/MgO catalyst presents olefins selectivity (propene and ethene) around 60% while the conventional Li/MgO catalysts show 100% selectivity to complete oxidation (CO_2).

Selectivity to olefins increases with temperature in both cases, but sol-gel Li/MgO is always more selective. Moreover in the case of sol-gel catalyst the main olefin specie formed is propene. Ratio $C_3^=/C_2^=$ is always above 1 varying from 4.5 to 1.2 when increasing temperature from 500 to 650°C. In the case of catalysts prepared by wet impregnation the ratio $C_3^=/C_2^=$ is always close to 1. Therefore the data clearly illustrate the advantage of sol-gel Li/MgO catalysts in propane ODH compared with conventionally prepared catalyst. Detailed testing of the sol-gel Li/MgO catalysts, varying the experimental conditions, Li loading and feed composition are in progress and will be discussed in a subsequent paper.

2.4 Discussion

2.4.1 MgO

The sol-gel process involves two main reactions i.e., hydrolysis and condensation [22]. In the case of *Mg-gel* obtained from $Mg(OCH_3)_2$ these reactions are:

$$Mg(OCH_3)_2 + xH_2O \rightarrow Mg(OH)_x(OCH_3)_{2-x} + xCH_3OH \quad (1)$$

$$\text{-Mg-}(OCH_3) + \text{OH-Mg-} \rightarrow \text{-Mg-O-Mg-} + CH_3OH \quad (2)$$

$$\text{-Mg-OH} + \text{OH-Mg-} \rightarrow \text{-Mg-O-Mg-} + H_2O \quad (3)$$

Gel formation can be attributed to presence of (i) chains of -Mg-O-Mg- bonds (chemical gel) and their internal interaction (Scheme 1) and/or (ii) smaller molecules of $Mg(OH)(OCH_3)$ which interact with each other by hydrogen bonding and/or electrostatic interaction (physical gel) as described in literature (Scheme 2) [16,23]. Our results from thermal analysis and IR spectroscopy indicate partial hydrolysis of the Mg-alkoxide during gel formation.

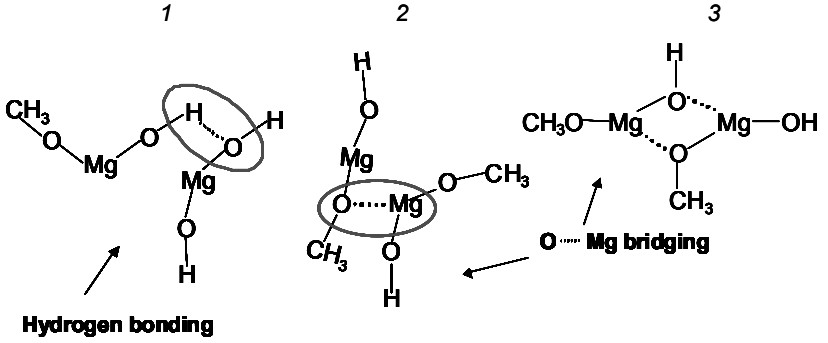

Scheme 2. Examples of interconnected gel molecules of $Mg(OH)(OCH_3)$ through hydrogen bonding (1) or oxygen-magnesium bonding (2, 3).[18-20]

In the case of partial hydrolysis (for e.g. 50% or x=1 in eq. (1), *i.e.,* formation of $Mg(OCH_3)(OH)$) or complete hydrolysis (100 % or x=2 in eq (1), *i.e.,* formation of $Mg(OH)_2$), one would expect for gel – oxide transformation under thermal treatment weight loss of 44 or 31 %, respectively. The experimental weight loss during *Mg-gel* decomposition to MgO is 34 %. From this we can calculate the molecular composition of the *Mg-gel* to be $Mg(OCH_3)_{0.15}(OH)_{1.85}$ suggesting about 92% hydrolysis. However, other reactions, such as condensation and dehydration (equation 2 & 3) also occur. These reactions cause rejection of methoxy groups (as methanol) or hydroxyls (as water) resulting in oligomers containing -Mg-O-Mg- type species. Observation of the band at 1100 cm^{-1} in IR spectra (Fig. 5), assigned to

the bending vibration of Mg-O-Mg bond [17], suggests that both condensation and dehydration occur at the gel stage. The extent of this will determine the amount of –(OH) and –(OCH_3) groups retained in the gel. Three observations indeed confirm significant presence of hydroxyl and methoxy groups at gel stage: (i) FTIR experiments show presence of strong methoxy bands in the gel (at 2800 cm^{-1}, Fig. 2), (ii) strong exothermic decomposition of the gel in air and (iii) the large amounts of CO_2 formed during gel combustion (Fig. 3, 4). Thus, hydrolysis occurs to a much smaller extent than estimated above (92%).

2.4.2 Li-Mg-gel

The presence of Li ions in the sol-gel system influences the extent of hydrolysis/condensation quite drastically. This can be concluded from the following observations: (i) lower intensity of -CH_3 stretching in the IR spectra (Fig. 2c as compared to Fig. 2a), (ii) lower weight loss during calcination for 5 wt% *Li-Mg gel* (24%) *vs Mg-gel* (34%) and (iii) lower amounts of CO_2 formed during combustion. These observations suggest that Li ions definitely enhance hydrolysis. Thus, the presence of Li ions changes the composition of the gel. Difference in the gel structure is also confirmed by N_2 adsorption isotherms shown in Fig 9, demonstrating that *Mg-gel* is typically mesoporous whereas 5 wt% *Li-Mg-gel* contains macropores.

Thus, addition of lithium precursor seems to generate a different ordering in the gel, as also supported by the fact that the isomorphic transition observed at 210°C for the *Mg-gel* is absent in the case of *Li-Mg-gels*. Reller *et al.* [24] qualitatively, attributed this transition for magnesia gel to either (i) a re-crystallization or (ii) formation of a new phase by intermediate species containing bridging of OH groups as shown in Scheme 2, case 1. The exact nature of these structures are neither relevant to this study nor taken up for further discussion, but the fact that such a transition is absent when Li ions are present in the gel confirms that the ordering in the presence of Li ions is different. It is thus likely that lithium ions are incorporated already in magnesia at *Li-Mg-gel* stage. The incorporated lithium can be directly bound in magnesium gel structure and located as a terminating entity, (-Mg-O-Li). A consequence of this is that the presence of lithium as a terminating entity will prevent further condensation and chain growth as shown in Scheme 3. Moreover chain termination by Li as -Mg-O-Li instead of -Mg-OH or -Mg-OCH_3 decreases the presence of hydroxyl or methoxy groups as observed in figure 2.

2.4.3 Li/MgO oxide

Samples containing 1 wt% Li/MgO obtained by sol-gel route posses low amount of free Li (about 0.6 wt% Li) and maintain high surface area even after treatment at higher temperatures (190 m^2/g, see Fig 8a). This indicates that small amounts of Li, even when present as free phase of Li_2CO_3, are not detrimental for making high surface area Li/MgO catalysts. The sol gel method applied to Li/MgO materials synthesis achieves two objectives simultaneously, (i) allows incorporation of Li in the magnesia under milder conditions during gelation and (ii) minimizes sintering during thermal treatments. The approach is less successful in the case of the 5 wt% Li containing sample. In this sample free Li carbonate phase (about 4.2 wt% Li) is present and, as expected, the oxide formed on calcinations at 500°C has a relatively low surface area (50 m^2/g). The effect of Li assisted sintering is also seen from the nitrogen sorption curves: MgO and 1 wt% Li/MgO show typical meso-porosity and high surface area whereas, the hysteresis loop for 5 wt% Li/MgO material indicates more macro-porosity.

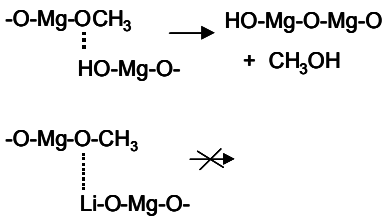

Scheme 3: Role of lithium, terminating chain at the gel stage during condensation reaction and chain growth.

Calcination of *Mg-gel* gives rise to presence of spherical like particles as observed by TEM. Extensive condensation and chain growth at the gel stage in the absence Li may lead to more random agglomerates and spherical type structures. On the contrary, short chains, formed in the presence of Li, tend to form a more ordered gel structure giving rise to cubic Li/MgO particles after calcination. A qualitative representation is shown below in Scheme 1. However, in this case due to the presence of Li, we cannot rule out that enhanced sintering is responsible for the observed changes in the particle shape [25].

Preparation of Li/MgO catalysts by conventional method (impregnation of bulk MgO with Li salts) leads to the formation of mixture of phases of Li_2CO_3 and MgO [26]. This is because Li_2O formed on calcinations easily sorbs CO_2 from atmosphere and forms Li_2CO_3. Only a high temperature treatment allows the incorporation of lithium (Li_2CO_3 melts / decomposes around 750°C) because it makes possible for Li^+ ions to diffuse into the MgO lattice replacing Mg^{2+} ions. The disadvantage of this is that this mobility of the Li species and high T facilitate sintering of MgO and subsequent loss of surface area. This is also seen

clearly from Fig. 8b. The high surface area MgO (250 m^2/g) is drastically reduced on impregnation with $LiNO_3$ and subsequent calcinations at 600°C and 700°C (1 wt% Li/MgO, respectively, 25 m^2/g and 10 m^2/g).

Both catalytic activity and selectivity in ODH of propane of the sol-gel catalyst are superior in comparison with Li/MgO prepared by conventional impregnation. This is probably the result of two effects: (i) the sol-gel derived catalyst has a significant higher surface area (130 vs 25 m^2/g) and (ii) the sol-gel derived catalyst contains a higher amount of Li incorporated in the MgO matrix. Both effects contribute to an increase in the number of active sites, *i.e.* $[Li^+\text{-}O^-]$. A third effect may contribute as well: the number of low-coordination sites is increasing when decreasing the size of the primary particles, and when lithium is incorporated and this could well influence the generation and/or properties of $[Li^+\text{-}O^-]$ sites on the surface. In future work we will study this effect with IR spectroscopy of CO adsorbed at low temperatures. The observed effect on activity is not very surprising. However, the effect on selectivity is not obvious at all taking into account the complex mechanism of catalytic ODH process, which includes radical generation at the active site in combination with radical chain reactions in gas-phase as well as quenching reactions on the catalyst surface [11].

The catalysts obtained have sufficient thermal stability for application in oxidative dehydrogenation and cracking as the operation temperature is typically below 650°C, in contrast to the classical application of Li/MgO catalysts for the oxidative coupling of methane at much higher temperatures (750°- 800°C).

2.5 Conclusions

High surface area nano scale Li/MgO oxide clusters can be synthesized by sol-gel method, co-gelling $Mg(OCH_3)_2$ and $LiNO_3$ in methanol/water solution followed by drying at 50 °C under vacuum and calcination at 500°C in air. Lithium ions are incorporated in the magnesia structure already at the gel stage, probably enhancing formation of $[Li^+O^-]$ type active sites at relatively low temperatures. Moreover the enhanced lithium incorporation can result also in an increased number of low coordinated sites. At this stage we cannot rule out any influence of low coordinated sites on the catalytic activity. When the Li loading is low (1 wt%), the structural and textural characteristics of the magnesia gel and eventually magnesium oxide are not significantly affected; the resulting Li/MgO retains high surface area and mesoporosity. At higher Li loading, the characteristics of the gel are changed: the gel is more ordered.

The sol-gel procedure allows significant incorporation of Li ions at temperatures below 650°C, i.e. temperature at which Li ions are not incorporated at all in impregnated Li/MgO catalysts. Consequently, less Li_2CO_3 is present in sol-gel derived catalysts during calcination. This effect is responsible for both high surface area obtained after calcination as well as for enhanced thermal stability of Li/MgO. Sol-gel catalysts are more active than catalysts prepared by wet impregnation. Olefins dominate even at 500°C when catalysts by wet impregnation produce only CO_2. Sol-gel derived Li/MgO is a very promising catalyst for the oxidative dehydrogenation of propane to olefins.

References

[1] C. Shi, M. Xu, M. P. Rosynek and J. H. Lunsford, J. Phys. Chem. 97 (1993) 216.

[2] M. A. Johnson, E. V. Stefanovich and T. N. Truong, J. Phys. Chem. B 101 (1997) 3196.

[3] L. Lefferts, K. Seshan, B. Mojet and J.G. van Ommen, Catalysis Today 100 (2005) 63.

[4] E.A. Mamedov and V. Cortes Corberan, Appl. Catal. A 127 (1995) 1.

[5] F. Cavani and F. Trifiró, Catalysis Today 24 (1995) 307.

[6] M. V. Landau, M. L. Kaliya, M. Herskowitz, P. F. van den Oosterkamp and P. S. G. Boque, Chemtech 26(2) (1996) 24.

[7] M. Herskowitz, M. Landau and M. Kaliya, US Patent number 6,130,183, October 2000.

[8] S. Zender, Hydrocarbon processing 77(2) (1998) 59.

[9] J. H. Lunsford, Adv. Catal. 35 (1987) 139.

[10] J. X. Wang and J. H. Lunsford, J. Phys. Chem. 90 (1986) 5883.

[11] L. Leveles, K. Seshan, J. A. Lercher and L. Lefferts, J. Catal. 218 (2003) 307.

[12] T. Ito, J. X. Wang, C. H. Lin and J. H. Lunsford, J. Am. Chem. Soc. 107 (1985) 5062.

[13] K. J. Klabunde, J. Stark and D. Zhang, J. Phys. Chem. 100 (1996) 12142.

[14] L. Leveles, PhD Thesis, University of Twente, The Netherlands, 2002.

[15] J. A. Roos, S. J. Korf, R. H. J. Veehof, J. G. van Ommen and J. R. H. Ross, Appl. Catal. 52 (1989) 147.

[16] Y. Diao, W. P. Walawender, C. M. Sorensen, K. J. Klabunde and T. Ricker, Chem. Mater. 14 (2002) 362.

[17] T. Lopez, R. Gomez, A. Ramirez-Solis, E. Poulain and O. Novaro, J. Molecular Catal. 88 (1994) 71.

[18] J. L. Boldú, E. Munoz, X. Bokhimi and O. Novaro, Langmuir 15 (1999) 32.

[19] R.C. Weast, in: Handbook of Chemistry and Physics, ed. CRC Press Inc., Florida, 64th edn., 1984, pp. B-106-108.

[20] K. S. Sing, Pure & Appl. Chem. 57 (4) (1985) 612.

[21] J. Hargreaves, G. Hutchings, R. W. Joyner and C. Kiely, J. Catalysis Today 13 (1992) 401.

[22] C.J. Brinker, in: Sol Gel Science, ed. Academic Press, New York, 1990, ch. 3, pp. 108.

[23] R. Portillo, T. Lopez, R. Gomez, A. Morales and O. Novaro, Langmuir 12 (1996) 40.

[24] H. Thoms, M. Epple, H. Viebrock and A. Reller, J. Mater. Chem. 5 (4) (1995) 589.

[25] A. G. Andersen and T. Norby, Catalysis Today 6 (1990) 575.

[26] X. D. Peng, D. A. Richards and P. C. Stair, J. Catal. 121 (1990) 99.

Chapter 3

Presence of Lithium Ions in MgO Lattice: Surface Characterization by Infra Red Spectroscopy and Reactivity towards Oxidative Conversion of Propane

Abstract

The surface morphology of Li-promoted MgO catalysts prepared using, respectively, sol-gel method (sg) and wet impregnation procedure (imp) has been studied with low temperature infrared spectroscopy of adsorbed CO molecules. The results show that step sites, as un-selective catalytic centers, are the major features existing on the surface of pure MgO and those are active toward the oxidative conversion of propane. However, the concentration of these sites is drastically reduced by the incorporation of lithium ions in the MgO lattice. In fact, the incorporated Li^+ ions tend to move into the surface region and occupy sites associated with lower coordination number (e.g., step sites). Li/MgO-sg catalysts are characterized by a higher concentration of incorporation of lithium compared to Li/MgO-imp. In the case of oxidative dehydrogenation/cracking of propane, Li/MgO-sg show higher activity and selectivity to olefins compared to materials prepared using wet impregnation. Catalytic performance differs strongly regarding (i) the amount of olefins formed, and (ii) the ratio of C_3H_6/C_2H_4. It is shown that high density of active sites is essential for further oxidative dehydrogenation of propyl radicals to propylene and suppression of cracking reactions pathway.

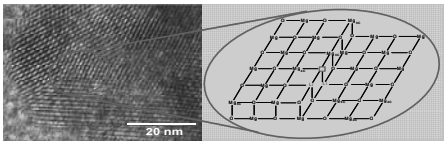

TEM picture over Li-promoted MgO catalysts

***Keywords**: Lithium ions incorporation; Surface Defect; Oxygen vacancy; Step site; Low temperature IR spectroscopy; Oxidative dehydrogenation/cracking of propane.*

3.1 Introduction

An efficient catalytic oxidative dehydrogenation (ODH) process of light alkanes (i.e., propane) attracts both scientific and industrial attention. In fact, this represents a direct route to highly desired olefins starting from available and cheap feedstock [1, 2]. However, despite enormous efforts, the development of an appropriate catalyst is still a challenge since (i) the formed olefins are generally prone to further oxidation under the reaction conditions and (ii) CO_x formation is favored [3]. Alkali metal-based oxide catalysts such as Li-promoted magnesia (i.e., Li/MgO), which are not susceptible to red-ox changes, are considered to be efficient catalysts which can provide higher olefin yields at a level of alkane conversion appropriate for industrial applications [4-6].

In the case of Li/MgO catalysts, lithium is an essential component which promotes the formation of defect sites such as $[Li^+O^-]$. These sites are considered to be responsible for the catalytic activity [7, 8] and able to activate alkanes, e.g., propane, *via* C-H bond cleavage leading to propyl radicals (eq. 1) [9, 10]:

$$[Li^+O^-] + C_3H_8 \rightarrow [Li^+OH^-] + C_3H_7^{\cdot} \quad (1)$$

However, Goodman and coworkers suggested, in the case of methane coupling, that $[Li^+O^-]$ centers are unlikely to be directly involved in the hydrocarbon activation step [11]. Rather, they promote the creation of F-type defects (oxygen vacancies containing one or two electrons), on the catalyst surface, which are considered to be responsible for the catalytic activity. As reported in literature, the identification and characterization of these two types of defects (F-centers and $[Li^+O^-]$) might be done using, respectively, high resolution electron energy loss spectroscopy (HREELS) and electron paramagnetic resonance (ESR) [11].

Interestingly, as repeatedly reported, the reaction during ODH of alkanes is initiated on the catalyst surface and continued mainly in the gas phase [12]. More specifically in the case of propane, the propyl radicals generated from propane on the catalyst surface (eq. 1) enter the gas phase and initiate homogeneous radical chain reactions leading to the desired products [13, 14]. Furthermore, gas phase propagation reactions are predominant at the higher temperatures, usually required to activate alkane molecules.

Although, non catalytic oxidative conversion of propane to propylene *vi*a thermal pyrolysis is feasible at higher temperatures [15, 16], Burch *et al.* demonstrated that only a combination of homogeneous and heterogeneous ODH routes, may offer the best opportunity

to obtain commercially accepted yields of propylene [17]. Varying the post catalytic volume of the reactor (in which only the homogeneous reactions are taking place) they recorded appreciable increase in conversion and yields to propylene (although the selectivity to olefins slightly decreased). Li/MgO catalysts, prepared conventionally by wet impregnation of MgO with aqueous solution of Li salts followed by drying and calcination, are generally characterized by low surface areas [14]. It was shown that for MgO (90 m^2/g), incorporation of Li is detrimental, causing substantial loss of surface area of Li/MgO (2 m^2/g) [18]. This is mainly due to (i) high temperature treatments required for lithium salt (*e.g.*, carbonate and/or nitrate) decomposition and Li^+ incorporation into the lattice structure of MgO to create $[Li^+O^-]$ active sites [19], and (ii) alkali metals facilitate sintering of oxides [18]. Thus, these catalysts with low surface areas possess low concentration of surface active sites and, hence, low catalytic activity. Moreover, this implies higher operation temperatures at which only homogeneous gas phase processes may occur (thermal pyrolysis). Moreover, chances of lithium loss by evaporation at the higher temperatures may have a marked influence on stability of the catalysts [20].

Fundamental understanding of the factors determining catalytic performance in ODH reaction i.e. (i) nature and role of the active site, and (ii) mechanistic reaction sequence, is important to tailor an improved Li/MgO catalyst.

In chapter 2 we reported that using sol-gel techniques small oxide clusters of MgO in the nanometer range could be synthesized [18]. Hattori reported [21], that nanoparticles of MgO posses a complex surface morphology due to an enhanced concentration of low coordinated Mg^{2+}_{LC} O^{2-}_{LC} pair sites. The coordination numbers are, respectively, 5 on the surface plane, 4 at the edges and steps, and 3 at the corners. They showed that Mg^{2+} ions with different coordination number could be probed by using low temperature IR spectroscopy of adsorbed carbon monoxide [22].

We have shown further that using sol-gel method, high surface area Li/MgO materials could be obtained [18]. In fact by co-gelling $Mg(OCH_3)_2$ and $LiNO_3$ in methanol/water solution, lithium ions can be incorporated in the magnesia structure at the gel stage, under milder (RT) conditions. Remarkably, the surface area after conversion of gel into oxide (calcinations at 600°C) was appreciably high even in presence of high lithium doping, which might help to, respectively, (i) enhance the number of defect sites $[Li^+O^-]$, and (ii) improve catalyst activity.

The aim of this paper is to characterize the surface chemistry of MgO and Li-promoted MgO catalysts and describe the effect of lithium incorporation in altering the concentration of the reactive step, edge and corner sites. Additionally, we aim to study the influence of catalyst surface chemistry on the reaction pathways leading to the products. We compare two set of LiMgO catalysts, prepared using, respectively, sol-gel method and the conventional wet impregnation method, and their catalytic performance in oxidative dehydrogenation/cracking of propane.

3.2. Experimental

3.2.1 Materials

Commercially available $Mg(OCH_3)_2$ solution (Aldrich, 8.7 wt.%, in methanol), methanol (Merck, GR for analysis), $LiNO_3$ (Merck >99.0%) and MgO (Merck 99.9%) were used. Water added to the solution was double de-ionized.

3.2.2 Catalysts preparation

A solution of $Mg(OCH_3)_2$ in methanol (0.4 M) containing $LiNO_3$ (in appropriate amounts to obtain 0, 1, 3 and 5 wt% Li in MgO) was mixed with water in methanol (0.8 M) at room temperature and allowed to stand for 24 h for gelation. After drying at 50°C in vacuum for 7 hours, the dried gels were calcined at 600ºC for 12h, for more details see chapter 2. These catalysts will be, hereafter, referred to as Li/MgO-sg.

Li/MgO catalysts containing varying amount of lithium (1÷5 wt%) were also prepared using $LiNO_3$ *via* wet impregnation of MgO, hereafter referred to as Li/MgO-imp, according to the method described in detail in [23]. The impregnation step was followed by drying and calcination at 700ºC for 15 h.

3.2.3 Catalysts characterization

Catalyst composition of the synthesized samples was monitored by atomic absorption spectroscopy (AAS). To investigate the catalyst phase composition X-ray diffraction patterns were recorded on a Philips PW 1830 diffractometer using Cu Kα radiation, λ= 0.1544 nm. XRD patterns were measured in reflection geometry in the 2θ range between 20° and 50°. Semi-quantitative experiments were carried out in order to quantify the amounts of different lithium phases present (i.e., Li_2CO_3) and estimate the amount of lithium incorporated into the

lattice of MgO forming solid solution. The relative intensities of the strongest lines [002] for Li_2CO_3 and [200] for MgO were plotted for a series of Li_2CO_3/MgO mechanical mixtures prepared. The line obtained was compared with the ones recorded for the catalysts prepared using sol-gel technique and wet impregnation, for more details see chapter 2 [18, 24].

Surface area has been measured with N_2 adsorption using a Micrometrics Tristar instrument. The samples were out gassed in vacuum at 200ºC for 24 h prior to the analysis. Infrared spectra of adsorbed CO molecules were recorded on self-supported wafers of the catalysts (0.1-0.2 g of powder) in 2210-2110 cm^{-1} range with a Bruker Tensor 27 FTIR with a data point resolution of 4 cm^{-1}. Measurements were performed over MgO, received from Merck, Li/MgO-imp, MgO-sg and Li/MgO-sg. The wafers were placed in a home made IR transmission cell similar to described in [25]. The cell was evacuated to 10^{-8} bar and simultaneously heated up to 350ºC (1 h, rate 2.5 ºC/min). Afterwards, the system was cooled down with liquid nitrogen to -193°C and switched to pure CO at a starting pressure of $2.8*10^{-2}$ mbar.

3.2.4 Catalytic measurements

Catalytic tests were performed in a kinetic setup employing a tubular fixed bed quartz reactor (internal diameter 4 mm) under plug flow conditions and at atmospheric pressure. Quartz rods of 3 mm diameter were inserted upstream and downstream of the catalyst bed to fill most of the free volume and to minimize gas phase reactions due to thermal activation (non catalytic) [17]. For the same purpose operation temperature was kept at 550ºC. To keep propane conversion level below 5 % the total flow rate was varied within 10 and 100 ml/min with a typical feed composition consisting of 2% CO_2, 10% C_3^o, 10% O_2 and rest He. Carbon dioxide was introduced to the feed in order to achieve a constant CO_2 concentration over the whole catalyst bed as CO_2 has a strong inhibiting effect on the reaction [26]. In addition, blank experiments were performed at 550ºC using a reactor filled with quartz wool. Under these conditions, propane conversion due to direct thermal activation of the gas phase was negligible.

A Varian 3800 GC equipped with a FID and a TCD detector was used to analyze the composition of reactants and products. It was possible to separate all the hydrocarbons on the Alumina Plot column and the rest i.e. oxygen, CO and CO_2 on the Porapak column combined with Molsieve-13X column. All reactants and products, except hydrogen, were quantified based on GC respond.

The catalysts used in catalytic reaction tests (typically 100 mg) were pressed, crushed and then sieved to 0.3-0.6 mm particles. Prior to each catalytic run, the sample was heated at 550ºC in O_2/He mixture for 1h. Comparison between catalysts prepared by wet impregnation and sol-gel method has been done under identical conditions of temperature, partial pressure and flow rate. Selectivity to the main products has been compared at the same level of propane conversion, achieved by varying the space velocity.

3.3 Results

3.3.1 Properties of catalysts tested

Chemical composition and specific surface areas for the catalysts investigated are compiled in Table 1. From XRD data (not shown here), MgO was the dominant crystalline phase in all the Li^+-doped MgO samples. Crystalline Li_2CO_3 phase was also observed especially in the case of samples containing high lithium doping. It is interesting to note, as earlier discussed in chapter 2 [14, 18], that neither $LiNO_3$ (used as lithium precursor) nor any other Li phases were observed. Moreover, based on semi quantitative XRD analysis, all the Li/MgO-sg catalysts show higher amount of lithium ions incorporated in MgO lattice in comparison with the respective Li/MgO-imp catalysts (table 1). Significantly, Li/MgO-sg catalysts show also higher surface areas (m^2/g, measured before and after catalytic test) than the respective materials prepared using wet impregnation. As shown in table 1, the specific surface area of MgO decreased while increasing the level of lithium doping.

The most drastic loss was recorded in the case of Li/MgO-imp materials which, at the same time, provide much less lithium incorporation. It should be stressed that the catalysts prepared by sol-gel method and wet impregnation have been calcined at different temperatures, respectively, 600ºC and 700ºC. Higher calcination temperature in the case of wet impregnation procedure is necessary to

Table 1.
Chemical composition and surface area of the Li/MgO catalyst prepared, respectively, using sol-gel method (sg) and wet impregnation (imp).

***Amount of lithium incorporated in MgO was estimated by XRD, for details see [18]**

Sample	Total Lithium (wt%)	Lithium incorporated (wt%)*	BET (m^2/g)
MgO-sg	0 %	0 %	60
1 wt% Li/MgO-sg	1 %	0.5 %	50
3 wt% Li/MgO-sg	3 %	0.7 %	30
5 wt% Li/MgO-sg	5 %	0.9 %	25
MgO (Merck)	0 %	0 %	30
1 wt% Li/MgO-imp	1 %	0.1 %	9.0
5 wt% Li/MgO-imp	5 %	0.5 %	4.0

decompose lithium salts and build lithium into the MgO lattice to create active centers [7, 8]. On the contrary, sol-gel method allows significant incorporation of lithium ions at lower temperatures, at the gel stage, and, therefore, the higher temperature treatment is not required [18]. Thus, sol-gel Li/MgO materials, given their high surface area and high amount of lithium incorporation, may be promising catalytic systems.

3.3.2 Surface investigation: infrared spectra of adsorbed CO molecules

The description of reactive surface sites by spectroscopy at low temperature represents a useful approach for the characterization of adsorption sites on the catalyst surface, although the conditions are much different than those present during catalytic reactions. In the case of MgO based materials, low coordinated surface sites, *i.e.*, $Mg^{2+}_{LC}O^{2-}_{LC}$ pairs, can behave as strong acid-base pairs. The weak adsorption of CO (hence the low temperatures required to observe them, at -193°C) on Lewis acid sites such as Mg^{2+}_{LC} produces IR bands at frequencies higher than the stretching frequency of the free CO molecule in the gas phase [27], and thus provides a tool for probing these surface sites.

3.3.2.1 Surface Lewis acid sites on MgO

Fig. 1 shows the IR spectra of CO adsorbed at -193°C on, respectively, MgO-sg and MgO (Merck). The main features are observed in the 2100-2200 cm^{-1} range typical for CO bond vibration. For both materials the same type of absorbance peaks are present. Based on the spectra shape (Fig.1) it is clear that more than one type of CO adsorbed specie result to be present. The adsorption at 2168-2164 and 2152-2157 cm^{-1} are associated with CO molecules adsorbed on 4 and 5 coordinated Mg^{2+} sites, respectively [27]. The band at 2145-2150 cm^{-1}, that has a frequency lower than the one of CO adsorbed on Mg^{2+}_{5C}, would suggest the presence of even less acidic Mg^{2+} ion than 5 coordinated. In particular, similar adsorption band (2148 cm^{-1}) was assigned to CO anchored *via* both the carbon and the oxygen atom to two cations at the step site [27], respectively, 5 and 4 LC Mg^{2+} sites. In this respect, Coluccia and

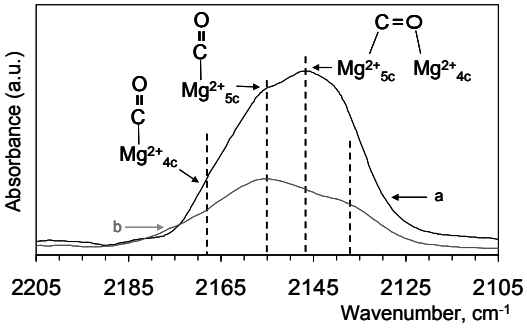

Fig. 1. IR spectra of CO adsorption at -193°C over (a) MgO-sg materials and (b) MgO (Merck).

coworkers suggested that the interaction of the oxygen atom of CO with a positive surface site lowers the stretching frequency typical for CO adsorbed at 5 coordinated Mg^{2+} sites [28]. The band at 2140-2145 cm^{-1} is not relevant due to the stretching mode of free CO molecules (2143 cm^{-1}). A qualitative comparison between the curves in Fig. 1 shows that all the bands recorded for MgO-sg have higher intensity and this can be related to the higher surface area. However, the band associated to CO anchored *via* both the carbon and oxygen atom at the step site is mainly dominating in the case of MgO-sg. This observation indicates a less regular surface of MgO-sg than the one of MgO (Merck); apparently more steps are present.

3.3.2.2 Surface Lewis acid sites on Li/MgO

Fig. 2 shows the IR spectra of CO adsorbed on Li/MgO-sg catalysts -193°C. In the case of 1 and 3 wt% Li/MgO the spectra show three bands at around 2164-2168, 2152-2155 and 2146-2148 cm^{-1}. All these components were also present in the spectra of CO adsorbed on MgO-sg (Fig.1, a) and assigned to CO, respectively, adsorbed on Mg^{2+}_{4C} and Mg^{2+}_{5C} single sites and anchored to Mg^{2+}_{4C} and Mg^{2+}_{5C} at the step site. A schematic representation of the existing Mg-O ion pairs with different coordination number is described in details in the discussion part. For the sample with the highest lithium loading (5 wt%) additional weak bands at 2200 and 2184 cm^{-1} were present. The band at 2200 cm^{-1} is attributed to CO molecule interacting with Mg^{2+}_{3C} site [27]. Based on DFT calculations, the adsorption at 2184 cm^{-1} can be attributed to the addition of a second CO molecule to the CO-Mg^{2+}_{3C} adduct, resulting in the formation of dicarbonyl species [27, 28]. In addition, changes in relative distribution of all the components present in the spectra were observed. The appearance of lower coordinated sites in presence of lithium due to decrease of particle size can be certainly excluded. As discussed earlier [18], addition of lithium causes substantial decrease in surface area and increase in particle size (Table 1). Thus, Mg^{2+}_{3C} sites must be due to the incorporation of lithium in the lattice structure of MgO. Fig. 3 shows the spectra of CO adsorption at -193°C on Li/MgO-imp catalysts. This results in spectra in which bands at 2165-2170 and 2155-2160 cm^{-1} dominate. The two main features

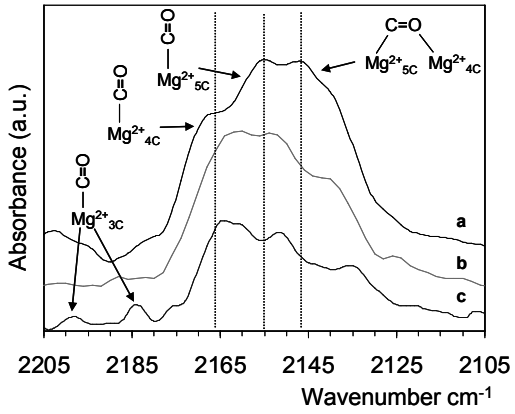

Fig. 2. IR spectra of CO adsorption at -193°C over (a) 1 wt% Li/MgO, (b) 3 wt% Li/MgO and (c) 5 wt% Li/MgO catalysts prepared using sol-gel method.

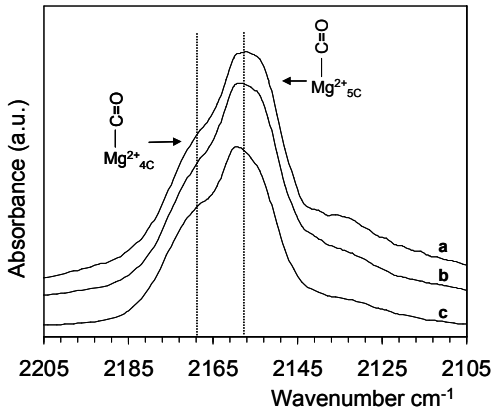

Fig. 3. IR spectra of CO adsorption at -193°C over (a) 1 wt% Li/MgO, (b) 3 wt% Li/MgO and (c) 5 wt% Li/MgO catalysts prepared using wet impregnation.

recorded at around 2168 and 2157 cm^{-1} were similarly observed in the case of MgO (Fig. 1, b) and assigned to 4 and 5 coordinated Mg^{2+} sites, respectively.

Remarkably, in contrast to Li/MgO-sg, increasing lithium doping does not change the ratios of the different low coordinated Mg^{2+} sites. Even for the highest lithium loading in Li/MgO-imp (5 wt %), the band around 2157 cm^{-1}, associated to Mg^{2+}_{5C}, is still dominant.

3.3.3 Catalytic activity for oxidative cracking of propane

We will now first discuss the results for the oxidative dehydrogenation/cracking of propane over pure MgO samples and then results for the Li-promoted MgO catalysts. Note that for all the samples tested the catalytic performance was compared under identical experimental conditions (temperature, flow rate, feed composition and total amount of catalyst forming the catalytic fixed bed reactor). Under the same conditions (550°C and GHSV= 120.000 h^{-1}) propane conversion in the empty reactor was below 1%. Thus, contribution of non catalytic activation of propane in our set of experiments can be neglected. Fig. 4 compares the rate of propane conversion for the tested MgO materials. In particular, MgO-sg showed a rate of propane conversion, expressed in $mol \cdot g^{-1} \cdot s^{-1}$, that is 4 times higher than MgO (Merck) (Fig.4, *a*). Remarkably, the conversion rate of propane was also higher when it was expressed in moles $m^{-2} \cdot s^{-1}$ (Fig. 4, *b*).

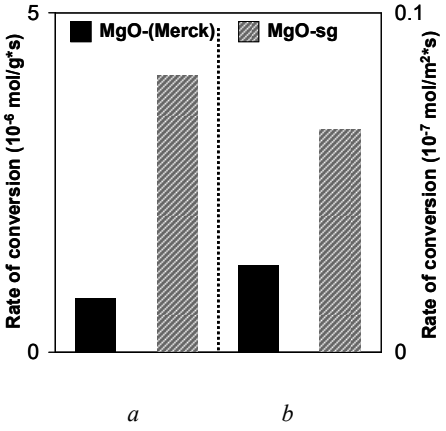

Fig. 4. Rate of propane conversion expressed as rates normalized to the catalyst weight (*a*) and specific surface area (*b*) for MgO (Merck) and MgO-sg at 550ºC. Conditions: 10% O_2, 10% Propane, 2% CO_2 and helium balance, GHSV= 120.000 h^{-1}.

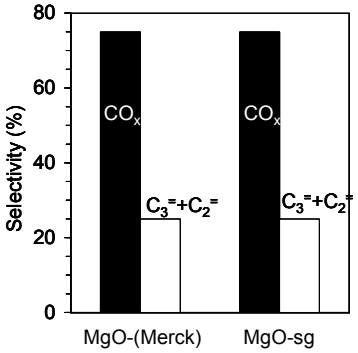

Fig. 5. Selectivity to olefins and CO_x for MgO-imp (Merck) and MgO-sg. Comparison was done at the same level of propane conversion, 5 mol%, obtained varying the space velocity (SV) at 550°C. Feed composition: 10% O_2, 10% Propane, 2% CO_2 and helium balance.

Fig. 5 represents the selectivity to all the products observed at the same level of propane conversion (5%). These do not show any difference. In both cases, CO_x is the most abundant product (80%) and olefins (20%) such as propylene and ethylene were also observed.

In principle, carbon oxides can be formed directly from propane or from propylene [29]. Since propane/propylene activation over the MgO-based catalysts may result in radical formation (propyl, ethyl, methyl) their interaction with gas phase O_2 can also result in CO_x formation. Therefore, interaction of MgO-sg with one of the products, *viz.* propylene, was also investigated. The rates of conversion of propane and propylene over MgO-sg and their selectivities to CO_x are shown in Fig. 6. Slightly lower rate of conversion has been found in the case of propylene. Obviously propylene activation resulted in higher selectivity to CO_x (90%). This agrees well with the results for low surface area MgO, as reported earlier [14]. In summary, MgO-sg is more active than MgO-(Merck), due to both higher surface area and presence of more defects. However, both materials show low olefins selectivity and mainly combustion properties. We shall now discuss the results obtained in the case of Li-promoted MgO. In Fig. 7 the rate of propane conversion expressed in $mol \cdot g^{-1} \cdot s^{-1}$ is shown for Li/MgO-sg catalysts with different lithium loading. The rate of conversion, in the case of 1 wt% Li/MgO-sg, was higher than that for MgO-sg although the latter had a higher surface area (see table 1). The incorporation of more Li^+ ions reduced the catalyst surface area even further. At the same time only a slight decrease in catalytic activity was observed.

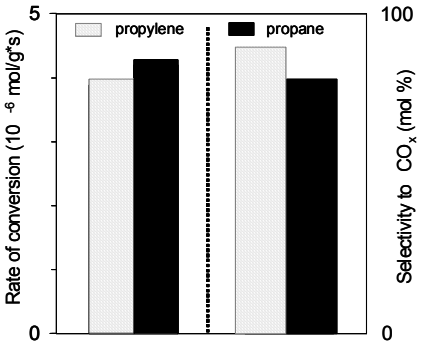

Fig. 6. Rate of conversion of propane and propylene and selectivity to CO_x for MgO-sg catalyst. Conditions: 2% CO_2, 10% oxygen, 10% propane or propylene and balance helium at T= 550ºC. Comparison at the same level of conversion (5 %) *via* varying SV.

The effect of lithium incorporation on the products selectivity is shown in Fig. 8. In particular, the propylene selectively increased by increasing lithium loading up to 3 wt% and then remained constant (50%). Ethylene selectivity (15%) appeared to be constant for all the Li-promoted MgO-sg catalysts, and it was higher than that over pure MgO-sg. Selectivity to CO_x (34%) was strongly decreased when increasing the lithium content, while the low methane selectivity remained constant (1%).

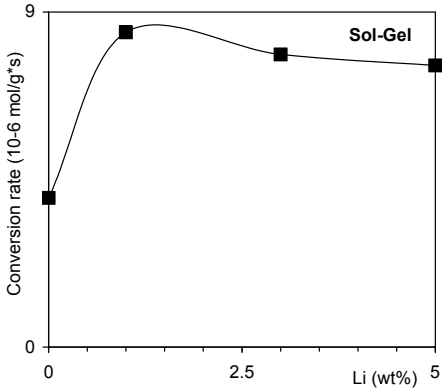

Fig. 7. Conversion rate of propane for Li/MgO catalysts prepared using sol-gel technique. Conditions: 10% propane, 10% oxygen and 2% carbon dioxide in helium; T=550ºC; GHSV=120.000 h^{-1}.

Further, a change in the reactivity of the catalyst surface of MgO due to lithium incorporation is also shown in Fig. 9, where the conversion rate of propylene is compared to the conversion rate of propane under identical conditions. It can be seen that Li/MgO-sg catalyst showed higher activity for propane than propylene. Thus, the interaction with propylene is partly suppressed because Li^+ ions incorporation in MgO makes the catalyst surface much less electrophilic. These findings are in agreement with early results reported by Leveles *et al.* in the case of Li/MgO-imp catalysts [14].

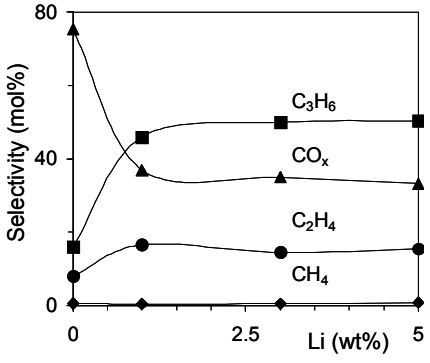

Fig.8 Selectivity towards the main products over Li/MgO-sg catalysts as function of the lithium content at 5% propane conversion obtained varying the space velocity; T=550°C.

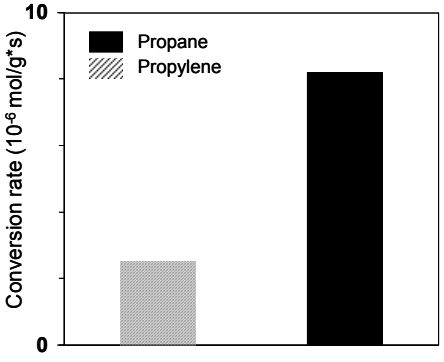

Fig.9 Rate of conversion of propane and propylene for 3 wt% Li/MgO-sg catalyst. Conditions: 2% CO_2, 10% oxygen and 10% propane/propylene in helium at 550ºC; GHSV= 120.000 h^{-1}.

3.3.3.1 Catalytic activity Li/MgO-sg vs Li/MgO-imp

Figure 10 compares the activity in oxidative cracking of propane for, respectively, 1 wt% Li/MgO-sg and 1 wt% Li/MgO-imp catalyst. Catalytic tests were performed under identical conditions of temperature, feed composition, space velocity and amount of catalyst, loaded into the reactor. It is obvious from the Figure 10 that Li/MgO-sg catalyst (having larger surface area, table 1) showed 5 times higher activity than Li/MgO-imp. The observed higher activity means higher number of active sites on the surface per gram of material, in agreement with higher surface area for Li/MgO-sg samples.

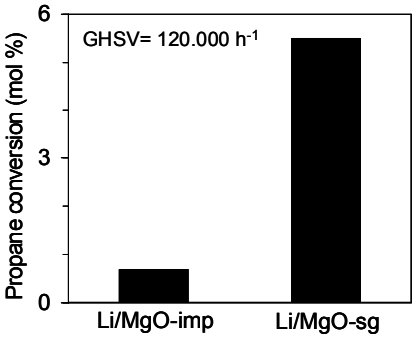

Fig. 10 Li/MgO (1 wt%) catalysts prepared using sol gel method (sg) and wet impregnation (imp) tested in ODH of propane at T=550ºC, GHSV=120.000 h^{-1}.

Selectivity to olefins as function of propane conversion is reported in Fig. 11 for both

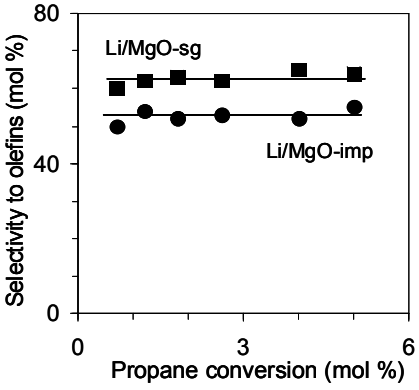

Fig.11 Selectivity to olefins function of propane conversion for 1 wt% Li/MgO catalyst prepared using sol-gel method (sg) and wet impregnation (imp), results obtained varying space velocity.

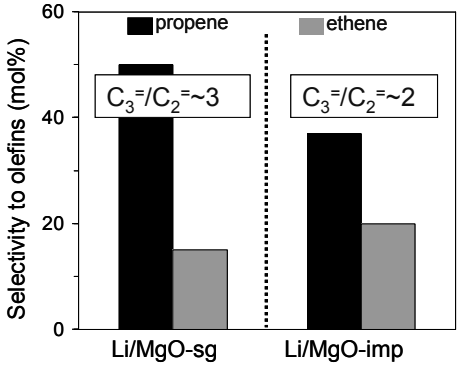

Fig.12 Selectivity to olefins ($C_3^= + C_2^=$) for 1 wt% Li/MgO catalyst prepared by sol-gel method (sg) and wet impregnation (imp) at a fixed level of propane conversion (5%) obtained varying space velocity; T=550ºC.

catalysts. Surprisingly, it can be seen that within the explored range of propane conversion, Li/MgO-sg catalyst showed better selectivity to olefins (65%) than Li/MgO-imp (55%). Further, the results in Fig. 12 show that the higher olefins selectivity observed for Li/MgO-sg catalysts is due to the relatively higher selectivity to propylene. This causes a much higher propylene/ethylene yield ratio as compared to Li/MgO-imp samples. To summarize, Li/MgO-

sg showed higher activity and selectivity to olefins and especially to propylene than catalysts prepared using wet impregnation.

3.4 Discussion

It has been earlier shown and concluded that, the oxidative conversion of propane on Li-doped magnesia proceeds through a heterogeneous-homogeneous reaction mechanism [12-14]. In these catalysts [$Li^{+}O^{-}$] type defect centers are claimed to be the active sites, which possess strong H-atom affinity and generate propyl radicals at the catalyst surface.

It is appropriate to discuss first the surface properties of MgO investigated by infrared spectroscopy and later relate the surface morphology to the catalyst performance. Although in the case of alkane activation, the nature of the active sites in pure MgO is not well defined/characterized yet, Hargreaves *et al.* [30] demonstrated (for methane activation) the importance of the MgO morphology. They suggested that the surface steps represent an active center improving the performance of an undoped MgO. Ricci *et al.* first [31] and Zecchina later [22] also confirmed this and reported that inverse sites (bottom line of stepped sites), formed by intersection of terraces, could play a role in chemisorption of hydrogen and CO. In principle, for pure MgO, characterized by "sodium chloride" type crystal structure, the stable exposed surface is the (100) containing equal quantities of magnesium and oxygen ions, both with 5 as coordination number. However, as earlier proposed and described by Coluccia and Tench [32, 33], Mg^{2+} O^{2-} pair sites of different low coordination numbers do exist on the external surface of MgO, for instance, at edges and corners.

Interestingly, Che *et al.* investigated the dissociation of water on low coordinated Mg^{2+}_{LC} O^{2-}_{LC} pair sites (LC= 5, 4 and 3) [34]. They suggested that for each surface pair site two types of OH groups are generally formed, Mg_{LC}-OH and O^{2-}_{LC}-H resulting, respectively, from the hydroxylation of Mg^{2+}_{LC} and protonation of O^{2-}_{LC} ions. Hence, hydroxyl groups formed by water activation on MgO might reduce the number of accessible low coordinated pair sites. Thus, it is appropriate to highlight here that IR studies showed, for all the samples tested (with and without lithium), the presence of a similar level of surface hydroxyl groups.

The surface sites of MgO can be titrated with CO at low temperature. Absorption bands at frequencies higher than 2143 cm^{-1} (stretching mode of the free CO molecules) are typical for CO molecules adsorbed on positively charged sites with the carbon pointing towards the Mg^{2+} cation [35]. The shift increases as the strength of the positive field increases. The positive field associated with a Mg^{2+}_{5C} site in a (100) plane, surrounded by five neighbors O^{2-}, is lower than the field of Mg^{2+}_{4C} on the edge where the charge is balanced by only four

neighboring ions. Further, this must be lower than the field of Mg^{2+}_{3C} on a corner position surrounded by only three O^{2-} anions. In the case of both MgO-sg and MgO (Merck) the recorded IR spectra are similar in band positions but differ in their intensities (Fig. 1). In the case of MgO-sg sample, all the bands possess higher intensity reflecting the higher concentration of the adsorption sites. Surface sites are similar for both MgO samples and include 5 and 4 coordinated Mg^{2+} ions (bands, respectively, at 2155 and 2164 cm^{-1}) [27]. Additionally, step sites are present (the band at 2148 cm^{-1}, as proposed by Zecchina *et al.*, corresponds to CO molecules anchored *via* both the carbon and oxygen atom to Mg^{2+} ions at the step site, see scheme 1) [36].

Remarkably, in the case of MgO-sg materials the contribution of the band at 2148 cm^{-1} is much higher suggesting the presence of a higher amount of surface step sites (scheme 1). In particular, these are mono-atomic step sites generated by two parallel planes.

Further, their presence implies a more irregular and complex surface morphology, *viz.* additional edges, see scheme 1 [37]. Therefore, the extra low coordinated sites observed, *i.e.*, four-coordinated ions, might also influence the catalytic activity [38]. Indeed, as shown in Fig. 4, the catalytic activity of undoped MgO sample is improved when prepared using sol-gel techniques. In the case of MgO-sg, the observed higher activity (4 times higher) can not be exclusively related to its specific surface area which is only 2 times larger than in the case of MgO (Merck) (table 1). Significantly, the presence of step sites in MgO seems to increase the number of active centers able to activate propane and thus the catalytic activity per square meter catalyst (Fig. 4). However, as shown in Fig. 5, both the MgO catalysts tested present the same low olefin selectivity. Thus, the additional active centers formed due to presence of step sites are unselective sites.

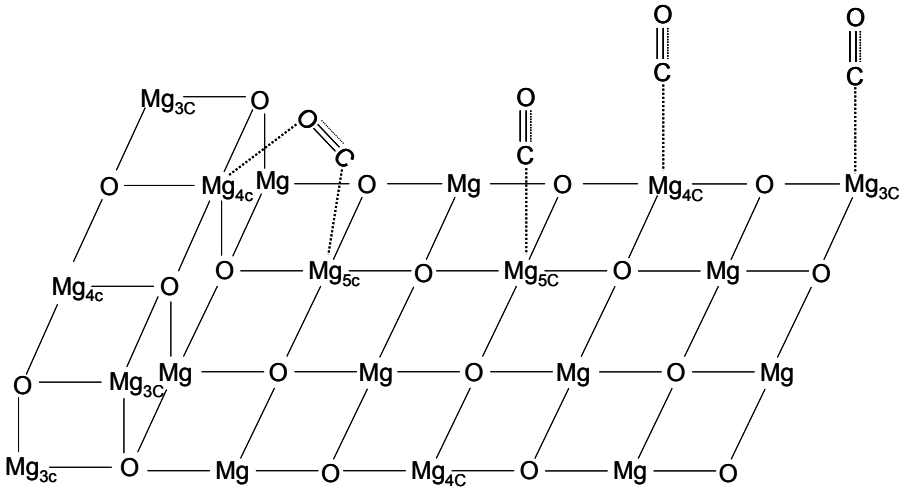

Scheme 1. CO molecule adsorbed and anchored at the surface of MgO catalyst [21].

Let us now discuss the effect of Li^+ ion incorporation in MgO. The similar ionic radii of Li^+ (r_{Li+}=0.76 Å) and Mg^{2+} (r_{Mg2+}=0.72 Å) allows easy accommodation of Li^+ in the lattice of MgO [39]. Replacement of Mg^{2+} by Li^+ creates lattice defects, *i.e.,* oxygen vacancies (positive hole) (scheme 2). Further, the proposed active site [Li^+O^-] is produced by a hole adjacent to Li^+ site trapping an oxygen atom (scheme 3) [40, 41].

$$\mathbf{Li_2O + 2Mg_{Mg}^{x} + O_O^{x} \rightarrow 2Li_{Mg}' + V_O^{\cdot\cdot} + 2Mg}$$

Scheme 2. Proposed mode of incorporation of Li^+ in MgO matrix as a substitutional ion at a cation site with compensating oxygen vacancies, the Kroger-Vink notation has been used.

$$\mathbf{2\,Li_{Mg}'\,O_O^{x} + V_O^{\cdot\cdot} + \tfrac{1}{2}O_2 \rightarrow 2\,Li_{Mg}'\,O_o^{\bullet} + O_O^{x}}$$

Scheme 3. Proposed mode of formation of [Li^+O^-] ($Li_{Mg}'\ O_o^{\bullet}$ above) active site in Li/MgO catalysts. A hole trapped at the O^{2-} is adjacent to Li^+ sites. The Kroger-Vink notation has been used [40, 41].

Infrared spectra, recorded for Li/MgO-sg samples (Fig. 2), show that, starting with 1 wt% lithium, mainly 4, 5 coordinated Mg^{2+} ions and step sites are present on the catalyst surface. In comparison to MgO-sg, the following two points have to be stressed: (i) 4 coordinated sites are definitely more prominent, and (ii) 5 coordinated Mg^{2+} ions and step sites posses the same intensity. Increasing lithium loading (*e.g.*, 3 wt% Li/MgO-sg), sites distribution is changed even more. The Mg^{2+} ions with coordination number 4 and 5 are equally detected whereas contribution of the step sites decreases. Remarkably, this effect is even more pronounced for 5 wt% Li/MgO-sg. In fact, the intensity of the signal corresponding to Mg^{2+}_{4C} site, dominates the spectrum, and, at the same time, contribution of new sites, 3 coordinated sites, is easily visible (Fig. 2).

It is generally accepted that the replacement of Mg^{2+} by Li^+ causes lattice defects, *viz.* oxygen vacancies, [42]. In fact, the presence of positive holes next to surface Mg^{2+} ions has the effect of lowering the coordination number of Mg^{2+}. Detailed studies are present in literature describing the role of low coordinated sites as trapping sites for dopant/hole centers [43]. Lewis *et al.* showed that substitutional Li^+ ions and the oxygen vacant defects are together at adjacent lattice site and both show a marked preference for the lower coordination step site [44]. Moreover, they reported that the resulting [Li^+O^-] site (scheme 3) are also stabilized on the MgO step site. In addition, Berger *et al.* also reported that, Li^+ ions, incorporated in MgO, tend to migrate and preferentially substitute the lowest coordination

Mg^{2+} cations (by definitions on the step site) to compensate for local deviations from stoichiometry [39].

In general, it is appropriate to stress here that lithium ions tend to segregate at the edges of MgO. These findings are logically connected to the results we observed with varying the amount of lithium loading from 1 to 5 wt%. In fact, our observations that higher lithium content lowers the concentration of step sites (Fig. 2) can be attributed to the decreased number of Mg^{2+} ions *via* decoration of step sites with lithium ions and oxygen vacancies (Mg^{2+} ions replacement). The possible siting of lithium ions and oxygen vacancy on the surface of Li/MgO-sg catalysts is schematically shown in scheme 4. Interestingly, the scheme 4a seems to better match the results we observed (Fig. 2). In fact, the simultaneous presence of lithium ions and oxygen vacancy at the step site can lower the concentration of step sites and increase the amount of Mg^{2+} sites with coordination number ≤ 4.

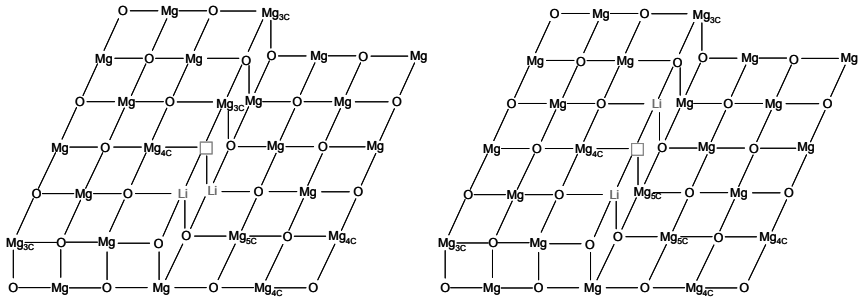

Scheme 4. Proposed configurations for lithium ions and oxygen vacancy siting at the step site on the surface of MgO.

However, the spectra of Li/MgO-imp catalysts do not show any significant changes varying the amount of incorporated Li^{+} (Fig. 3). In contrast to the results observed for Li/MgO-sg samples (Fig. 2), the band associated to 5 coordinated Mg^{2+} dominates all the spectra. Moreover, the signal related to 4 coordinated Mg^{2+} is also present but the ratio between 4 and 5 coordinated sites, even in the case of high lithium doping, was not appreciably influenced. Remarkably, in the case of Li/MgO-imp catalysts formation of sites with coordination numbers lower than 4 were not recorded. This can be explained by a lower concentration of incorporated Li^{+} ions in Li/MgO-imp samples in comparison with Li/MgO-sg (table 1). In addition, because of the higher calcination temperature, Li/MgO-imp catalysts possess lower amounts of morphological defects (*i.e.*, edges and kinks). This causes less

segregation and migration of lithium ions and oxygen vacancy to preferential surface sites associated with low coordinated numbers.

In summary, Li/MgO catalysts, prepared using sol-gel method, are characterized by an enhanced concentration of Li^+ ions incorporated in MgO. Incorporation of Li^+ in MgO not only increases the overall concentration of holes, but also promotes their segregation to surface sites. It is thus likely that the oxygen taken up by the positive holes may give rise to surface $[Li^+O^-]$ sites (active and selective catalytic centers for oxidative cracking of propane) which make Li/MgO-sg catalysts more active than Li/MgO-imp.

In order to discuss the performance of the catalyst tested it is essential to know the reaction mechanism for propane ODH; therefore we first summarize prior knowledge. Leveles *et al.* reported that for oxidative conversion of propane on Li-promoted magnesia, alkane activation *via* a C-H bond splitting is the rate determining step [14]. Propane activation takes place on the $[Li^+O^-]$ active site by homolytic hydrogen abstraction, forming $[Li^+OH^-]$ and propyl radicals (eq. 1). There is general evidence that the two different primary radicals formed after heterogeneous activation, n- and iso-propyl radicals, are released from the catalyst surface to the gas phase and radical chain reactions lead to final products [14]. For the propyl radicals formed, two different decompositions routes have been proposed in gas phase: (i) the iso-propyl radicals can undergo scission of C-H bond at the α-position and decompose into propylene and H radical, and (ii) the n-propyl preferentially follows a C-C cleavage in the ß-position forming methyl radical and ethylene (scheme 5). Thus, the cleavage of C-H bond (dehydrogenation) versus cleavage of C-C bond (cracking) is the process controlling the selectivity to, respectively, propylene and ethylene. At relative low T (<600°C), and low conversion level of propane, when contribution from thermal gas phase reactions is less, propylene to ethylene ratio higher than 1 was observed [14]. At higher temperatures (≥600°C) decrease of dehydrogenation and increase of cracking was recorded.

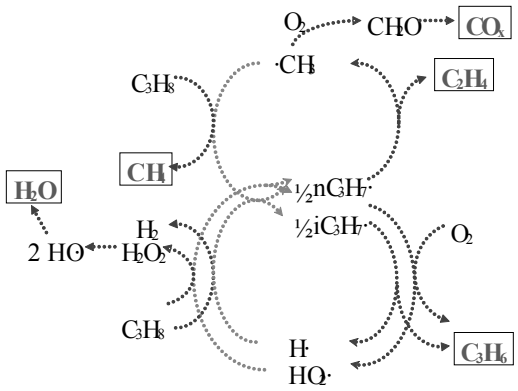

Scheme 5. Proposed reaction mechanism for gas phase propyl radicals [13].

As shown in Fig. 10 the catalytic activity of Li/MgO-sg catalyst in oxidative/cracking of propane is superior in comparison with LiMgO-imp catalysts at T=550°C. This is obviously due to the higher surface area and higher amount of incorporated Li^+ ions in MgO, which contribute to increase the number of $[Li^+O^-]$ active sites, as discussed above. Surprisingly, we also observed that Li/MgO-sg catalysts show an improved selectivity to olefins (Fig. 11) and higher propylene to ethylene ratio in comparison with Li/MgO-imp (Fig. 12). Indeed, as Kondratengo *et al.* recently reported, in the case of propane ODH over vanadium oxides systems increasing density of active sites affected olefin distribution [45]. In particular they suggested that high density of oxidizing sites is essential for further ODH of propyl radicals to propylene and therefore suppression of concurrent cracking reaction pathway to ethylene.

Similarly, in the case of Li/MgO-sg catalysts, with high density of active sites (per volume of catalytic bed), heterogeneous H-atom abstraction from $C_3H_7^{\bullet}$-radicals yielding propylene (eq. 2) can be more efficient than reaction of $C_3H_7^{\bullet}$-radicals in gas phase (scheme 5) and this can affect the propylene to ethylene ratio.

$$[Li^+O^-] + C_3H_7^{\bullet} \rightarrow [Li^+OH^-] + C_3H_6 \qquad (2)$$

Propane activation on $[Li^+O^-]$ active centers, leading to propyl radical, is a single site interaction. The chance that propyl radicals formed may further react with a second $[Li^+O^-]$ active site leading to propylene (multiple site interactions) strongly depends on their density. This seems to be the case for the oxidative dehydrogenation /cracking of propane over Li/MgO-sg catalysts. Due to the surface properties of Li/MgO-sg materials, a higher number of active sites per cm^3 of reactor volume was achieved, compared to Li/MgO-imp (same amount of catalysts in the reactor).

Thus, Li/MgO-sg catalysts possessing higher surface area and higher concentration of active sites are intrinsically more active and selective to propylene at low temperature (550ºC) due to the contribution of heterogeneous H-abstraction from propyl radicals to yield propylene (selective quenching reaction, scheme 6). This is also in an agreement with Lunsford *et al.* [46] who suggested, in the case of methane coupling, that the radicals generated by heterogeneous activation can also remain on the catalyst surface and undergo further reactions before desorption to yield products [46].

Finally, substantial changes in the surface morphology due to lithium incorporation which result in the appearance of Mg^{2+} ions with a coordination number ≤ 4 (Fig.2) do not

change products selectivities (Fig. 8). However, their presence substantially helps in creating [Li^+O^-] sites

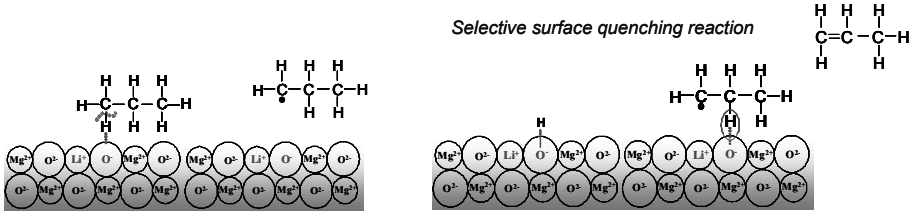

Scheme 6. Selective quenching reaction to yield propylene proposed for Li/MgO-sg catalysts.

3.5 Conclusions

Detailed study of MgO and Li-promoted MgO demonstrates the importance of the catalyst morphology and defects structure in the oxidative conversion of propane over these materials. We conclude that 4 coordinated $Mg^{2+}O^{2-}$ ions pair at step sites on the MgO surface seem to play a crucial role, increasing the number of un-selective active centers. However, Li^+ ions incorporated in MgO preferentially move to surface step sites replacing Mg^{2+} ions. Decoration of step sites with lithium ions and oxygen vacancies is observed with increasing the amounts of lithium doping. This is associated to an enhanced surface reactivity and concentration of low coordinated Mg^{2+} ions. Li/MgO-sg catalysts possessing higher concentration of incorporated Li^+ ions show enhanced olefins selectivity during the oxidative dehydrogenation/cracking of propane. The high density of active centers per unit volume of catalytic bed results to be essential for further oxidative dehydrogenation of propyl radicals to propylene and suppression of cracking reactions pathway.

References

[1] F. Cavani, N. Ballarini and A. Cericola, Catalysis Today 127 (2007) 113.

[2] J.F. Brazdil, Top. Catal. 38 (2006) 289.

[3] F. Cavani, F. Trifiro', Catalysis Today 24 (1995) 307.

[4] M.V. Landau, M.L. Kaliya, M. Herskowitz, P.F. van der Oosterkamp, P.S.G. Boque, Chemtech 26 (2) (1996) 24.

[5] M. Herskowitz, M. Landau, M. Kaliya, US Patent 6,130,183 (October 2000).

[6] S. Zender, Hydrocarbon Process. 77 (2) (1998) 59.

[7] J.X. Wang, J.H. Lunsford, J. Phys. Chem. 90 (1986) 5883.

[8] I. Balint, Ken-Ichi Aika, J. Chem. Soc. Faraday Transactions 91(12) (1995) 1805.

[9] J.H. Lunsford, Langmuir 5(1) (1989) 12.

[10] J.H. Lunsford, Adv. Catal. 35 (1987) 139.

[11] M.C. Wu, C.M. Troung, K. Coulter, D.W. Goodman, J. Vas. Sci. Technol. A 11(4) (1993) 2174.

[12] V.P. Vislovskiy, T.E. Suleimanov, M.Y. Sinev, Y.P. Tulenin, L.Y. Margolis, V. Cortes Corberan, Catalysis Today 61 (2000) 287.

[13] L. Leveles, K. Seshan, J.A. Lercher, L. Lefferts, J. Catal. 218 (2003) 296.

[14] L. Leveles, K. Seshan, J.A. Lercher, L. Lefferts, J. Catal. 218 (2003) 307.

[15] S.A.R. Mulla, O.V. Buyevskaya, M. Baerns, Appl. Catal. A 226 (2002) 73.

[16] A.A. Lemonidou, A.E. Stambouli, Appl. Catal. A 171(2) (1998) 325.

[17] R. Burch, E.M. Grabb, Appl. Catal. A 100(1) (1993) 111.

[18] C. Trionfetti, I.V. Babich, K. Seshan, L. Lefferts, Appl. Catal. A 310 (2006) 105.

[19] T. Ito, J.X. Wang, C.H. Lin, J.H. Lunsford, J. Am. Chem. Soc. 107 (1985) 5062.

[20] S.J. Korf, J.A. Roos, N.A. De Bruijn, J.G. van Ommen, J.R.H. Ross, Appl. Catal. 58 (1990) 131.

[21] H. Hattori, Appl. Catal. A 222 (2001) 247.

[22] E. Spoto, E.N. Gribov, G. Ricciardi, A. Damin, D, Scarano, S. Bordiga, C. Lamberti, A. Zecchina, Progress in Surface Science 76 (2004) 71.

[23] L. Leveles, PhD Thesis, University of Twente, The Netherlands, 2002.

[24] C. Trionfetti, I.V. Babich, K. Seshan, L. Lefferts, Top. Catal. 39(3-4) (2006) 191.

[25] M. Vaarkamp, B.L. Mojet, M.J. Kappers, J.T. Miller, D.C. Koningsberger, J. Phys. Chem. 99 (1995) 16067.

[26] D. Wang, M. Xu, C. Shi, J.H. Lunsford, Catalysis Letter 18 (1993) 323.

[27] R. Soave, G. Pacchioni, Chem. Phys. Letters 320 (2000) 345.

[28] G. Martra, T. Cacciatori, L. Marchese, J.S.J. Hargreaves, I.M. Mellor, R.W. Joyner, S. Coluccia, Catalysis Today 70 (2001) 121.

[29] C. Shi, M.P. Rosynek, J.H. Lunsford, J. Phys. Chem. 98 (1994) 8371.

[30] J.S. Hargreaves, G.J. Hutchings, R.W. Joyner, C.J. Kiely, J. Catal. 135 (1992) 576.

[31] D. Ricci, C. Di Valentin, G. Pacchioni, P.V. Sushko, A.L. Shluger, E. Giamello, J. Am. Chem. Soc. 125 (2003) 738.

[32] S. Coluccia, A.M. Deane, A.J. Tench, J. Chem. Soc. Faraday Trans. I 74 (1978) 2913.

[33] A.J. Tench, G.T. Pott, Chem. Phys. Letter 26 (1974) 590.

[34] C. Chizallet, G. Costentin, H. Lauron-Pernot, M. Che, C. Bonhomme, J. Maquet, F. Delbecq, P. Sautet, J. Phys. Chem. C 111 (2007) 18279.

[35] A. Pelmenschikov, G. Morosi, A. Gamba, S. Coluccia, G. Martra, L. G. M. Pettersson, J. Phys. Chem. B 104 (2000) 11497.

[36] S. Coluccia, M. Baricco, L. Marchese, G. Martra, A. Zecchina, Spectrochimica Acta 49 (1993) 1289.

[37] E.A. Colbourn, W.C. Mackrodt, Solid State Ionics 8 (1993) 221.

[38] M.L. Bailly, C. Chizallet, G. Costentin, J.M. Krafft, H.L. Pernot, M. Che, J. Catal. 235 (2005) 413.

[39] T. Berger, J. Schuh, M. Sterrer, O. Diwald, E. Knozinger, J. Catal. 247 (2007) 61.

[40] C.R.A. Catlow, R.A. Jackson, J.M. Thomas, J. Phys. Chem. 94 (1990) 7889.

[41] P.J. Gellings, H.J.M. Bouwmeester, Catal. Tod. 58 (2000) 1.

[42] I. Balint, Ken-Ichi Aika, Appl. Surf. Science, 173 (2001) 296.

[43] S.P. Mehandru, A.B. Anderson, J.F. Brazdil, J. Am. Chem. Soc. 110 (1998) 251.

[44] D. Lewis, R.W. Grimes, C.R.A. Catlow, J. Mol. Catal. A: Chemical 100 (1995) 103.

[45] E.V. Kondratenko, M.Y. Sinev, Appl. Catal. A 325 (2007) 353.

[46] M. Xu, T.H. Ballinger, J.H. Lunsford, J. Phys. Chem. 99 (1995) 14494.

Chapter 4

Lithium ions incorporation in MgO for oxidative dehydrogenation/cracking of propane: active site characterization and mechanism of regeneration

Abstract

In the case of Li-promoted MgO two different mechanisms for regeneration of the active site are found when varying the temperature between 550 and 700ºC. Propane titration showed that the active site is deactivated through formation of hydroxyl groups that are stable at 550ºC and below in absence of oxygen. On the contrary at 700ºC, propane titration showed that hydrocarbon activation is accompanied by evolution of water molecules. Thus, the active site is deactivated trough the removal of lattice oxygen atoms. In addition, simultaneous evolution of hydrogen molecules pulsing propane indicate that propane conversion on Li-promoted MgO catalysts follows a mixed heterogeneous-homogeneous radical chemistry. No CO_x was observed while pulsing propane at both temperatures. Moreover CO_x molecules were not detected even during catalyst regeneration by pulsing oxygen showing that Li/MgO materials are not affected by coke formation. Formation of CO_x molecules seems to be feasible exclusively by co-feeding propane and oxygen.

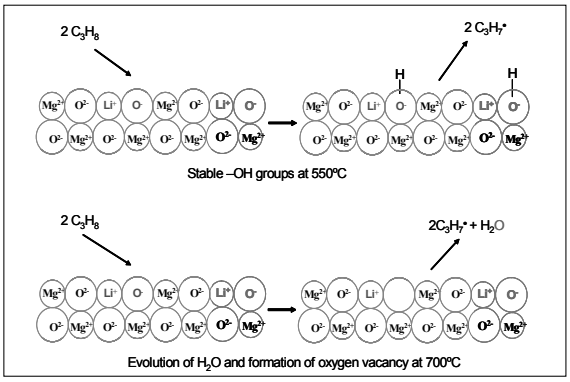

Proposed mechanism of active site deactivation for Li-promoted MgO catalysts at, respectively, 500 and 700 ºC.

*Keywords: Oxidative dehydrogenation/**cracking of propane; Li-promoted MgO; Active site regeneration; De-hydroxylation reaction.***

4.1. Introduction

Traditionally, olefins are produced by non-catalytic thermal conversion of hydrocarbons, i.e. steam cracking, which is industrially well proven but characterized by severe conditions and homogeneous phase radical chemistry that maximizes ethylene selectivity instead of propylene [1-3].

However, commercially available catalytic routes for olefins production, *viz.* catalytic dehydrogenation, also present several drawbacks because of thermodynamic equilibrium constraints and coking that restricts catalyst stability [4]. In this respect, oxidative dehydrogenation reactions (ODH) are considered as the most promising way to avoid thermodynamic limitations, minimize coking and limit the necessity of external heating during the production of olefins from light alkanes [5]. Indeed, when an oxidant, *e.g.*, molecular oxygen, is added to the feed gas the process becomes thermodynamically favorable because of water formation.

In the case of ODH of propane, mainly two types of catalytic materials are discussed which differ in the nature and properties of surface-oxygen species taking part in the hydrocarbon activation. The first type of materials, classified as redox type catalysts, is mainly based on vanadium oxides as main component [6]. For these catalysts lattice oxygen is available for the catalytic cycle and considered to be responsible for the selective and non-selective reaction pathways leading to olefins, CO_x and water [7]. The second class of materials, *i.e.*, non-redox type of catalysts, is based on MgO doped with alkali [8, 9]. For these materials lattice oxygen cannot be consumed and replenished during the catalytic cycle [10]. As reported often in the case of methane coupling, the catalytic activity of Li-promoted MgO is determined by surface $[O^-]$ species and their existence in MgO was mainly shown using the electron paramagnetic resonance (EPR) technique [11-13]. Lunsford suggested that the $[O^-]$ species was created by the substitution of Li^+ for Mg^{2+} ions to allow charge balance and stabilized on the MgO lattice as $[Li^+O^-]$ centers [14]. Remarkably, $[O^-]$ are reported to be very stable at high temperatures and can exist in the crystal lattice of metal oxides even in the absence of oxygen in the gas phase [15].

It is experimentally proved, in the case of Li/MgO catalysts, that the first step in oxidative conversion of methane involves the homolytic scission of C-H bonds forming surface -OH groups and alkyl radicals (eq. 1) [16]:

$$[O^-]_{(s)} + CH_4 \rightarrow [OH^-]_{(s)} + CH_3^{\bullet} \qquad (1)$$

The resulting radicals are released from the catalyst surface and subsequently initiate gas phase-chain propagation reactions to yield products [17].

Assuming the proposed surface initiation as a primary step, Leveles *et al.* recently suggested a reaction mechanism to describe the oxidative conversion of propane over Li/MgO catalysts. Indeed, the mechanism involves a sequence in which the $[Li^+O^-]$ active site abstracts a hydrogen from propane forming n- or iso-propyl radicals that undergo radical chain reactions in the gas phase [8, 9].

However, several uncertainties still exit concerning the way how the catalytic sequence is closed *via* the regeneration of the active site. One of the difficulties is to identify the mechanism how the hydrogen is removed from the surface $[OH^-]$ group. Ito and Lunsford suggested regeneration of surface hydroxyl groups to occur *via* de-hydroxylation reaction and hence removal of lattice oxygen that leaves an anion vacancy (eq. 2) [18, 19]:

$$2[OH^-]_{(s)} \rightarrow [O^{2-}]_{(s)} + [V_a] + H_2O \qquad (2)$$

Oxygen removal implies redox changes in the material, however, if this is the case for Li/MgO material is not established. In fact, water formation during ODH experiment is generally not easily detected and quantified even when using on-line gas chromatography. This becomes even more difficult when the catalysts are prepared using high temperature treatments ($T \geq 700°C$) and thus possess low surface areas that result in low concentration of surface $[Li^+O^-]$ centers and hence low catalytic activity.

In chapter 3 we compared the surface properties and catalytic performance of Li/MgO catalysts prepared using wet impregnation procedures (imp) and sol-gel technique (sg) resulting, respectively, in low and high surface area materials [20]. We reported, based on spectroscopic studies, that Li/MgO-sg catalysts show an enhanced concentration of incorporated Li^+ ions. Interestingly, these tend to be localized in the MgO surface that also presents an enhanced concentration of defects which might also affect catalytic activity. In agreement with this observation/hypothesis, Li/MgO-sg catalysts showed higher catalytic activity for the oxidative propane conversion.

The aim of this paper is to quantify the number of active centers responsible for the catalytic activation of propane in Li-promoted MgO catalysts, prepared using wet impregnation and sol-gel technique. This might help to describe, respectively, (i) the role of Li^+ incorporation in MgO in creating the active sites, and (ii) the properties of surface $[O^-]$ species stabilized as $[Li^+O^-]$ centers. In particular, we will attempt to investigate this by

following possible reduction and re-oxidation processes. In the end we aim to establish the elementary reaction steps taking place on the catalyst surface during the active sites regeneration.

4.2 Experimental

4.2.1 Materials

Commercially available $Mg(OCH_3)_2$ solution (Aldrich, 8.7 wt.%, in methanol), methanol (Merck, GR for analysis), $LiNO_3$ (Merck, > 99.0%) and MgO (Merck 99.9%) were used. Water added to the solution was double de-ionized.

4.2.2 Catalyst preparation

A solution of $Mg(OCH_3)_2$ in methanol (0.4 M) containing $LiNO_3$ (in appropriate amounts to obtain 1, 3 and 5 wt.% Li in MgO) was mixed with water in methanol (0.8 M) at room temperature and allowed to stand for 24 h for gelation (wet gels). After drying at 50ºC in vacuum for 7 h the dried gels were calcined at 600ºC and 700 in air according to the method described in chapter 2 [21]. These catalysts will be, hereafter, referred to as Li/MgO-sg. In addition, Li/MgO catalysts containing varying amounts of Li (1 and 5 wt%) were also prepared using $LiNO_3$ *via* wet impregnation of MgO, hereafter referred to as Li/MgO-imp, according to the method described in detail in [9]. The impregnation step was followed by drying and calcination at 700ºC.

4.2.3 Catalyst characterization

Catalyst composition and the total concentration of impurities in the samples were measured by chemical analysis (AAS) and XRF (Philips PW1480). In addition to MgO the following were detected (maximum amount wt% shown in parentheses): Cs_2O (0.0002), SiO_2 (0.1), BaO (0.002), CaO (0.03), K_2O (0.002) and S (0.04).

Presence of different lithium phases as well as the amount of lithium incorporated in MgO was valuated by X-ray diffraction, see chapter 2 [21, 22]. Patterns were recorded with a Philips PW 1830 diffractometer using Cu Kα radiation, λ= 0.1544 nm. Catalysts compositions and the amount of incorporated lithium in MgO are presented in Table 1. Surface area was measured with N_2 adsorption measurements and experiments were carried out using a

Micrometrics Tristar instrument. The samples were out gassed in vacuum at 200ºC for 24 h prior the analysis.

4.2.4 Pulse experiments

Reduction-oxidation cycles were carried out in a quartz reactor (internal diameter 4 mm) under plug flow conditions at atmospheric pressure. The catalyst bed was packed between two quartz-wool plugs. Approximatively 100 mg of catalyst was used. In all experiments the catalyst was activated in 10% O_2 in He for 1 h at temperatures 50°C higher than that desired for the experiments (550 and 700°C). The reduction was performed by treating the catalysts in 10% H_2 in He at 550°C for 1 h. After purging the sample in He for 30 minutes, pulses of 2% O_2 in He flow as carrier (loop volume 500 µl) were sent through the catalytic bed. The outlet of the reactor was directly connected to a gas chromatography (GC). The pulses were sent *via* a Porapak column to a thermal conductivity detector (TCD) to observe and quantify the consumption of oxygen.

Propane and hydrogen titration tests were also carried out in a kinetic setup employing a quartz fixed bed reactor. Quartz beads were inserted upstream and downstream of the catalyst bed to minimize the empty volume. After activation (10% O_2 in He) the system was purged in He flow (total flow rate 3 ml/min) until a constant level of oxygen (zero level) was recorded. Each pulse (loop size 300 µl) containing only one reactant, *i.e.*, propane, hydrogen and oxygen diluted in He (95%) was sent separately to the catalyst bed. The feed and the effluent compositions were monitored by sampling on-line to a quadruple mass spectrometer (Pfeiffer AG Balzers, OmniStar) equipped with Channeltron and Faraday detectors (2-200 amu).

4.2.5 Carbon dioxide sorption experiments

Sorption measurements were used to investigate the interaction of CO_2 on the surface of pure MgO and Li-promoted MgO catalysts. Experiments were carried out with a Mettler-Toledo TGA-SDTA apparatus at temperatures between 100 and 700°C. Typically 40 to 80 mg of sample was used in a 70 µl alumina crucible. A gas flow of 50 ml/min with a composition of 10% CO_2 in Argon was used. Prior the experiments the samples were pretreated at 700ºC in Argon until a constant weight was measured.

4.3 Results

4.3.1 Properties of the catalysts tested

Table 1 shows the list of all the catalysts tested. The catalyst surface area and the relative amount of incorporated Li in MgO (estimated by XRD) are also shown. Li/MgO-sg catalysts possess, respectively, higher surface areas and amounts of lithium built into MgO lattice than Li/MgO-imp catalysts (Table 1). In fact, as we reported in our earlier contributions about catalyst preparation [21], during the sol-gel method lithium ions can be incorporated in the magnesia gel structure and high temperatures treatments are not required.

Table 1. Chemical composition and surface area of the Li/MgO catalyst prepared, respectively, using sol-gel method (sg) and wet impregnation (imp).

*Amount of lithium incorporated in MgO was estimated by XRD, for details see [22]

Sample	Total Lithium (wt%)	Lithium incorporated (wt%)*	BET (m^2/g)
MgO-sg	0 %	0 %	60
1 wt% Li/MgO-sg	1 %	0.5 %	50
3 wt% Li/MgO-sg	3 %	0.7 %	30
5 wt% Li/MgO-sg	5 %	0.9 %	25
MgO (Merck)	0 %	0 %	30
1 wt% Li/MgO-imp	1 %	0.1 %	9.0
5 wt% Li/MgO-imp	5 %	0.5 %	4.0

4.3.2 Li/MgO active sites titration: reduction/oxidation cycles and CO_2 sorption

In previous papers, Leveles *et al.* proposed that the formation of $[Li^+CO_3^-]$ species by CO_2 interaction with the $[Li^+O^-]$ active site can be observed and quantified [9]. This would make CO_2 a suitable probe molecule in order to titrate and quantify the number of catalytically active $[O^-]$ species. Thus, the interaction of CO_2 molecules with the Li/MgO catalysts was studied using TGA. Figure 1 shows a typical experimental result during the sorption/desorption cycles of CO_2 at temperatures between 100 and 700°C over 1 wt% Li/MgO-sg catalysts. The experiments were carried out under conditions where the desorbed

CO_2 molecules from $[Li^+CO_3^-]$ surface specie may be differentiated from those attributed to the decomposition of Li_2CO_3. Switching on CO_2 containing inert gas (Ar) to the sample in TGA results in a weight increase for all the tested temperatures (Fig. 1 left-hand). Adsorption of CO_2 reached steady state after 20 minutes at 700°C. Switching off CO_2 from the gas stream did not cause any changing in weight at low temperature *i.e.*, 100ºC while at temperature higher than 500°C it resulted in a weight decrease of the sample due to CO_2 partially desorbed (Fig.1 right-hand). In particular, at temperature of 700ºC, CO_2 desorption did not reach steady state during the measurements. On the contrary, desorption at 550°C quickly reached the equilibrium already after 10 minutes. The adsorption/desorption cycles were performed at 550°C in TGA for all the catalysts prepared using sol-gel method and wet impregnation (samples containing varying amounts of lithium) and the results are reported in Table 2. The first column shows the number of moles of CO_2 desorbed at 550°C expressed per m^2 of catalyst. Appreciably, for both Li/MgO-sg and Li/MgO-imp catalysts the concentration of CO_2 desorbed increased with increasing lithium content. Interestingly, we observed that the amounts of CO_2 desorbed per m^2 of catalyst for Li/MgO-sg samples were in the same range as obtained for Li/MgO-imp catalysts (table 2). We can conclude from this that the surface area of Li/MgO catalysts can be tuned without altering nature and properties of the materials (see table 1 and 2).

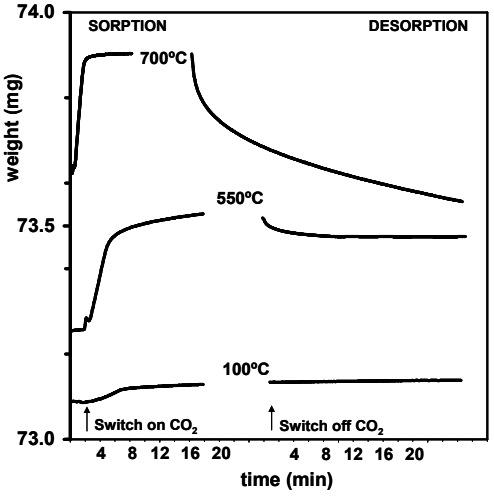

Fig. 1. Sorption and desorption curves measured in TGA on 1 wt% Li/MgO sol-gel catalyst. Conditions: 10% CO_2 in Ar; total flow 50 ml/min.

The second method to quantify the number of surface $[Li^+O^-]$ active sites consists of measuring the amount of oxygen consumed while pulsing O_2 containing stream over catalysts (pretreated in hydrogen at T=550°C followed by purging with He). The typical result of this experiment is presented in Fig. 2 for 1 wt% Li/MgO-sg catalyst. The oxygen TCD signal shows that the catalyst treated in hydrogen consumed all the oxygen molecules from the first pulse and nearly half of the second pulse (~10^{-6} moles of oxygen atoms). An investigation of the reaction taking place during reduction and oxidation processes over Li/MgO catalysts will

be shown in the next paragraph and discussed afterwards. Quantitative data (using TCD) for oxygen consumption during pulsing at 550°C for all the catalysts prepared using sol-gel method and wet impregnation are shown in Table 2.

Table 2.
Results of oxygen titration obtained from reduction/oxidation cycles (column 2-4) for MgO and Li/MgO catalysts prepared using sol-gel method (sg) and wet impregnation (imp). The amount of CO_2 desorbed per m^2 of catalyst at 550°C (column 1) is also shown.

Sample	Moles of CO_2 desorbed per m^2 of cat. ($*10^{-7}$)	Amount of O_T as % of total available oxygen	Amount of O_T as % of surface available oxygen	Moles of O_T per m^2 of cat. (10-7)
MgO-sg	0.08	0.01	0.3	0.4
1 wt% Li/MgO-sg	2.7	0.04	1.5	2.1
3 wt% Li/MgO-sg	4.9	0.04	2.7	3.5
5 wt% Li/MgO-sg	7.5	0.06	4.5	5.9
MgO (Merck)	0.003	0.005	0.3	0.4
1 wt% Li/MgO-imp	2.0	0.008	1.6	2.0
5 wt% Li/MgO-imp	6.9	0.011	4.6	6.0

The column 2 in table 2 shows the amount of titrated oxygen atoms (O_T) expressed as percentage of the total number of oxygen present in the sample. Furthermore, in column 3 and 4 the amount of O_T is calculated as, respectively, (i) percentage of total surface oxygen atoms and (ii) moles of oxygen atoms per m^2 of catalyst. These two were calculated taking in consideration the surface area of each catalyst and assuming the face (001) of MgO as the only one exposed (surface oxygen density of 12.5 oxygen atoms/$Å^2$).

In summary, Table 2 shows that for both Li/MgO-sg and Li/MgO-imp catalysts the number of titrated surface oxygen species increased with increasing lithium content (column 2). Moreover, the number of moles of titrated oxygen atoms normalized per m^2 of catalysts is the same (column 4). The results from adsorption/desorption of CO_2 and reduction/oxidation cycles show a good correlation (column 1 and 4). However, an appreciable difference was observed only in the case of MgO. In this case, the number of moles of $[O^-]$ specie (normalized per m^2) estimated using CO_2 sorption is much lower than the one calculated from the re-oxidation experiments.

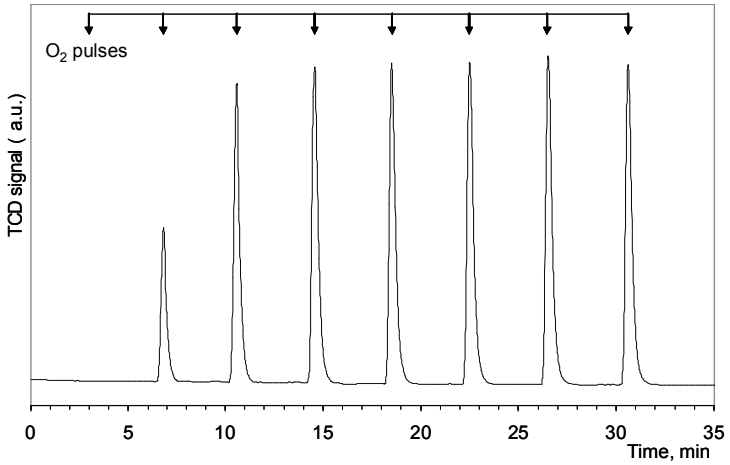

Fig. 2. TCD signal during oxygen pulsing of pretreated 1 wt% Li/MgO catalyst prepared using sol-gel method. Pretreatment: 10% hydrogen, 1h at 550°C. Carrier (He) flow: 30 ml/min.

4.3.3 Regeneration of the active site: hydrogen and propane pulses at 550°C.

A typical experimental result during subsequent pulsing of H_2 and O_2 over 5 wt% Li/MgO-sg catalyst at 550°C is presented in Figure 3. Prior to the experiments all the catalysts were treated in 10% oxygen in He at 600°C for 1h and then purged in He flow for 30 minutes to remove any oxygen molecules physisorbed on the surface. Results in Figure 3 show that hydrogen pulses resulted in partial consumption of hydrogen without formation of any product water. Moreover, after two pulses (out of five) no appreciable consumption of hydrogen was recorded (surface deactivation). After purging in He for a few minutes (to remove adsorbed hydrogen) subsequent O_2 pulses were sent through the catalytic bed. Consumption of oxygen and formation of H_2O were simultaneously observed (surface regeneration, Fig. 3). Catalyst re-oxidation seemed to be facile since most of hydrogen was removed after the first O_2 pulse.

Second set of H_2 and O_2 pulses produced the same results, Respectively, H_2 consumption without H_2O production and simultaneous O_2 consumption and H_2O production. The mechanism of this re-oxidation will be discussed later in the manuscript.

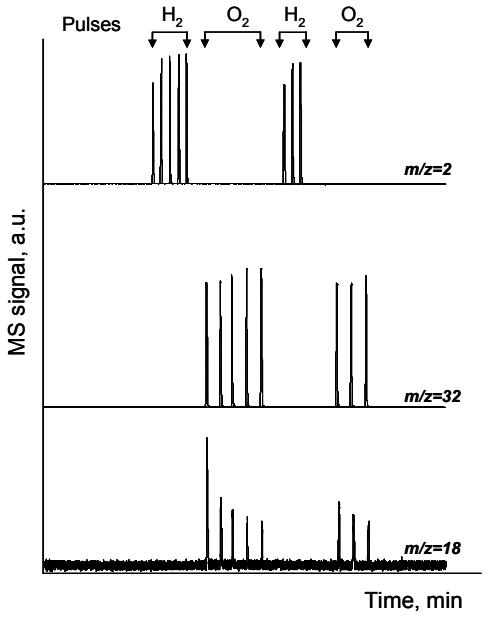

Fig. 3. MS signal intensity during hydrogen and oxygen pulsing at 550ºC of pretreated Li/MgO sol-gel catalyst; pretreatment in 10% oxygen in He, 1h at 600ºC and then purged 30 min in pure He.

We shall now discuss the results obtained in the case of subsequent pulses of propane and oxygen. In Figure 4 a typical experimental result over 5 wt% Li/MgO-sg catalyst is shown. During propane pulses consumption of propane was observed which can be attributed to the activation of propane on the catalyst surface. In addition, formation of hydrogen was simultaneously detected (Fig.4). In particular, the MS signal intensity of H_2 quickly drops down after the first propane pulse (fast surface deactivation). Interestingly, this contribution can be attributed to reactions taking place in the gas phase and discussed later. After purging the sample in He pulses of O_2 were sent through the catalytic bed. As it was previously observed (Fig. 3), simultaneous oxygen consumption and formation of water was recorded (Fig. 4). Remarkably, formation of CO_x was not detected during pulsing C_3^0 and even during pulsing of O_2 (results not shown here). Thus, the catalysts do not seem to suffer from coke formation. To summarize, all the observations here reported suggest that formation of water in the catalytic cycle occurs exclusively with gas phase oxygen.

4.3.4 Regeneration of the active site: hydrogen and propane pulses at 700°C.

Experimental results during subsequent pulses of H_2 and O_2 at 700ºC over 5 wt% Li/MgO-sg catalyst are shown in Figure 5. In contrast to the results showed in Figure 3 during repetitive H_2 pulses, consumption of hydrogen was accompanied by the evolution of molecules of water (Fig. 5). Remarkably, formation of water involves necessarily the partial removal of oxygen atoms from the lattice of Li/MgO catalysts and additionally formation of oxygen vacancies (eq. 2). Surprisingly, at 700°C Li/MgO catalysts show appreciable hydrogen consumption. After purging the samples in He, consecutive oxygen pulses were

performed and showed exclusively consumption of oxygen. In fact, not even a trace of water formation was detected (Fig. 5).

The results of subsequent pulses of propane and oxygen at 700°C over 5 wt% Li/MgO sol-gel catalyst are presented in Figure 6. In particular, during pulses of propane, (i) consumption of propane, (ii) evolution of hydrogen, and (iii) formation of water molecules were simultaneously observed (Fig.6).

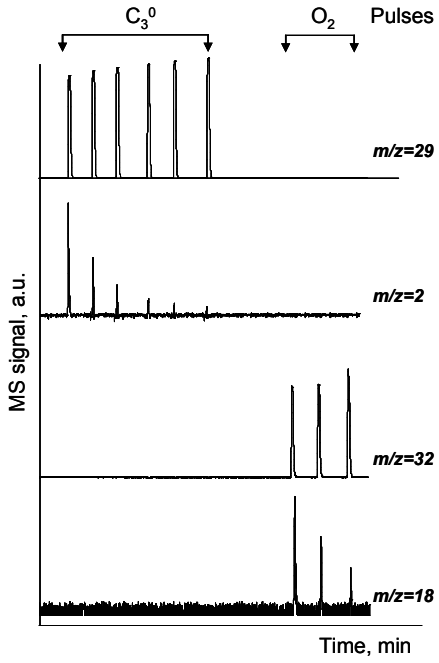

Figure 4. MS signal intensity during propane and oxygen pulsing at 550ºC of pretreated Li/MgO sol-gel catalyst; pretreatment in 10% oxygen in He, 1 h at 550ºC and then purged 30 min in pure He.

Remarkably, in contrast to the results obtained at 550°C (Fig. 4) formation of H_2O showed the removal of oxygen atoms from the catalyst lattice structure during pulses of propane (eq. 2). Surprisingly, formation of CO and CO_2 molecules was not recorded. In the case of CO, a quantitative detection was less spectacular at 700°C and CO traces can not be excluded completely. This is due to the large presence of products having fragmentation pattern similar to carbon monoxide, m/z=28 (*i.e.*, propylene and ethylene) [23]. As expected, pulses of oxygen showed clearly consumption of oxygen but no traces of water formation (Fig.6). Moreover, CO and CO_2 were also not detected suggesting again that the catalyst is not affected by coke formation.

4.4 Discussion

It is a general knowledge that the conversion of light alkanes (C_1-C_4 range) on Li-promoted MgO proceeds *via* a heterogeneous-homogeneous mechanism, in which alkyl radicals are generated on the catalyst surface and released to the gas phase [24, 25]. In the case of oxidative conversion of propane, Leveles *et al.* [9] demonstrated the crucial role of lithium in creating an active catalytic site. Moreover, Ito *et al.* showed that Li^+ ions occupying Mg^{2+} sites can stabilize the nearby [O^-] species resulting in [Li^+O^-] defects sites [18]. Thus,

propyl radicals can be formed *via* homolytic hydrogen abstraction on [Li^+O^-] centers to form surface hydroxyl groups [OH^-]. Subsequently, these sites may be regenerated with the help of gas phase oxygen molecules [26].

We shall first discuss our attempts to quantify the number of surface [Li^+O^-] active sites. Furthermore, the mechanism of regeneration of the active site will be clarified. Presence of [O^-] ions on several metal oxides has been proposed and based only on electron magnetic resonance technique (ESR). In this respect, the only reactions studied on the surface of such metal oxide systems are those in which stable paramagnetic radicals are formed. Examples of these reactions are [27, 28]:

$$O^- + O_2 \rightarrow O_3^- \quad (3)$$

$$O^- + CO_2 \rightarrow CO_3^- \quad (4)$$

In addition, CO_2 molecule adsorbed on [Li^+O^-] was detected by *in-situ* IR spectroscopy and it was concluded that [$Li^+CO_3^-$] species is the precursor for Li_2CO_3 formation [29]. Thus, CO_2 can poison, reversibly, the active sites. But at the same time CO_2 also stabilizes the catalyst against deactivation in oxidative coupling at relatively high temperature [30] by forming carbonates species, preventing the formation of volatile Li(OH) compounds [31]. Based on previous studies from Leveles and coworkers [9] the number of [Li^+O^-] active sites can be quantified using CO_2 as probe molecule and involving its reversible adsorption/desorption reaction on the [Li^+O^-] sites. In particular, the following assumptions were made: (i) CO_2 molecules are reversibly adsorbed on the Li/MgO surface exclusively forming [$Li^+CO_3^-$], and (ii) the number of moles of desorbed CO_2 molecules is equal to the number of moles of active [O^-] species. Fig. 1 shows two distinct modes of CO_2 adsorption. At relative low temperature *i.e.*, 100°C the adsorption is irreversible. The adsorbed CO_2 molecules give rise to the formation of $MgCO_3$ and Li_2CO_3 and switching off CO_2 from the stream does not result in any desorption of carbon dioxide.

On the contrary, at T≥550°C the adsorption is, at least partly, reversible. In particular, at the temperature of 550°C a fast but incomplete CO_2 desorption is recorded (Fig. 1). It is here appropriate to stress that 550°C is higher than the temperature of $MgCO_3$ decomposition (450°C) [32] and lower than Li_2CO_3 decomposition (700°C) [32]. Therefore, at T=550°C MgO would not show any sorption of CO_2 and this contribution can be ruled out (see Table 2). Thus, the desorption phenomena at 550°C can be associated to the release of CO_2 from unstable [$Li^+CO_3^-$] $^-$species (eq. 5)

$$[Li^{+}O^{-}] + CO_2 \Leftrightarrow [Li^{+}CO_3^{-}] \quad (5)$$

Non-removed CO_2 should be related to formation of Li_2CO_3 which is stable at this temperature. Moreover, complete desorption of CO_2 is recorded at temperatures above 700°C due to the contribution of Li_2CO_3 decomposition (Fig. 1). In summary, considering the number of moles of CO_2 desorbed at 550°C equal to the number of moles of surface $[O^-]$ species we found that the concentration of $[Li^+O^-]$ active sites increases with increasing lithium content, Table 2 (for both Li/MgO-sg and Li/MgO-imp samples).

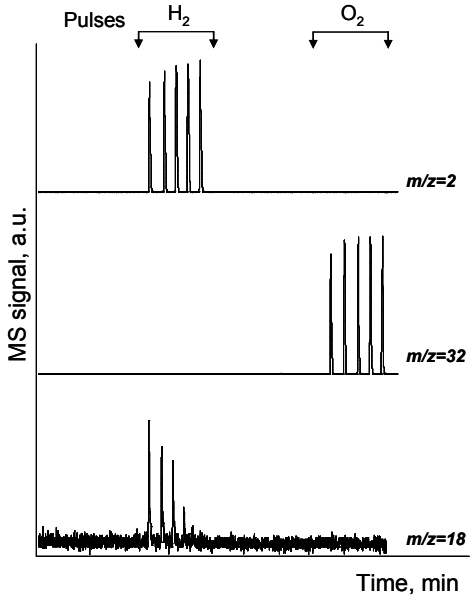

Figure 5. MS signal intensity during hydrogen and oxygen pulsing at 700ºC of pretreated Li/MgO sol-gel catalyst; pretreatment in 10% oxygen in He, 1 h at 700ºC and then purged 30 min in pure He.

Let us now discuss the results obtained from treating the catalyst in hydrogen and then pulsing oxygen through the catalytic bed. Interestingly, Leveles *et al.* observed that at 600°C the samples pretreated in hydrogen markedly lose their reactivity in propane oxidative dehydrogenation [9]. This fact can be explained by deactivation of surface active sites which are involved in oxidation of propane. Interestingly, they proposed that the catalytic activity of Li/MgO catalysts can be attributed to removable lattice oxygen. Thus, they suggested that active $[O^-]$ species possess peculiar properties and these can be removed during hydrogen treatment at high temperatures and replenished exclusively upon oxygen treatment [9]. However, this would imply the formation/evolution of species containing oxygen i.e., H_20 during hydrogen treatment but no direct observation of that was reported [9]. Similarly, the results presented in Fig. 2 show appreciable consumption of oxygen during oxygen pulses preformed at 550°C over samples pretreated in hydrogen. At this stage, we attribute the estimated oxygen consumption to the removal of hydrogen adsorbed on the catalyst surface. In particular, we calculated the number of $[Li^+O^-]$ active sites assuming that, respectively, (i) adsorbed H_2 molecules can be split homolitically on surface active $[O^-]$ species forming hydroxyl groups (eq. 6) and (ii) each $[O^-]$ specie belongs to the $[Li^+O^-]$ active site.

$$H_2 + 2O^- \rightarrow 2[OH^-] \quad (6)$$

Interestingly, for both Li/MgO-sg and Li/MgO-imp catalysts oxygen consumption increases with increasing lithium content (Table 2) reflecting the increased number of active sites. Interestingly, the concentration of active sites estimated from desorbed CO_2 and oxygen consumption is in the same range (Table 2). To summarize, in the explored range of lithium doping, Li/MgO-sg samples having higher surface area than Li/MgO-imp materials posses the same number of active sites per m^2 of catalyst (Table 2).

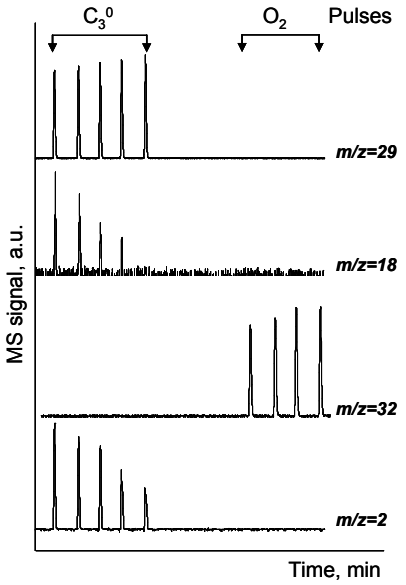

Figure 6. MS signal intensity during propane and oxygen pulsing at 700ºC of pretreated Li/MgO sol-gel catalyst; pretreatment in 10% oxygen in He, 1 h at 700ºC and then purged 30 min in pure He.

It is now appropriate to discuss the mechanism of active site regeneration for Li/MgO catalysts. To our knowledge, the only complete mechanism for the oxidative conversion of alkane (i.e., CH_4) over Li-promoted MgO, including activation and regeneration of the active site, was proposed by Ito and Lunsford [18, 19]. For the present case, as discussed above, let us speculate that the oxidative dehydrogenation/cracking of propane proceeds along the same mechanism. Similar to eq. 1 the first step includes hydrogen abstraction by $[Li^+O^-]$ defects with formation of two surface $[OH^-]$ groups:

$$2[Li^+O^-] + 2C_3H_8 \rightarrow 2[Li^+OH^-] + 2C_3H_7^{\cdot} \quad (7)$$

The formed propyl radicals are released to the gas phase where they undergo radical chain reactions. The second step, according to eq. 2, involves dissociation of one surface $[OH^-]$ group into a lattice O^{2-} ion and a mobile surface proton. This proton migrates to another $[OH^-]$ group to form a water molecule which desorbs from the surface leaving behind an anion vacancy (V_a):

$$2[Li^+OH^-] \rightarrow [Li^+O^{2-}] + [Li^+V_a] + H_2O \quad (8)$$

The final step [18, 19] is the regeneration of the active site, which involves electron transfer to the anion vacancy and the dissociative chemisorption of oxygen, respectively, eq. 9 and 10:

$$[Li^{+}O^{2-}] + [Li^{+}V_a] \rightarrow [Li^{+}O^{-}] + [Li^{+}V_a^{-}] \quad (9)$$

$$[Li^{+}V_a^{-}] + O_2 \rightarrow [Li^{+}O^{-}] + O \quad (10)$$

However, certain features in the Ito-Lunsford mechanism appear to be unlikely especially at lower temperatures. In particular, removal of oxygen from the lattice is not facile and this would be the rate-limiting step of the complete catalytic cycle (instead of hydrogen abstraction) [18]. Moreover, migration of a proton, as in reaction 8 would require, respectively, (i) substantial energy to overcome electrostatic barrier [33], and (ii) the proximity of $[Li^{+}O^{-}]$ centers [34].

Alternatively, Sinev [35, 36] proposed a new mechanism of regeneration of the active sites that does not require the removal of lattice oxygen and thus the formation of oxygen vacancies. In fact, the re-oxidation of the catalyst can proceed by the mechanism of oxidative dehydrogenation of surface OH groups and require the scission of strong O-H bonds. More specifically, regeneration reactions proposed by Sinev are summarized here [37]:

$$O_2 + [OH^{-}] \rightarrow [O^{-}] + HO_2^{\bullet} \quad (11)$$

$$HO_2^{\bullet} + [OH^{-}] \rightarrow [O^{-}] + H_2O_2 \quad (12)$$

$$H_2O_2 \rightarrow 2^{\bullet}OH \quad (13)$$

$$^{\bullet}OH + [OH^{-}] \rightarrow [O^{-}] + H_2O \quad (14)$$

It is appropriate to stress that the overall equation of regeneration is the same as in the mechanism proposed by Ito and Lunsford [18]. In fact, it involves the participation of two surface $[OH^{-}]$ groups and the formation of water molecules. However, it does not require removal of lattice oxygen. As we mentioned above, for both Li/MgO-sg and Li/MgO-imp catalysts during pulses of propane and hydrogen at 550°C initial conversion of reactants and catalyst deactivation was observed (Fig. 3 and 4). Additionally, the deactivation was not accompanied by water formation. This implies surface deactivation without any lattice oxygen removal and, most likely, formation of oxygen vacancies as intermediate stage does not take place. To conclude, under these conditions surface $[OH^{-}]$ groups are formed and result to be stable in absence of gas phase oxygen. Thus, Li/MgO catalysts do not show any reducibility at 550°C.

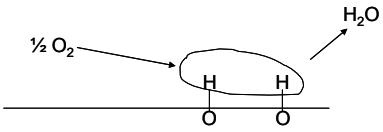

Scheme 1. Schematic drawing: mechanism of regeneration of the active sites as suggested by Sinev [35].

Remarkably, only during the interaction of oxygen with the catalysts pretreated in propane or hydrogen the evolution of water was observed. This may suggest, as proposed by Sinev, that at 550°C the re-oxidation of Li/MgO catalysts proceeds as some sort of oxidative dehydrogenation of surface hydroxyl groups (Scheme 1 and eq. 11-14). Our observations suggest that only at higher temperatures (700°C) and relevant to methane coupling discussed by Lunsford, the catalyst regeneration goes *via* the traditional scheme of re-oxidation, according to Ito and Lunsford mechanism that implies a de-hydroxylation step involving the formation of oxygen vacancies.

Finally we would like to discuss the formation of hydrogen observed during pulses of propane. Typically, homolytic C-H bond splitting forming propyl radicals is the rate determining step [38]. For the propyl radicals formed, mainly two different decompositions routes have been proposed in gas phase in absence of oxygen. In general, there is a slight preference for, (i) C-H bond scission at the α-position to yield propylene and H radical and (ii) C-C cleavage in the ß-position forming methyl radical and ethylene [8]. However, a series of gas phase reactions involving propyl radicals that lead to the formation of H_2 molecules are suggested in literature and here reported [8, 39].

$$i\text{-}C_3H_7^{\cdot} \rightarrow C_3H_6 + H^{\cdot} \quad (15)$$

$$H^{\cdot} + C_3H_8 \rightarrow H_2 + C_3H_7^{\cdot} \quad (16)$$

This argument can be logically connected to the amounts of hydrogen that we observed during pulses of propane. In fact, our observations suggest that catalytic formation of alkyl radical and homogeneous gas phase radical reactions take place even during pulse experiments. Furthermore, comparison between the MS signal intensities of hydrogen formed during propane pulses at 550°C and 700°C (see Fig. 4 and 6) supports the role for homogeneous gas phase reactions which are favored at higher temperatures.

To conclude, carbon oxides formation was thoroughly investigated in the case of oxidative coupling of methane. However, current knowledge of the mechanism involved in generating carbon oxides is very limited. In fact, the origin of carbon oxides might be described either heterogeneously or homogeneously. In addition, in the case of propane, CO_x might form directly from (i) propane, and (ii) any other intermediates such as alkenes or alkyl radicals, generated during propane activation [40, 41]. In this respect, Lin *et al.* proposed that

an important source of carbon oxides is the homogeneous oxidation of methyl radicals with gas phase oxygen through the formation of methyl peroxy radicals ($CH_3O_2^{\cdot}$) [42]. In fact, their subsequent reactions in the gas phase produce carbon oxides. On the other hand, Nelson *et al.* proposed a mechanism involving surface reactions of $CH_3O_2^{\cdot}$ species to CO_x [43]. Tong and Lunsford investigated yet another way for the formation of carbon dioxide, during the catalytic coupling of methane, which involves the heterogeneous oxidation of methyl radicals by collision methyl radicals with the metal oxide surfaces [44]. In our experiments, during pulses of propane, evolution of CO and CO_2 in the gas phase was not observed. Therefore, we conclude that CO and CO_2 formation during the oxidative conversion of propane over Li/MgO catalysts is not caused by active lattice oxygen. Carbon oxides might be formed mainly in the gas phase (when propane and oxygen are simultaneously present). However, the role of adsorbed oxygen molecules on the catalyst surface can not be ruled out and it is not here investigated.

4.5 Conclusions

Our findings demonstrate that the number of surface [O^-] active sites in Li-promoted MgO catalysts can be independently estimated by studying, respectively, the interaction of H_2 and O_2, and the sorption/desorption cycles of CO_2. The results obtained from the two methods are in good agreement. We conclude that the surface areas of Li-promoted MgO catalysts can be tuned using different preparation methods maintaining the same number of [Li^+O^-] active sites per m^2 of material.

Propane activation occurs *via* abstraction of hydrogen on the [Li^+O^-] centers forming hydroxyl groups. Our investigations of active sites regeneration suggested that at 550°C water formation during oxidative dehydrogenation proceeds without removal of lattice oxygen. Further, CO_x formation is not caused by participation of lattice oxygen. In contrast, at higher temperatures (*i.e.*, 700°C) evolution of water seems to involve lattice oxygen as in redox routes involving anion vacancies.

References

[1] R.K. Grasselli, D.L. Stern, J.G. Tsikoyiannis, Appl. Catal. A: Gen. 189 (1999) 1.

[2] F. Nierlich, Hydrocarbon Proc. 71 (1992) 45.

[3] Petrochemistry activity review, http://www.cefic.org/

[4] M.M. Bhasin, J.H. McCain, B.V. Vora, T. Imai, P.R. Pujado, Appl. Catal. A: Gen. 221 (2001) 397.

[5] E.A. Mamedov, V. Cortes Corberan, Appl. Catal. A: Gen. 127 (1995) 1.

[6] F. Cavani, F. Trifiro, Catal. Today 36 (1997) 431.

[7] H.H. Kung, Adv. Catal. 40 (1994) 1.

[8] L. Leveles, K. Seshan, J.A. Lercher, L. Lefferts, J. Catal. 218 (2003) 296.

[9] L. Leveles, K. Seshan, J.A. Lercher, L. Lefferts, J. Catal. 218 (2003) 307.

[10] F. Cavani, F. Trifiro', Catal. Today 24 (1995) 307.

[11] J.X. Wang, J.H. Lunsford, J. Phys. Chem. 90 (1986) 5883.

[12] J.H. Lunsford, Langmuir 5(1) (1989) 12.

[13] J.H. Lunsford, Adv. Catal. 35 (1987) 139.

[14] M.C. Wu, C.M. Troung, K. Coulter, D.W. Goodman, J. Vas. Sci. Technol. A 11(4) (1993) 2174.

[15] I. Balint, Ken-Ichi Aika, J. Chem. Soc. Faraday Transactions 91(12) (1995) 1805.

[16] K.D. Campbell, J.H. Lunsford, J. Phys. Chem. 92 (1988) 5792.

[17] D.J. Driscoll, J.H. Lunsford, J. Phys. Chem. 89 (1985) 4415.

[18] T. Ito, J.X. Wang, C.H. Lin, J.H. Lunsford, J. Am. Chem. Soc. 107 (1985) 5062.

[19] D.J. Driscoll, W. Martir, J.X. Wang, J.H. Lunsford, J. Am. Chem. Soc. 107 (1985) 58.

[20] C. Trionfetti, I.V. Babich, K. Seshan, L. Lefferts, Langmuir, submitted

[21] C. Trionfetti, I.V. Babich, K. Seshan, L. Lefferts, Appl. Catal. A: Gen. 310 (2006) 105.

[22] C. Trionfetti, I.V. Babich, K. Seshan, L. Lefferts, Top. Catal. 39 (3-4) (2006) 191.

[23] http://webbook.nist.gov/chemistry/

[24] R. Burch, E.M. Crabb, Appl. Catal. A: Gen. 100 (1993) 111.

[25] V.P. Vislovskiy, T.E. Suleimanov, M.Y. Sinev, Y.P. Tulenin, L.Y. Margolis, V. Cortes Corberan, Catalysis Today 61 (2000) 287.

[26] M.A. Johnson, E. Stefanovich, T.N. Truong, J. Phys. Chem. 101 (1997) 3196.

[27] C. Shi, M.P. Rosynek, J.H. Lunsford, J. Phys. Chem. 98 (1994) 8371.

[28] Ken-Ichi Aika, J.H. Lunsford, J. Phys. Chem. 81 (14) (1977) 1393.

[29] S.C. Bhumkar, L.L. Lobban, Ind. Eng. Chem. Res. 31 (1992) 1856.

[30] D. Wang, M. Xu, C. Shi, J.H. Lunsford, Catal. Lett. 18 (1993) 323.

[31] S.J. Korf, J.A. Roos, N.A. de Bruijn, J.G. van Ommen, J.R.H. Ross, J. Chem. Soc. Chem. Commun. (1987) 1433.

[32] R.C. Weast, Handbook of Chemistry and Physics, 64th ed., CRC Press Inc., Florida, 1984, pp. B106 and B108.

[33] A.L. Shluger, R.W. Grimes, C.R.A. Catlow, N. Itoh, J. Phys. Condens. Matter 3 (1991) 8027.

[34] A.M. Ferrari, G. Pacchioni, J. Phys. Chem. 99 (1995) 17010.

[35] M.Y. Sinev, V.Y. Bychkov, V.N. Korchak, O.V. Krylov, Catal. Today 6 (1990) 543.

[36] M.Y. Sinev, Catal. Today 24 (1995) 389.

[37] M.Y. Sinev, V.Y. Bychkov, Kinet. Katal. 34 (1993) 309.

[38] M. Machli, C. Boudouris, S. Gaab, J. Find, A.A. Lemonidou, J.A. Lercher, Catal. Today 112 (2006) 53.

[39] M.Y. Sinev, Z.T. Fattakhova, Y.P. Tulenin, P.S. Stennikov, V.P. Vislovskii, Catal. Today 81 (2003) 107.

[40] K. Otsuka, K. Jinno, A. Morikawa, J. Catal. 100 (1986) 353.

[41] J.A. Roos, S.J. Korf, R.H.J. Veehof, J.G. van Ommen, J,R.H. Ross, Appl. Catal. 52 (1989) 147.

[42] C.H. Lin, T. Ito, J.X. Wang, J.H. Lunsford, J. Catal. 111 (1988) 302.

[42] P.F. Nelson, C.A. Lukey, N.W. Cant, J. Catal. 120 (1989) 216.

[43] Y. Tong, J.H. Lunsford, J. Am. Chem. Soc. 113 (1991) 4741.

Chapter 5

Oxidative conversion of propane in a microreactor in the presence of plasma over MgO based catalysts – An experimental study

Abstract

In this work, oxidative cracking of propane was studied in a microreactor containing a catalyst. A dielectric barrier discharge (DBD) allows one to generate a cold microplasma, which activates propane forming radicals, at room temperature and atmospheric pressure. Homogeneous and well crystalline thin layers of MgO and Li/MgO catalysts, 25 µm thicknesses, were deposited in the microchannel using sol-gel method and by micropipetting. Li/MgO catalyst showed higher propane conversion and olefins selectivity compared to MgO. The latter one suggests that (i) radicals formed by DBD in gas phase are differently terminated depending on the catalyst surface; (ii) the surface of Li/MgO catalyst present more selective sites than MgO, such as [Li^+O^-] centers and F-type defects that are generated and able to react at RT. Surprisingly large amounts of products with higher molecular weight than propane i.e., C_4 , C_4^+ were also observed due to only C-C bond formation.

Keywords*: Dielectric barrier discharge; Plasma; Microreactor; Sol-gel Li/MgO; Propane; Oxidative cracking; Oxidative coupling.*

5.1 Introduction

Formation and reaction of gas phase free radicals generated on a catalyst surface has raised increasing interest in recent years, especially in the case of reactions occurring at higher temperatures [1]. Radical species have been proposed as intermediates in numerous catalytic reactions involving partial oxidation of hydrocarbons to olefins and oxygenates, these are the so called heterogeneously initiated homogeneous processes [2]. In these cases, activation of hydrocarbons occurs on the catalytic site, via homolytic splitting of C-C or C-H bonds, resulting in the formation of radicals. There is general evidence that the radicals thus generated are released from the catalyst surface to the gas phase and radical chain reactions lead to final products [1-2]. Alternatively, these radicals can also remain on the catalyst surface and undergo further reactions before desorption, to yield products [3].

Contribution of such homogeneous gas phase routes in heterogeneous catalysis has been especially discussed in the last 20 years in the case of oxidative coupling of methane to higher hydrocarbons [4] and oxidative dehydrogenation of light alkanes (ODH) to olefins [5]. By varying the post catalytic volume of the reactor (in which the reaction is carried out) and recording that this causes an increase in conversion [3], it was concluded that gas phase radical reactions form a major contribution in such processes. In addition, direct evidence for the presence of surface-generated gas-phase radicals has been provided by spectroscopic methods, in particular by techniques like matrix isolation electron spin resonance (MI-ESR) and infrared spectroscopy (MI-IR) in tandem with a catalytic reactor [6-7].

In the case of oxidative dehydrogenation of alkanes, using Li/MgO catalysts, EPR studies showed the existence of $[Li^+O^-]$ defect sites to be the active centers [8]. These sites are responsible for the activation of C-H bonds of alkanes in the presence of oxygen at higher temperatures. During the hydrocarbon conversion, the initial step is the hydrogen atom abstraction by oxygen ions [9], forming hydroxyl groups and alkyl radicals (Eq.1):

$$[Li^+ O^-] + C_3H_8 \rightarrow [Li^+ OH^-] + C_3H_7\cdot \qquad (1)$$

These propyl radicals undergo radical chain reactions in the gas phase [5, 10]. Thus the catalyst affects the activation of propane and product selectivity is determined by the gas phase homogeneous reactions. However, Kondratengo et al. recently reported, in the case of vanadium oxide systems, that increasing the density of active sites affected olefin distribution [11]. In particular, for a high density of oxidizing sites, heterogeneous H-atom abstraction

from C_3H_7· radicals yielding propene can be more effective than the reaction of C_3H_7· radicals in the gas phase [11].

Remarkably, in the case of Li/MgO catalyst, an increase of olefin selectivity could be achieved by increasing the number of active sites per volume of catalytic bed [12]. We suggested recently, that the propyl radicals formed could undergo a second hydrogen abstraction at the active sites leading to propene (Eq. 2) [12]:

$$[Li^+ O^-] + C_3H_7^\bullet \rightarrow [Li^+ OH^-] + C_3H_6 \quad (2)$$

Generally, propane activation by C-C, C-H bond scission requires higher temperatures (T > 550ºC) even in the presence of a strong [H·] abstractor such as $[Li^+O^-]$. This is a drawback because substantial loss of catalyst surface area occurs due to sintering of Li/MgO [13, 14]. This may result in a lower contribution from the heterogeneous formation of propene (eqn. 2). This can be investigated in two ways i.e., (i) to allow initial alkane activation at lower temperatures, and (ii) to carry out the reaction in small and confined reactor space, enhancing radical surface interactions. We propose to achieve this by carrying out the oxidation of propane in the presence of plasma in a microreactor (μ-reactor). Advantage of using a microreactor allows one to generate non-thermal plasma at higher pressures, *i.e,* without the need for vacuum.

Stable and cold gaseous plasma can be generated at room temperature inside a microreactor by dielectric barrier discharge [15]. This plasma consists of energetic electrons which can activate propane as a result of inelastic collisions [16]. Ions and radicals are thus formed at room temperatures at which the catalyst surface area is not affected. Additionally, performing the reaction in a micro scale system (channel dimensions 10-1000 μm) with intrinsically high surface to volume ratio provides extreme quenching conditions on the catalyst surface [17-18].

Thus a microplasma reactor containing catalyst may be used to convert hydrocarbons i.e., light alkanes into more valuable molecules at room temperature and atmospheric pressure by cleavage/formation of C-H and C-C bonds [19]. Incorporation of a stable catalyst layer on the reactor wall is crucial in such a situation. In the case of catalytic reactions many attempts have been made to deposit catalysts on the walls of microreactors, instead of introducing powder type materials in the microchannels in a packed-bed fashion which leads to a high pressure drop [20].

The objective of the present study is to (i) develop a microreactor containing Li/MgO catalyst, (ii) demonstrate activation of C-C, C-H bonds at room temperature using plasma, (iii) allow efficient contact of radicals with the catalyst surface at low temperature and (iv) investigate the effect of this interaction on the products selectivity. Oxidative conversion of propane to olefins is the targeted reaction.

5.2 Experimental

5.2.1 Microplasma reactor

Figures 1 & 2 show, respectively, the top and schematic cross sectional view of the microplasma reactor used in this study. It consists of a Pyrex rectangular chip of 50 mm length x 15 mm width. Microchannels with dimension of 30 mm length x 5 mm width and a channel depth of 500 µm were realized in the chip by means of chemical etching using aqueous HF. Sandwich thermal bonding of three Pyrex plates (one with, two without a channel) allowed fabrication of the microreactor. Details of the processing scheme are given elsewhere [21]. Gas in- and out-lets holes were created by powder blasting using Al_2O_3 particles. The bottom surface of the reactor channels were also treated by powder blasting to increase roughness and allow better catalyst deposition (adhesion). The reactor was then cleaned in an ultra sonic bath to remove contamination. Two copper ribbon electrodes were attached, externally, on the top and bottom side of the chip. The copper electrodes were connected, using adhesive copper foils, to a power supply in order to be able to generate plasma by Dielectric Barrier Discharge (DBD) at atmospheric pressure. A high voltage (5-10 kV) sine wave with a frequency around 60 kHz was applied to one electrode while the other was

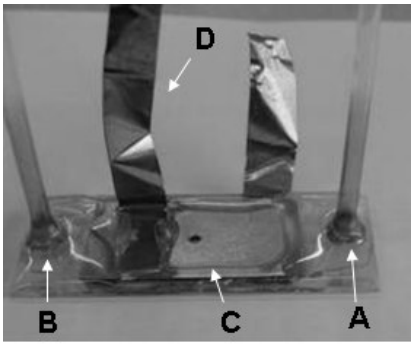

Fig. 1. Top view of the employed microplasma reactor made of Pyrex. The inlet and out let are indicated (A, B). The copper plate is also well visible (C). This is connected to a power supply using adhesive copper foils (D).

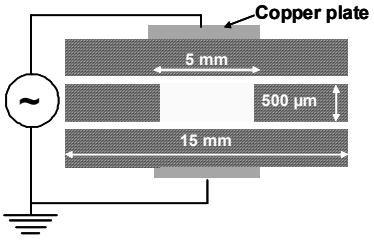

Fig. 2. Schematic drawing of the cross sectional view of the employed microplasma reactor. The 3 Pyrex plates forming the microreactor are schematically represented.

grounded. This generated an output power between 2 to 25 watts. The absorbed power by plasma was calculated from the corresponding V-Q Lissajous figures [22].

The plasma generated in the DBD configuration consists of high energy electrons and is characterized by a large number of microdischarge filaments (ionization of the medium by the electrons), each lasting nano-seconds [23]. These high energy electrons (in the range 3-4 eV) are able to activate hydrocarbons and oxygen at room temperature and atmospheric pressure [24].

The short life time of the current spikes (ns) helps in minimizing local heating. Moreover, the small volume and the large surface to volume ratio of the microreactor allow fast removal of the heat produced during oxidation of propane. Optical emission spectra were recorded with an Ocean Optics HR 4000 spectrometer with fiber optic coupling to the microreactor.

5.2.2 Catalyst deposition in the microchannels

The channels of the microreactor were coated with a catalyst layer using a sol-gel method [13]. Chemicals used were: $Mg(OCH_3)_2$ solution (Aldrich, 8.7wt%, in methanol), methanol (Merck), $LiNO_3$ (Merck), HNO_3 (Merck) an doubly de-ionized water. A solution of $Mg(OCH_3)_2$ in CH_3OH was mixed with DI water in methanol (0.8 M) containing $LiNO_3$ in appropriate amount (0-5 wt%) and a small amount of HNO_3 in order to get a stable sol [25].

This stable sol was used as the precursor for catalyst synthesis and introduced in the open channel by micropipetting [26]. The method consists of injecting the precursor/sol from a micro syringe until filling the length of the microchannel. The sol was kept in contact with air for 45 minutes at 40ºC and a thin film of gel was formed. The procedure was repeated till about 10 mg of catalyst was deposited on the open microchannel. Since the area outside the channel needs to be kept clean for subsequent sealing with the top plate by thermal bonding, the catalyst precursor must be injected precisely into the channel. The gel formed was dried at 50ºC on a hotplate for 12 h in air and subsequently calcined in a furnace at 500ºC for 1 h, heating rate 5ºC/min.

5.2.3 Catalyst characterization

The catalyst layer deposited in the microchannel reactor was characterized using different techniques like X-ray diffraction (XRD), optical microscopy and BET. A portion of the open

microchannel where the catalyst layer is deposited as described above was used for the purpose of these analyses.

Chemical composition of the catalyst was determined with XRF analysis and atomic adsorption composition. The following elements and compounds as impurities (traces) were detected: Mg, O, Li, Cl, S, BaO and CaO. X-ray patterns were recorded by a Philips PW1830 diffractometer using Cu K_α radiation, λ=0.1544 nm, in the 2θ range between 30° and 60°. Surface areas were estimated using the BET method using a Micrometrics Tristar system. The samples were out-gassed in vacuum at 200°C for 24 hours prior to the analysis. For the optical microscopy a Philips microscope DB600 was used.

5.2.4 Catalytic tests

Steady state measurements of the oxidative conversion of propane were performed in the microreactor in the presence of plasma. Empty μ-reactors as well as μ-reactors containing catalyst layers (MgO or 5 wt% Li/MgO) were used at identical conditions. The total gas flow rate was 15 ml. min^{-1} and the feed composition, 10% propane and 1 to 10% oxygen in helium. The reactor was operated at room temperature and atmospheric pressure.

A Varian 3800 GC was used to analyze reactants and products. The GC was equipped with FID and TCD detectors. It was possible to separate all the hydrocarbons on an Alumina Plot column and the remaining components *i.e.* oxygen, CO and CO_2, on a Porapak Q column in combination with a Molsieve-13X column. In the case of μ-reactors containing catalyst, prior to each run, the sample surface was pretreated using pure oxygen plasma. Even, after long operation of the microreactors (up to 1h) stability and data reproducibility were observed.

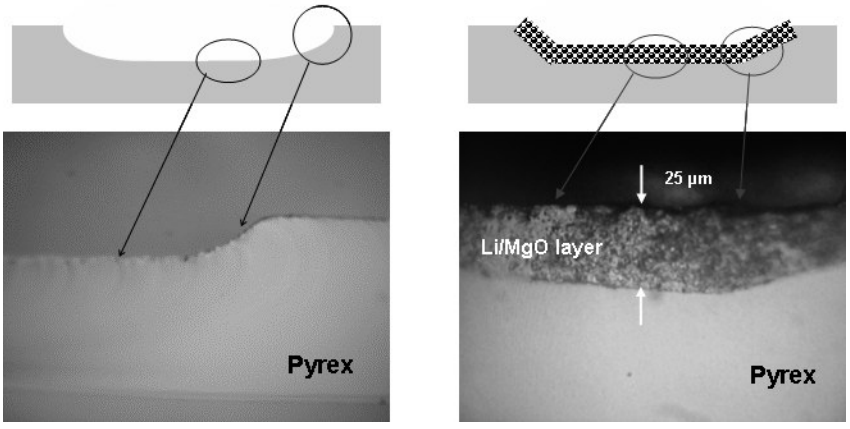

Fig. 3. Optical microscopy - Cross sectional views of the base of the microchannel (a) after powder blasting and (b) after catalyst deposition (5 wt% Li/MgO) by sol gel and micropipetting.

5.3 Results

5.3.1 Catalyst characterization

Optical micrographs of the cross section of the microchannel reactor with and without catalyst are shown in Figures 3a and b, respectively. It can be seen from the images that a ~25 μm uniform catalyst layer could be deposited in the open microchannel by micropipetting. Similar results were also obtained for all the catalysts studied. Table 1 shows the BET surface area of the microreactor chips with and without the catalyst layers. The empty microreactor has a low surface area (< 1 m^2/g). The table shows that it is possible to prepare thin catalyst layers having high surface areas using the described sol-gel method. Indeed the fact that milder heat treatments, during the sol gel method, can prevent sintering effects has already been observed in preparing catalyst particles of Li/MgO [13]. Thus, using the sol gel and micropippetting method we are able to make a high surface area catalyst layer on a Pyrex microchannel.

Table 1.

Calculated surface area per gram of catalyst deposited in the microchannels using sol gel method and calcined at 500ºC for 1 h.

Samples	BET (m^2/g) Surface area
Empty μ-reactor	<1 m^2/g
μ-reactor + MgO	120 m^2/g
μ-reactor + 1 wt% Li/MgO	100 m^2/g
μ-reactor + 5 wt% Li/MgO	80 m^2/g

*Surface area is calculated per gram of microreactor

XRD patterns of the catalyst layers deposited in the microreactor are shown in Fig. 4. The spectra typically contain lines corresponding to MgO. No other phases which contain Lithium, including $LiNO_3$, were detected. The peaks corresponding to the MgO phase became narrower for the samples containing lithium. In general, results show that crystalline catalyst layers can be obtained after calcination at 500ºC and that the crystallinity is enhanced in lithium containing samples [13].

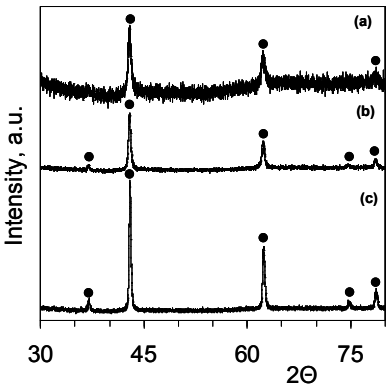

Fig. 4. XRD patterns for MgO (a), 1 wt% Li/MgO (b) and 5 wt% Li/MgO (c) catalyst layers deposited in the microchannel reactor. • MgO phase.

We will now first discuss the results for the oxidative conversion of propane in an empty μ-reactor in the presence of plasma and then show results for the μ-reactor containing catalyst layers.

5.3.2 Propane conversion in the presence of plasma

5.3.2.1 μ-reactor without catalyst

Figure 5 shows the influence of the absorbed power, during plasma formation, on the propane conversion in the absence of oxygen. These experiments were performed between 0 and 6 W of absorbed power (5-10 kV applied voltage) because the non-thermal plasma was stable in this range. The dominant reaction path that occurs in the non-thermal plasma is electron impact homogeneous bond splitting. In fact, as shown in fig. 5, propane conversion increases with increasing energy input due to the increase of (i) the number of electrons and (ii) their average energy [27-28]. Remarkably, propane conversions up to 30 mol% could be achieved near room temperature in the presence of plasma. Further experiments were carried out applying 3 Watt of power. Typical propane conversion in this situation was about 15 mol%.

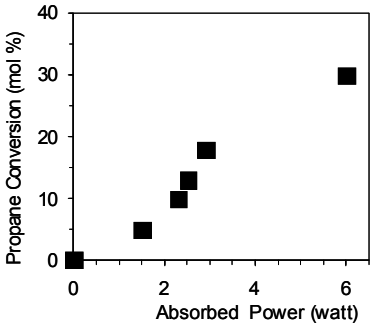

Fig. 5. Influence of the absorbed power by plasma on the conversion of propane. Conditions: 10% propane in helium, flow rate 10 ml. min^{-1}, 1 atm, and 25ºC.

Figure 6 shows the optical emission spectrum of a C_3H_8-He plasma with 3 W power input. Electronic excitation of 'CH' corresponding to the $A^2\Delta \rightarrow X^2\Pi$ transition at 431.5 nm was used to determine the kinetic gas temperature in this emission region [22]. The resolution of the spectrometer, calibrated using a UV lamp, was determined to be 0.7 nm (full width at half maximum). This is not enough to resolve the individual rotational lines of the Q, R and P branches of the CH band. However, rotational temperature, which reflects the gas temperature inside the filamentary discharge, was calculated by comparing the CH band (in Fig 6) with those in spectra simulated as a function of temperature using LIFBASE software [29]. The best fit was obtained in the region of 25-75˚C. Remarkably, a thermocouple inserted inside the

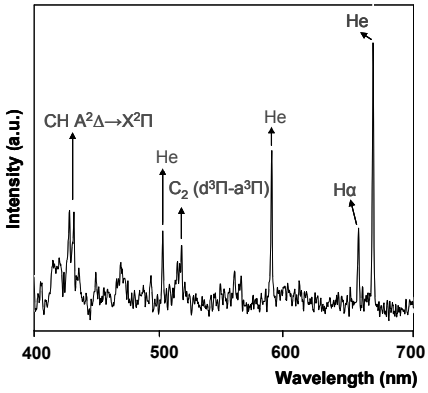

Fig. 6. Optical emission spectrum for a gas mixture of 10% propane in helium in the presence of plasma; 3W power was applied.

microchannel measured 75˚C at the highest power of 24 watt supplied from the source. In the case of the 3W used in our experiments the average gas temperature of 25 ± 50°C was obtained. Thus propane activation occurs close to room temperature.

Existence of CH and H bands in the spectra shown in Fig. 6 indicates decomposition of propane *via* C-C and C-H bond scission. Based on the propane conversion in Fig 5 and the corresponding selectivity observed (results not shown here), the kinetic data were fitted with a set of reaction equations [27-28] and the results indicated that mainly radicals, for e.g., C_3H_7·, C_2H_5·, CH_3· and H· were present in the gas phase as a result of inelastic electron collisions.

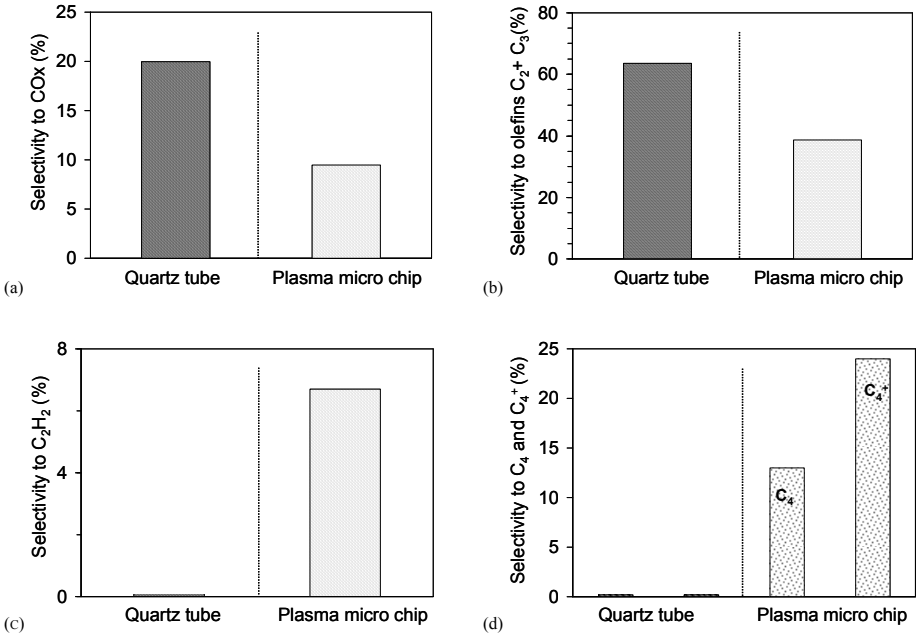

Fig. 7. Results of the oxidative conversion of propane. Selectivity to the products observed, respectively, for empty, quartz tube reactor at 600ºC [5] and plasma microreactor at room temperature and at the same level of propane conversion achieved by varying SV: (a) CO_x, (b) products from C_2 to C_3, (c) C_2H_2, (d) C_4 and C_4^+. Conditions: 10% propane, 1% oxygen in helium.

In the presence of oxygen, under identical conditions (3W of input power, 10 % propane and 1% oxygen in helium), the propane conversion was higher i.e. 22 mol% instead of 15 mol%, indicating that oxygen plays a role in the propane conversion. Figure 7 shows the typical product distribution obtained in an empty plasma microchip reactor at room temperature in the presence of oxygen. Results from an empty quartz tube reactor (internal diameter 4 mm) operating with the same feed composition (10% propane and 1% oxygen in

helium), and heated up to 600˚C are also given [5]. The selectivities presented are at the same level of propane conversion, *i.e.* 20%.

It is obvious from Figure 7 that the product selectivities show striking differences in the two cases. To start with, in the case of the plasma microreactor there was less CO_x formation (Fig. 7a), however the total olefin selectivity unexpectedly was also lower (Fig. 7b). Most remarkably, in the case of the microreactor, a substantial amount of ethyne was observed (Fig. 7c). Furthermore, large amounts (37 mol%) of products with higher molecular weights than propane, i.e., C_4, C_4^+, were also observed (Fig. 7d). A presence of products containing four or more C atoms requires C-C bond formation under the conditions present in the microreactor.

5.3.2.2 μ-reactor with catalyst

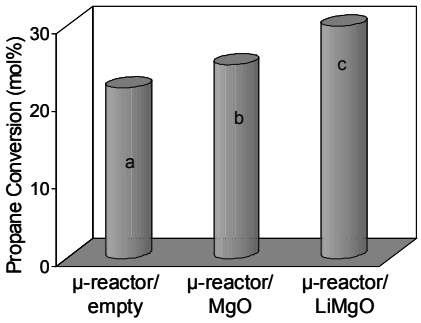

Fig. 8. Propane conversion in microreactor in the presence of plasma at RT (a) empty reactor, (b) reactor containing MgO and (c) reactor containing Li/MgO. Conditions: flow rate 15 ml/min, feed composition 10% propane and 1% oxygen in He; 3W power was applied.

Figure 8 compares propane conversions for an empty μ-reactor with those obtained for a μ-reactor containing, respectively, MgO or 5 wt% Li/MgO catalyst. In order to make a proper comparison, all the experiments were carried out under the same conditions of flow rate, feed composition and applied power (3W). Clearly, in the presence of catalyst, conversion of propane increases. Most remarkably an increase in propane conversion was also observed in the presence of lithium, the conversion increased from 24% for MgO, to 30% in the case of 5 wt% Li/MgO. Figure 9 shows the selectivity to CO_x in the case of μ-reactors containing MgO or 5 wt% Li/MgO catalysts. As can be seen from the figure, the microreactor containing MgO gave more combustion than the one with Li/MgO catalyst. These findings are similar to those we reported earlier [10] in the case of oxidative cracking of propane at high temperature employing a fixed bed reactor at 600˚C; MgO showed selectivity to CO_x up to 80% and this dropped to 40% in the presence of lithium. Figure 10 shows the selectivity to olefins as a function of the oxygen partial pressure. In the explored range of oxygen partial pressures, the chip containing Li/MgO catalyst showed constant selectivity meanwhile it decreased in the case of MgO.

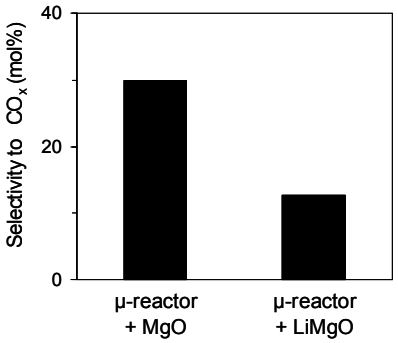

Fig. 9. Recorded selectivity to CO_x during oxidative conversion of propane in the presence of plasma in a microreactor containing (i) MgO and (ii) 5 wt% Li/MgO. Conditions: flow rate 15 ml/min, feed composition 10% propane and 1% oxygen in He at RT.

This indicates that MgO is much less selective than Li/MgO towards olefins. Figure 11 shows the selectivity to all the products obtained with propane and oxygen in the presence of plasma in the μ-reactor containing 5wt% Li/MgO catalyst. Propene is the most abundant olefin (13%) followed by ethene (10%). Appreciable amounts of alkanes, methane (12%) and ethane (10%) were also observed. COx was about 13%. Just as in the case of the reactor without catalyst, an appreciable amount of ethyne (8%) was formed. Most remarkably, again, very high selectivity to $\geq C_4$ was observed (C_4 -12%, C_4^+ - 22%). To summarize, the product distributions obtained with 5 wt% Li/MgO catalyst at 600˚C in a fixed bed reactor [10] and at 25˚C in a μ-reactor in presence of plasma are given again in Table 2. This allows an easy comparison of all the data discussed so far.

5.4 Discussion

It has been shown earlier [10, 30] that, for Li/MgO catalysts, propane activation requires the presence of oxygen and higher temperatures (T > 600˚C). In these catalysts [Li^+O^-] type defect centers are the active sites and their formation requires the higher temperatures. The [Li^+O^-] site is claimed to have high H-atom affinity and, at relative high temperature, is able to abstract H· from propane molecules forming n- and iso-propyl radicals as primary intermediates [31, 32]. These propyl radicals are formed depending on whether primary or secondary hydrogen is abstracted from propane. At the higher temperatures required for the reaction, endothermic decompositions are favored and the two types of radicals (n & iso) undergo different uni-molecular reaction routes in the homogeneous phase: iso-propryl can undergo C-H bond scission at the α-position and yields propene and a hydrogen atom, while n-propyl preferentially follows β-

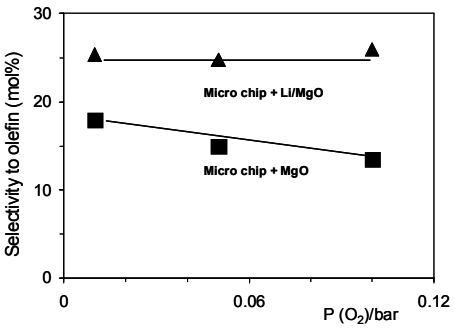

Fig. 10. Influence of oxygen partial pressure on selectivity to olefins Conditions: 10% propane, 1-10% oxygen in helium.

scission of the C-C bond, therewith forming a methyl radical and ethylene [33]. The various products formed can be accounted for by a series of radical chain reactions in the gas phase, details of which were discussed earlier [34]. It is now appropriate to discuss what happens in the presence of plasma. The non-thermal plasma generated at atmospheric pressure by dielectric barrier discharge consists of current filaments, namely microdischarges, distributed in the space between the two electrodes (see Fig. 12). The number of microdischarges depends on (i) the voltage applied on the electrodes (ii) the distance between the electrodes (iii) the relative permittivity of the dielectric barriers and (iv) the processing gas [35]. The relative permittivity of a dielectric barrier can strongly determine the amount of charge that can be stored for a certain value of applied electric field. This parameter plays a critical role in plasma formation [36].

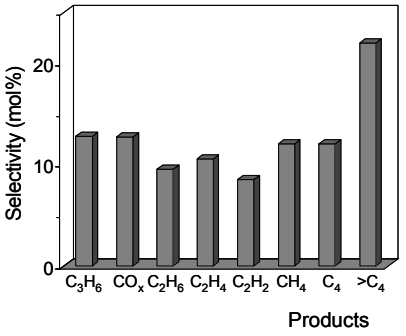

Fig. 11. Selectivity to the main products for a plasma microreactor containing 5 wt% Li/MgO catalyst. Conditions: flow rate 15 ml/min, feed composition 10% propane, 1% oxygen and balance helium at room temperature. Formation of hydrogen was detected but not quantified.

In a plasma microreactor, C_3H_8 molecules are directly activated/converted *via* collisions with energized electrons. Activation produces radicals such as $C_3H_7\cdot$ due to cleavage of C-H bonds (Eq. 3). These can initiate radical chain reactions. Thus, reaction 3 is strongly influenced by the number of charges transferred or accumulated on the dielectric surface [37] and therefore by the relative permittivity.

$$C_3H_8 + e^- \rightarrow C_3H_7\cdot + H\cdot + e^- \qquad (3)$$

As shown in Fig. 8, at a fixed applied voltage, the reactivity of a microplasma towards propane is improved when a layer of MgO is deposited on the Pyrex surface of the chip (Fig. 12). At room temperature the permittivity (ε) of MgO is 9.7 $C^2/N*m^2$, which is double that of Pyrex, 4.8 $C^2/N*m^2$ [38]. Because of the higher permittivity, in the case of MgO a higher amount of charges can be accumulated on the surface. Thus, plasma reactivity is expected to be improved [39]. Indeed, in the present of catalyst layers, we observed additional microdischarges distributed over the entire electrode area [28]. This higher number of charges transferred allows more impacts (and higher in-elastic collisions) giving rise to excitation of a higher number of propane molecules.

Table 2.

Catalytic performance of Li/MgO catalysts respectively tested in (i) a fixed bed reactor at 600ºC [10] and (ii) plasma microreactor at room temperature.

		Selectivity (%)					
		C_3H_6	$(C_2H_4 + C_2H_6)$	C_2H_2	CH_4	CO_x	$>C_4^*$
Fixed Bed/ Li/MgO	**600ºC**	**30**	**32**	**-**	**4**	**34**	**-**
Microchip/ Li/MgO	**RT**	**13**	**20**	**8**	**12**	**13**	**34**

Conditions: 10% propane, 1÷10% oxygen in helium; similar conversion level of propane ~ 30% obtained by varying the space velocity (SV); *C_4= 12%, C_4^+=22%.

In the case of Li/MgO catalyst layer, the reactivity is even slightly more improved than for MgO. Though the thickness of the layers has been kept the same, in presence of lithium the MgO layer is more crystalline (Fig. 4). Huang *et al.* [40] have shown that, in the case of ZrO_2, an increase of crystallinity results in an increase in permittivity. The higher crystallinity of the Li/MgO layer can contribute towards enhanced propane activation *via* improved permittivity, as described in the previous paragraph. The improved crystallinity for the Li/MgO results from a 'Li assisted ordering' in the gel during sol-gel transformation, reported earlier by us [13].

In addition, propane activation can also occur *via* an indirect route, *i.e.* activation of gas phase oxygen by the plasma. Among the atomic processes taking place in a non-thermal plasma, the electron impact dissociation of O_2 to form charged and neutral oxygen has been reported in literature and is described in reaction equations 4 and 5 [41].

$$e^- + O_2 \rightarrow 2O + e^- \rightarrow O^- + O \quad (4)$$

$$e^- + O_2 \rightarrow O_2^* + e^- \rightarrow O + O + e^- \quad (5)$$

The O^- species, present in the homogeneous phase, has been reported to cause C-H bond scission in alkanes e.g., methane [42], ethane [43]. In the case of propane this will result in the formation of propyl and hydroxyl radicals as shown below:

$$[O^-] + C_3H_8 \rightarrow [OH^-] + C_3H_7\cdot \quad (6)$$

In fact, the increased propane conversion observed while co-feeding oxygen (22%) in the μ-reactor without catalyst (propane conversion was 15% in the absence of oxygen under

identical conditions, results not shown here) supports the above argument (reaction 6). We observed earlier [5] that by adding oxygen the number and the concentration of chain carrier radicals increased [5]. In fact C_3H_7· radicals react fast with O_2 forming hydro-peroxyl (HO_2·) radicals, which can react with propane molecules to form H_2O_2. Decomposition of H_2O_2 results in hydroxyl radicals (OH·) which become the main chain propagators.

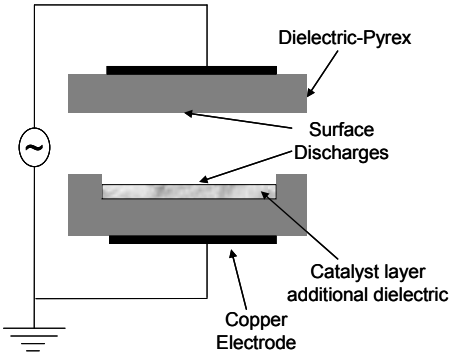

Fig. 12. Sketch of the elements constituting a microplasma reactor.

Furthermore, let us now discuss the role of Li on the observed selectivity. Interestingly, in the plasma microreactor, addition of lithium to MgO results in an enhanced activity and selectivity to propylene (Fig. 13) at similar levels of conversion (see Fig. 8b, c). Thus, Li/MgO is intrinsically more selective and the better selectivity observed, may only be addressed to more selective quenching reactions taking place on the catalyst surface. In the case of Li/MgO catalysts, as discussed earlier, [Li^+O^-] is suggested to be the active oxidation site [29] for the selective conversion of propane to olefins. Hydrogen abstraction occurs at the [Li^+O^-] site [44, 45], as shown in equation 1. The propyl radicals undergo transformations in homogeneous phase to give olefins [10, 31, 46].

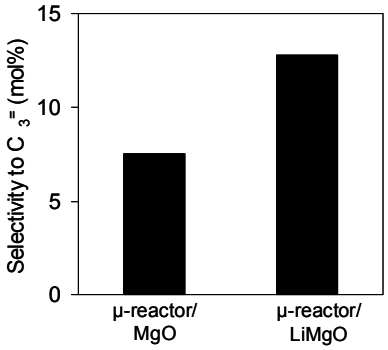

Fig. 13. Selectivity to propylene for MgO and Li/MgO catalysts in a microreactor in presence of plasma at RT. Comparison made at similar levels of propane conversion.

Significantly, we have also shown [12] that by preparing Li/MgO catalysts (e.g. with a sol gel method) with increasing active sites concentration allows interaction between propyl radicals formed and the catalyst surface *via* a second hydrogen abstraction leading to propylene (equation 2).

It is generally accepted that incorporation of Li in MgO occurs only at higher temperatures (T > 500ºC) and formation of the [Li^+O^-] site occurs *via* the following defect reactions 7 and 8 (Kroeger-Vink notation) [47, 48].

$$Li_2O + 2Mg_{Mg}^{x} + O_O^{x} \rightarrow 2Li_{Mg}' + V_O^{\cdot\cdot} + 2MgO \qquad (7)$$

$$2\ Li_{Mg}'\ O_O^x + V_O^{\cdot\cdot} + \tfrac{1}{2}O_2 \rightarrow 2\ Li_{Mg}'\ O_o^{\bullet} + O_O^x \quad (8)$$

$[Li^+O^-]$ sites are defect sites and their existence at lower temperatures has been investigated and confirmed, using EPR spectroscopy, by Lunsford and coworkers [49-51] In agreement with this, we propose that $[Li^+O^-]$ defect sites may already be present at the low temperature under our conditions. Thus propyl radicals formed already at room temperature in the presence of plasma (equation 3) can interact selectively with these $[Li^+O^-]$ sites and give improved propylene yields as suggested earlier (see equation 2).

Alternatively, the presence of plasma can also help to create other defect sites which are able to selectively terminate radicals. Detailed studies are present in literature describing emission of UV light during dielectric barrier discharge (DBD) [52]. The optical emission spectrum recorded during plasma formation (Fig. 6) shows that UV light is generated inside the microreactor. Nelson *et al.* [53] and later E. Knozinger *et al.* [54] reported, using EPR studies, that interaction between UV light and MgO particles can give rise to surface paramagnetic centers (trapped electrons, typically F-centers, $[V_O^{\bullet}]$). Quantification of the UV emission power can not be done in our conditions, however, we cannot rule out UV activation. Goodman *et al.* suggests that oxygen vacancy, containing one or two electrons (F-type defects), is able to activate C-H bonds during methane oxidative coupling [55]. Bond scission occurs and the H· is trapped at the defect site. Thus, the presence of $[V_O^{\bullet}]$ type defect sites caused by the plasma, may allow H· abstraction from propane and even propyl radicals, and in the latter case enhanced selectivity to propene can be expected.

In our experiments, we observe appreciable amounts of ethyne. Activation of methane is known to yield ethyne in the presence of plasma [56, 57]. Two routes are often suggested. Firstly, ethyne can be formed by extensive dehydrogenation of C_2 species present during methane conversion [58] We also observe C_2 specie during our experiments (Fig. 6). Further, CH type species are formed in the presence of plasma (Fig. 6). Dimerization of such species can result in ethyne. Such a possibility is also suggested by Kado *et al*. during methane conversions [59]. Hydrogen redistribution during this reaction, forming dehydrogenated products as ethyne, may be the reason for the appreciable amount of methane observed.

This argument can also be logically connected to the large amounts of C_4 and C_4^+ products that we observe. The role of plasma is in the activation of propane and formation of radicals at ambient temperatures as stated previously. Formation of C_4 and C_4^+ products from propane essentially requires C-C bonds formation. C-C bonds formation is an exothermic

process and therefore favored at lower temperatures. Coupling reactions between radicals also imply a decrease in entropy because the number of molecules/radicals is decreasing by definition. Therefore, it is not surprising to see C-C bond formation reactions under our conditions. In the conventional fixed bed reactors, propane activation occurs at higher temperatures (T > 600˚C) in the presence of catalyst. These conditions favor the rupture of C-C bonds (causing increase in entropy) and thus we see only products of cracking (Table 2), *i.e.*, with molecular weights lower than that of propane. Considering that similar amounts of $C_4 + C_4^+$ products are formed in the case of both the μ-reactor with and without catalyst, it is suggested that the coupling of the radicals generated occurs in the homogeneous phase predominantly.

5.5 Conclusions

Oxidative conversion of propane was carried out using a μ-reactor in the presence of a cold plasma. Under these conditions it is possible to oxidize propane at RT and atmospheric pressure.

A homogeneously uniform layer of Li/MgO catalyst could be synthesized by a sol-gel method and deposited onto the open channel of the reactor by micropipetting. Enhanced olefin selectivity in the presence of Li/MgO catalyst indicates the possible formation of active defect sites at these mild conditions due to the influence of the plasma.

Conditions present in the investigated microplasma reactor, in particular the low temperature used during propane activation, favor the formation of C-C bonds. C_4 and C_4^+ are the major products and the coupling of the radicals occurs predominantly in the homogeneous phase.

References

[1] Driscoll, D. J.; Campbell, K.; Lunsford, J. H. Advances in Catalysis 1987, 35, 139.

[2] Vislovskiy, V. P.; Suleimanov, T. E.; Sinev, M. Y.; Tulenin, Y. P.; Margolis, L. Y.; Cortes Corberan, V. Catalysis Today 2000, 61, 287.

[3] Buyevskaya, O. V.; Baerns, M. Catalysis Today 1998, 42, 315.

[4] Couwenberg, P. M.; Chen, Q.; Marin, G. B. Industrial & Engineering Chemistry Research 1996, 35 (11), 3999.

[5] Leveles, L.; Seshan, K.; Lercher, J. A.; Lefferts, L. J. Catal. 2003, 218, 296.

[6] Lunsford, J. H. Langmuir 1989, 5, 12.

[7] Tevault, D. E.; Lin, M. C.; Umstead, M. E.; Smardzeqski, R. R. Int. J. Chem. Kinet. 1979, 11, 445.

[8] Wang, J. X.; Lunsford, J. H. J. Phys. Chem. 1986, 90, 5883.

[9] Balint, I.; Aika, Ken-ichi J. Chem. Soc., Farday Trans. 1997, 93 (9), 1797.

[10] Leveles, L.; Seshan, K.; Lercher, J. A.; Lefferts, L. J. Catal. 2003, 218, 307.

[11] Kondratenko, E. V.; Sinev, M. Y. Applied Catalysis A: General 2007, 325, 353.

[12] Trionfetti, C.; Babich, I. V.; Seshan, K.; Lefferts, L. Topics in Catalysis, 2006, 39 (3-4), 191.

[13] Trionfetti, C.; Babich, I. V.; Seshan, K.; Lefferts, L. Applied Catalysis A: Gen. 2006, 310, 105.

[14] Cavani, F.; Trifiro, F. Catalysis Today 1995, 24, 307.

[15] Kim, H. Plasma Processes and Polymers 2004, 1, 91.

[16] Kogelschatz, U. Plasma Chemistry and Plasma Processing 2003, 23 (1), 1.

[17] de Mello, A.; Wootton, R. Lab on a chip 2002, 2, 7N.

[18] Jensen, K. F. Chemical Engineering Science 2001, 56, 293.

[19] Eliasson, B.; Liu, C.; Kogelschatz, U. Ind. Eng. Chem. Res. 2000, 39, 1221.

[20] Ajmera, S. K.; Delattre, C.; Schmidt, M. A.; Jensen, K. F. J. Catal. 2002, 209, 401.

[21] Tiggelaar, R. M.; Benito-Lopez, F.; Hermes, D. C.; Rathgen, H.; Egberink, R. J. M.; Mugele, F.; Reinhoudt, D. N.; van den Berg, A.; Verboom, W.; Gardeniers, J. G. E. Chemical Engineering Journal 2007, 131, 163.

[22] Nozaki, T.; Muto, N.; Kadio, S.; Okazaki, K. Catalysis Today 2004, 89, 67.

[23] Kogelschatz, U. Plasma Physics and Controlled Fusion 2004, 46, B63.

[24] Okumoto, M.; Kim, H. H.; Takashima, K.; Katsura, S.; Mizuno, A. IEE Transaction on Industry Applications 2001, 37 (6), 1618.

[25] Diao, Y.; Walavender, W. P.; Sorensen, C. M.; Klabunde, K. J.; Ricker, T. Chem. Mater. 2002, 14, 362.

[26] Chen, H.; Bednarova, L.; Besser, R. S.; Lee, W. Y. Applied Catalysis A: General 2005, 286, 186.

[27] Agiral, A.; Trionfetti, C.; Seshan, K.; Lefferts, L.; Gardeniers, J. G. E. Abstract of papers, ICPIG Meeting, Czech Republic, July 2007.

[28] Agiral, A.; Trionfetti, C.; Seshan, K.; Lefferts, L.; Gardeniers, J. G. E. Abstract of papers, ISPC18 Meeting, Japan, August 2007.

[29] Lugue, J.; Crosley, D. R. 1999 Lifbase: Database and Spectral Simulation Program (ver.1.6) SRI International Report MP 99-009

[30] Leveles, L.; Fuchs, S.; Seshan, K.; Lercher, J. A.; Lefferts, L. Applied Catalysis A: Gen. 2002, 227, 287.

[31] Zhang, Hong Sheng; Wang, Ji Xiang; Driscoll, D. J.; Lunsford, J. H. J. Catal. 1988, 112(2), 366.

[32] Wang, D.; Xu, M.; Shi, C.; Lunsford, J. H. Catalysis Letters 1993, 18, 323.

[33] Yamauchi, N.; Miyoshi, A.; Kosaka, K.; Koshi, M.; Matsui, N. J. Phys. Chem. A 1999, 103(15), 2723.

[34] Sinev, M. Y. Res. Chem. Intermed. 2006, 32, 205.

[35] Li, R.; Yamaguchi, Y.; Yin, S.; Tang, Q.; Sato, T. Solid State Ionics 2004, 72, 235.

[36] Xu, X. Thin Solid Film 2001, 390, 237.

[37] Pons, J.; Moreau, E.; Touchard, G. J. Phys. D : Appl. Phys. 2005, 38, 3635.

[38] Lewis, T.J.; Wright, A. J. Appl. Phys. 1970, 3, 1329.

[39] Li, R.; Tang, Q.; Yin, S.; Sato, T. Fuel Processing Technol. 2006, 87, 617.

[40] Huang, A. P.; Chu, P. K.; Yan, H.; Zhu, M. K. J. Vac. Sci. Technol. B 2005, 23(2), 566.

[41] Cosby, P. C. J. Chem. Phys. 1993, 98(12), 9560.

[42] Nozaki, T.; Hattori, A.; Okazaki, K. Catalysis Today 2004, 98, 607.

[43] Zhang, X.; Zhu, A.; Li, X.; Gong, W. Catalysis Today 2004, 89, 97.

[44] Driscoll, D. J.; Martir, W.; Wang, J. X.; Lunsford, J. H. J. Am. Chem. Soc. 1985, 107, 58.

[45] Sinev, M. Y.; Bychkov, V. Y.; Korchak, V. N.; Krylov, O. V. Catalysis Today 1990, 6, 543.

[46] Sinev, M. Y. J. Catal. 2003, 216, 468.

[47] Gellings, P. J.; Bouwmeester, H. J. M. Catalysis Today 2000, 58, 1.

[48] Catlow, C. R. A.; Jackson, R. A.; Thomas, J. M. J. Phys. Chem. 1990, 94, 7889.

[49] Ito, T.; Wang, J. X.; Lin, C. H.; Lunsford, J. H. J. Am. Chem. Soc. 1985, 107, 5062.

[50] Bothe-Almquist, C. L.; Ettireddy, R. P.; Bobst, A.; Smirniotis, P. G. J. Catal. 2000, 192, 174.

[51] Aika, Ken-ichi; Lunsford, J. H. J. Phys. Chem. 1978, 82 (16), 1794.

[52] Lu, X. ; Laroussi, M. J. Appl. Phys. 2005, 98, 23301.

[53] Nelson, R. L.; Tench, A. J. J. Chem. Phys. 1964, 40(9), 2736.

[54] Sterrer, M.; Diwald, O.; Knozinger, E.; Sushko, P. V.; Shluger, A. L. J. Phys. Chem. B 2002, 106, 12478.

[55] Wu, M. C.; Truong, C. M.; Coulter, K.; Goodman, D. W. J. Vac. Sci. Technol. A 1993, 11(4), 2174.

[56] Yang, Y. Plasma Chemistry and Plasma Processing 2003, 23(2), 327.

[57] Zhang, X.; Zhu, A.; Li, H.; Gong, W. Catalysis Today 2004, 89, 97.

[58] Kim, S. S.; Lee, H.; Na, B. K.; Song, H. K. Korean J. Chem. Eng. 2003, 20(5), 869.

[59] Kado, S.; Urasaki, K.; Sekine, Y.; Fujimoto, K.; Nozaki, T.; Okazaki, K. Fuel 2003, 82.

Chapter 6

Alkane activation at ambient temperatures – Unusual selectivities, C-C, C-H bond scission vs C-C bond coupling

Abstract

In this work a cold plasma generated by dielectric barrier discharge (DBD) in a microreactor was used to convert alkanes, in the range C1-C3, at atmospheric pressure. Alkanes activation via C-H and C-C cleavage to form radicals was detected at temperatures close to ambient. Remarkably, large amounts of products with higher molecular weight than the starting hydrocarbon were observed in all the experiments. Results clearly show that C-H activation at lower temperature favorably lead to C-C bond formation.

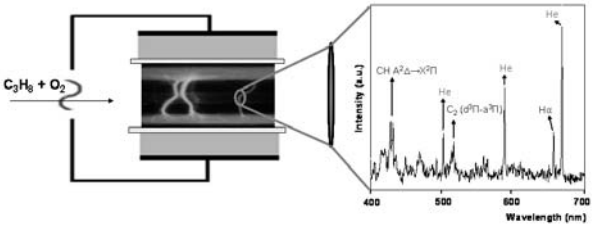

Cold Plasma generated in a microreactor by dielectric barrier discharge for propane conversion at low temperatures.

Keywords*: Microreactor; Plasma reactions; C-H bond activation; Light alkanes; C-C coupling reactions.*

6.1 Introduction

Availability and low cost of light alkanes (C_1-C_4 range) make them interesting as feedstock for commercial fuels and chemicals [1]. However, the rate limiting step in their use is reported to be the selective activation/scission of a C-H bond [2]. In fact, direct conversion of alkanes is a challenging problem due to the strong C-H (e.g., 415 kJ/mol, for methane) and C-C bonds (350 KJ/mol for ethane) present [3].

Two commonly attempted solutions to the problem are (i) to use oxygen to activate the bonds and (ii) to use selective catalysts for efficient conversions. Even then, higher temperatures are required to get appreciable alkane conversions. For e.g., oxidative methane conversion requires temperatures in the range of 850ºC, for ethane 750ºC and even for LPG range hydrocarbons (C_3+C_4) temperatures above 600ºC are required.[4] Activation of C-C and C-H bonds at higher temperatures, even in the presence of heterogeneous catalyst systems, tend to be initiated by homogeneous splitting of the bond, creation of radicals and radical chain reactions leading to products [5-7]. High temperatures alkane conversions have inherent difficulties, viz. (i) they lead to extensive endothermic C-C and C-H bond cleavage causing formation of cracking products or coke, respectively (ii) cause loss of catalyst activity due to sintering and (iii) favor non-selective combustion of alkanes. Alkane activation at lower temperatures, even though challenging, is very interesting from a commercial point of view.

Plasma processes have recently been utilized in many chemical reactions. Plasmas generate active species (i.e., electrons, ions and radicals) and allow operation at lower temperature as compared to catalytic processes [8, 9].

In particular, methane conversion with plasma is being widely investigated using glow discharge and corona discharge [10, 11]. Typically, these technologies showed, respectively, (i) gas temperatures which were higher than ambient, (ii) deterioration of electrodes because of their direct contact with the plasma and (iii) constriction of the plasma volume (because of electrode's geometry). In order to overcome these limitations, plasmas generated between two parallel electrodes by dielectric barrier discharge (DBD), at atmospheric pressure, were used [12]. Pioneering work by Kogelschatz and coworkers reported the direct conversion of CO_2 and CH_4 to synthesis gas and higher hydrocarbons, *i.e.*, C_2-C_6, in a quartz reactor using a dielectric barrier discharge [13, 14]. Additionally, they also demonstrated the feasibility of performing the reaction of methane with carbon dioxide over various zeolite catalysts promoted by DBD at generally ambient conditions [15, 16]. In the case of a DBD, the cold

gaseous plasma [17] is reported to be able to activate hydrocarbons as a result of electron impact collisions [18].

In this study, we report oxidative conversion of light alkanes, C_1-C_3 range, in the presence of cold plasma in a microreactor [19]. The use of a microreactor for plasma processing [20] helps to work at higher pressures instead of the vacuum required in conventional systems [13]. Generation of a DBD at atmospheric pressure in a small and confined reactor space may imply a (i) stronger electric field, (ii) more uniform and dense plasma and (iii) better control of the residence time. The addition of small amounts of oxygen helps to achieve higher levels of hydrocarbon conversion [21]. Thus, C-C and C-H bond activation at lower temperatures and its influence on product selectivities are discussed.

6.2 Experimental part

Figure 1 shows, respectively, the top view (left) and schematic cross sectional view (right) of the microplasma reactor used in this study. It consists of a Pyrex rectangular chip of 50 mm length x 15 mm width. Microchannels with dimension of 30 mm length x 5 mm width and a channel depth of 500 μm were realized in the chip by means of chemical etching using HF [21]. Sandwich thermal bonding of three Pyrex plates (one with and, respectively, the bottom and top plate without a channel) allowed fabrication of the microreactor (Figure 1, right) [19]. Gas in- and out-lets were created by powder blasting using alumina particles. Two copper ribbon electrodes were attached, externally, on the top and bottom side of the chip. The copper electrodes were connected to a power supply (<25 watts). A high voltage (5-10 kV) sine wave (60 kHz) was applied to one electrode while the other was grounded.

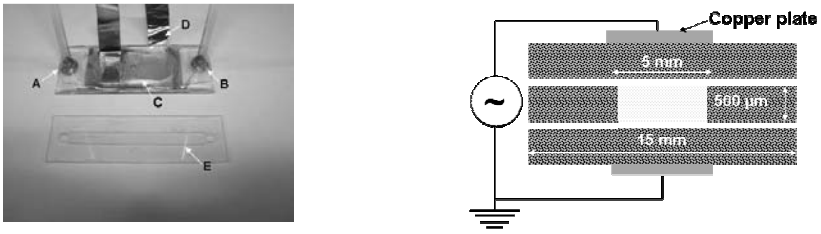

Fig. 1. Employed microplasma reactor made of Pyrex. (Left) Top view, the inlet and outlet are indicated (A, B), the copper plate (C) is connected to a power supply using adhesive copper foils (D). The microchannel (E) is also shown in the picture. (Right) Schematic drawing of the cross sectional view; the 3 Pyrex plates forming the microreactor are schematically represented.

This generated plasma by Dielectric Barrier Discharge (DBD) at atmospheric pressure. The absorbed power by plasma was calculated from the corresponding V-Q Lissajous figures [22]. Experiments were carried out with stable plasma at 3 Watt of absorbed power. Typically

around 15-20% alkane conversions were observed under these conditions. Operating with absorbed power higher than 3 Watt the carbon balance is less spectacular. Alkane conversion increased but selectivity to products of coupling dropped. The increased average electron energies causes (i) enhanced oxygen activation and (ii) formation of coke and/or oxygenates compounds. In order to determine the temperature in the gaseous plasma, optical emission spectra were recorded with an Ocean Optics HR 4000 spectrometer with fiber optic connected to the microreactor. Additionally, the temperature of the gas, outside the plasma region, was monitored with a Type-K thermocouple. Activation of C_1, C_2, C_3 alkanes, in presence of oxygen, was attempted in a microreactor in presence of plasma. The total gas flow rate was varied between 10 and 20 ml/min and the feed composition consisted of 10% alkane and 1% oxygen in helium. The 10:1 alkane to oxygen ratio reported represents an optimum condition. In the case of higher amounts of oxygen, formation of coke and oxygenates was also observed (carbon balance was around 85%). The reactor was operated at room temperature and atmospheric pressure. A Varian 3800 GC was used to analyze reactants and products. The GC was equipped with FID and TCD detectors. It was possible to separate all the hydrocarbons on an Alumina Plot column and the remaining components i.e., O_2, CO and CO_2, on a Porapak Q column in combination with a Molsieve-13X column.

6.3 Results and discussion

Optical emission spectroscopy is one of the important methods for determining the temperature and composition of plasma. Figure 2 shows the optical emission spectrum for C_3H_8-He plasma under our experimental conditions. Features of the electronic excitation of the 'CH' radical corresponding to the $A^2\Delta \rightarrow X^2\Pi$ transition at 431.5 nm, C_2 radical species pertaining to $d^3\Pi$-$a^3\Pi$ transition at 520 nm (Swan band), and lines corresponding to hydrogen radicals (Hα, Balmer series) and Helium [22] can be observed. It has been reported earlier that the rotational fine structure in the emission spectrum of CH radicals, observed during the activation of methane, can be used to determine gas phase temperature using the Boltzmann plot [22, 23].Accordingly, 'CH' excitation line observed at 431.5 nm was used to determine the kinetic gas temperature during our experiments. The resolution of the spectrometer, calibrated using a UV lamp, was determined to be 0.7 nm (full width at half maximum). This is not enough to resolve the individual rotational lines of the Q, R and P branches of the CH band.[24] Thus, rotational temperature, which reflects the gas temperature inside the filamentary discharge, was predicted comparing the CH band shown in Fig. 2 with those in the spectra simulated as a function of the rotational temperature using LIFBASE software [25]. Spectrometer resolution was the only input used for the software. The best fit was obtained in the region of 25-75ºC. Additionally, the temperature of the gas outside the

discharge area has been directly monitored by inserting a thermocouple inside the microchannel and measured as 75ºC at the highest power input of 25 W. In the case of the 3W used in our experiments (lower end of the power input) the average gas temperature was close to ambient. In the presence or absence of oxygen, the intensity of the CH band emission only varied slightly and in both cases the estimated rotational temperature remained close to ambient [26].

Two important points can be stressed from the results so far, i.e., (i) under the alkane activation conditions that we apply, the temperature is close to ambient and (ii) existence of CH and H bands in the spectra (shown in Figure 1) indicates decomposition of propane via C-C and C-H bond scission.

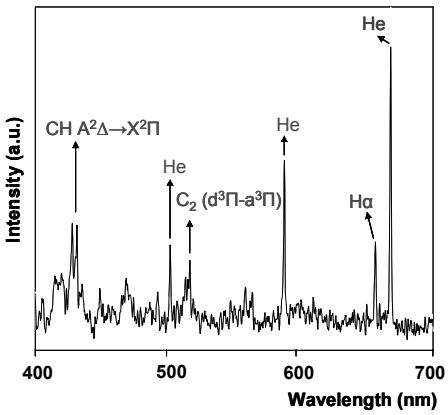

Fig. 2. Optical emission spectrum for a gas mixture of 10% propane in helium in the presence of plasma; 3W power was applied.

The results obtained with different hydrocarbons in the presence of oxygen in cold plasma microreactor are discussed below. In the case of propane, under the conditions discussed in the experimental section, 22 mol% conversion was observed. Figure 3 shows selectivities to all the products observed. Carbon balance was 95 ±5%, and no carbon deposition was observed in the reactor. It can be seen from the figure that, propene is the most abundant olefin (14%) followed by ethylene (12%). Additionally, alkanes, methane (8%) and ethane (14%) were also observed. Selectivity to combustion products (CO_x) was about 10%. As often observed during alkane activation by plasma [27, 28], we observed ethyne (6%) in the product stream. Most remarkably, very high selectivity to $\geq C_4$ components was observed (C_4 – 13%, C_4^+ - 24%). In order to highlight this, typical product distribution obtained in an empty quartz tube reactor (internal diameter 4 mm) operating at 600˚C (same feed composition) [29] is given in Fig. 4 and compared with the results discussed above. The selectivities presented are obtained at the same level of propane conversion, 20%. We did not observe any products containing more number of carbon atoms than the starting feed (C_3) in the case of the high temperature experiment. Unlike propane, ethane and methane contain only primary carbon atoms. In order to check if the homologation, observed during propane conversion in the microreactor, is also possible in the case of ethane and methane, their activation in the presence of plasma was attempted. Table 1 shows the products selectivity

recorded for the conversion of ethane (10% in He with 1% O_2) in the presence of plasma in microreactor.

Ethane conversion was about 15 mol%, mass balance was close 100% and again no carbon deposition was observed in the reactor. Ethane is, thus less active than propane, as expected. Methane was the most abundant product (27%) while ethylene the most abundant olefin (23%). Selectivities towards CO_x was about 13% and ethyne 15%. Again, appreciable amount (22 mol %) of C-C coupling products was observed. Selectivity to C_4 was about 10 mol % and 12 mol % C_3 products were also observed. Table 2 shows the products selectivity recorded during the conversion of methane (10 mol%). Interestingly, C_2 products were the most abundant species (49%) and much more ethane (40%) than ethylene (9%) was observed. Appreciable amounts of C_3 (11%) and C_4 (2%) products, demanding multiple C-C coupling were also found. Detailed studies of oxidative conversion of alkanes, even in the presence of catalysts, indicate that rather high temperatures are required because of the high energetic requirements for the C-H bond split. In the case of experiments conducted in the microreactor in presence of plasma, we deduced from the rotational band for the CH radical (Figure 1) that the temperature of the reaction system was close to room temperature. Observation of CH, C_2 and H radical species in the optical emission spectra thus confirmed activation by cleavage of the C-C and C-H bonds at ambient temperatures. This is consistently observed for all three hydrocarbons studied viz, propane, ethane and methane [24].

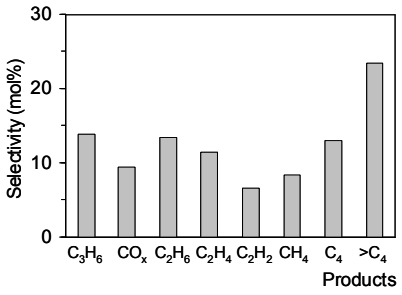

Fig. 3. Selectivity to the main products for a plasma microreactor. Conditions: flow rate 15 ml/min, feed composition 10% propane, 1% oxygen and balance helium; activation at room temperature. Formation of hydrogen was detected but not quantified.

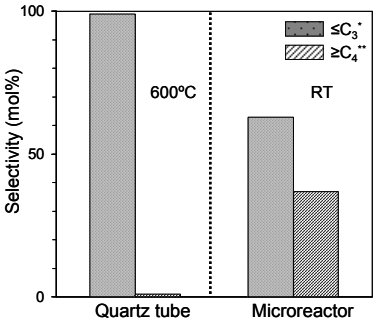

Fig. 3. Oxidative conversion of propane. Selectivity to the products observed, respectively, for empty, quartz tube reactor at 600ºC [29] and plasma microreactor at room temperature and at the same level of propane conversion achieved by varying SV. Conditions: 10% propane, 1% oxygen and balance helium. *≤C_3 corresponds to CO_x, C_2H_4, C_2H_6, C_3H_6; **≥C_4 corresponds to C_4 and C_4^+ (alkane+olefins).

We have previously discussed propane oxidation around 600ºC in the presence of Li/MgO catalyst [7]. In that respect, we observed that molecules with carbon atoms number $\leq C_3$ (Figure 3) such as C_3H_6, C_2H_4, CO_X and CH_4 were the only species detected. We also showed that heterogeneous propane activation predominantly takes place [29] via abstraction of hydrogen at the $[Li^+O^-]$ active site and propyl radicals formed [7]. These radicals are released to the gas phase where they undergo radical chain reactions [5-7]. The product selectivities could be explained by a series of propagation/termination reactions [7].

Let us now discuss what happens in the presence of plasma. The non-thermal plasma generated at atmospheric pressure by dielectric barrier discharge consists of high energy electrons and is characterized by a larger number of current filaments, microdischarges (ionization of the medium by the electrons), each lasting a few nano-seconds [20, 26].

The short life time of the current spikes (ns) helps in minimizing local heating. Moreover, the small volume and the large surface to volume ratio of the microreactor allow fast removal of the heat produced during oxidation of propane. The microdischarges are distributed in the space between the two electrodes and their number depends on (i) the voltage applied on the electrodes (ii) the distance between the electrodes (iii) the relative permittivity of the dielectric barriers (Pyrex) and (iv) the processing gas [30]. In the presence of plasma C_3H_8 molecules can be directly activated/converted via collisions with energized electrons. Activation produces radicals such as C_3H_7• due to cleavage of C-H bonds ($C_3H_8 + e^- \rightarrow C_3H_7$• + H• + e-) [31]. In presence of Helium, as batch gas, this mechanism might become more efficient because the mean free path of the electrons increases [32] due to the small cross section of highly excited helium species created during electric discharge. These excited species of helium, can also possess higher energy, up to nearly 20 eV, enough to activate hydrocarbon by collisions [33].

Propane activation can also occur *via* an indirect route, i.e. activation of gas phase oxygen by plasma. Among the atomic processes taking place in a non-thermal plasma, the electron impact dissociation of O_2 to form charged and neutral oxygen has been reported in literature and is described in the following reaction equations ($O_2 + e^- \rightarrow 2O + e^- \rightarrow O^- + O$) and ($O_2 + e^- \rightarrow O_2^* + e^- \rightarrow O + O + e^-$) [34, 35].

The O^- species, present in the homogeneous phase, have been reported to cause C-H bond scission in alkanes e.g., methane [36], ethane [37]. In the case of propane this will result in the formation of propyl and hydroxyl radicals as here shown ($C_3H_8 + O^- \rightarrow C_3H_7$• + OH^-). In addition, as Leveles *et al.* observed addition of oxygen can enhance the number and the

concentration of chain carrier radicals. The reaction between C_3H_7• radicals with O_2 helps formation of hydroperoxyl (HO_2•) radical that further reacts with a propane molecule forming H_2O_2. Decomposition of the latter gives two hydroxyl radicals (OH•) which become the main chain propagators [29]. All those factors can initiate radical chain reactions, but the main difference is that these propagation and termination reactions now take place at ambient temperature.

Table 1.

Oxidative conversion of ethane. Selectivity (mol%) to the products observed in a plasma microreactor. Conditions: 10% ethane and 1% oxygen in helium, flow rate 15 ml/min, RT; 15% conversion level of ethane (mol%).

CO_x	C_3H_8+C_3H_6	C_2H_4	C_2H_2	CH_4	C_4
13	12	23	15	27	10

In the case of propane, we observed large amounts (37%) of products with molecular weight higher than propane, i.e., C_4, C_4^+. The presence of products containing four or more C atoms requires C-C bond formation under the conditions present in the microreactor. Significantly, oxidative conversion of ethane and methane investigated in the plasma microreactor also showed higher tendency to form products that require C-C bond Figure 1. To recall, in the case of ethane appreciable amounts of C_3 and C_4 were detected. Even more remarkably, in the case of methane, products of homologation to C_2 and multiple coupling to C_3 and C_4 were the most abundant (70%). In comparison, efforts to make C_2 products by the oxidative coupling of methane, extensively studied over the years [38] had the inherent difficulty that methane activation required high temperatures and at the high temperatures C-C bond formation would be expected to be less favorable. Typically, formation of C-C bonds is an exothermic process and therefore favored at lower temperatures. Coupling reactions between radicals also imply a decrease in entropy because the number of molecules/radicals decreases. Therefore, it is not surprising to see C-C bond formation reactions under the mild conditions present during our experiments. C-C bond coupling is also observed during olefin metathesis type reactions, also at room temperature, but mandate the presence of a transition metal catalyst. Current scenarios for upgrading light hydrocarbons (increasing molecular weight) for e.g., alkylation [39], metathesis [40, 41] or oligomerisation [42, 43] reactions (e.g., SHOP process [44, 45]) involve at least one olefin. However, in our studies direct homologation of alkanes is observed. This represents an interesting novelty to upgrade cheap low molecular weight alkanes to commercially useful fuels and/or feedstock materials for the chemical industry.

Table 2.

Oxidative conversion of methane. Selectivity (mol%) to the products observed in a plasma microreactor. Conditions: 10% methane and 1% oxygen in helium, flow rate 15 ml/min, RT; 10% conversion level of methane (mol%).

CO_x	C_3H_8+C_3H_6	C_2H_4+C_2H_6	C_2H_2	C_4
30	11	49	8	2

6.4 Conclusions

The oxidative conversion of C_1-C_3 alkanes was investigated in the presence of cold plasma in a microreactor at atmospheric pressure. Formation of radicals as intermediates has been detected at ambient temperatures. Radicals thus formed, undergo C-C bond coupling reactions unlike C-H, C-C bond scission typically observed at higher temperatures. This is a promising route for the direct utilization of alkanes as feedstock for fuels or chemicals.

References

[1] F. Cavani, N. Ballarini, A. Cericola, Cat. Today 2007, 127, 113.

[2] J.H. Lunsford, P. Qiu, M. P. Rosynek, Z. Yu, J. Phys. Chem. B 1998, 102(1), 167.

[3] T.V. Choudary, E. Aksoylu, D. Wayne Goodman, Catalysis Reviews 2003, 45 (1), 151.

[4] V.P. Vislovskiy, T.E. Suleimanov, M.Y. Sinev, Y.P. Tulenin, L.Y. Margolis, V. Cortes Corberan, Cat. Today 2000, 61, 287.

[5] D.J. Driscoll, K. Campbell, J.H. Lunsford, Advances in Catalysis 1987, 35, 139.

[6] V.R. Choudhary, S.A.R. Mulla, V.H. Rane, Applied Energy 2000, 66(1), 51.

[7] L. Leveles, K. Seshan, J.A. Lercher, L. Lefferts, J. Catal. 2003, 218, 307.

[8] F.M. Aghamir, N.S. Matin, A.H. Jalili, M.H. Esfarayeni, M.A. Khodagholi, R. Ahmadi, Plasma Sources Sci. Technol. 2004, 13, 707.

[9] A. Huang, G. Xia, J. Wang, S.L. Suib, Y. Hayashi, H. Matsumoto, J. Catal. 2000, 189, 349.

[10] A. Marafee, C. Liu, G. Xu, R. Mallinson, L. Lobban, Ind. Eng. Chem. Res. 1997, 36, 632.

[11] S.Y. Savinov, H. Lee, H.K. Song, B.K. Na, Ind. Eng. Chem. Res. 1999, 38(7), 2540.

[12] H.K. Jeong, S.C. Kim, C. Han, H. Lee, H.K. Song, K.B. Na, Korean J. Chem. Eng. 2001, 18(2), 196.

[13] B. Eliasson, C.J. Liu, U. Kogelschatz, Ind. Eng. Chem. Res. 2000, 39, 1221.

[14] K. Zhang, U. Kogelschatz, B. Eliasson, Energy & Fuel 2001, 15, 395.

[15] K. Zhang, B. Eliasson, U. Kogelschatz, Ind. Eng. Chem. Res. 2002, 41, 1462.

[16] M. Kraus, B. Eliasson, U. Kogelschatz, A. Wokaun, Phys. Chem. Chem. Phys. 2001, 3, 294.

[17] H. Kim, Plasma Proc. and Polym. 2004, 1, 91.

[18] U. Kogelschatz, Plasma Chem. and Plasma Proc. 2003, 23 (1), 1.

[19] R.M. Tiggelaar, F. Benito-Lopez, D.C. Hermes, H. Rathgen, R.J.M. Egberink, F. Mugele, D. N. Reinhoudt, A. van den Berg, W. Verboom, H.J.G.E. Gardeniers, Chem. Eng. J. 2007, 131, 163.

[20] U. Kogelschatz, Contrib. Plasma Phys. 2007, 47 (1-2), 80-88.

[21] C. Trionfetti, A. Agiral, K. Seshan, J.G.E. Gardeniers, L. Lefferts, J. Phys. Chem. C, 112 (2008) 110.

[22] T. Nozaki, N. Muto, S. Kado, K. Okazaki, Cat. Today 2004, 89, 67.

[23] S. Kado, K. Urasaki, Y. Sekine, K. Fujimoto, T. Nozaki, K. Okazaki, Fuel 2003, 82, 2291.

[24] T. Nozaki, Y. Unno, Y. Miyazaki, K. Okazaki, J. Phys. D: Appl. Phys. 2001, 34, 2504.

[25] J. Lugue, D.R. Crosley, Lifbase: Database and Spectral Simulation Program (ver.1.6) SRI International Report MP 99-009, 1999.

[26] M. Okumoto, H.H. Kim, K. Takashima, S. Katsura, A. Mizuno, IEE Trans. Ind. Applicat. 2001, 37 (6), 1618.

[27] S.S. Kim, H. Lee, B.K. Na, H.K. Song, Korean J. Chem. Eng. 2003, 20(5), 869.

[28] Y. Yang, Plasma Chem. and Plasma Proc. 2003, 23(2), 327.

[29] L. Leveles, K. Seshan, J.A. Lercher, L. Lefferts, J. Catal. 2003, 218, 296.

[30] R. Li, Y. Yamaguchi, S. Yin, Q. Tang, T. Sato, Solid State Ionics 2004, 72, 235.

[31] J. Pons, E. Moreau, G. Touchard, J. Phys. D : Appl. Phys. 2005, 38, 3635.

[32] M.A. Tas, PhD thesis.

[33] D.W. Lee, J.H. Lee, B.H. Chun, K.Y. Lee, Plasma Chem. and Plasma Proc. 2003, 23 (3), 519.

[34] P.C. Cosby, J. Chem. Phys. 1993, 98(12), 9560.

[35] B. Eliasson, U. Kogelschatz, J. Phys. B: At. Mol. Phys. 1986, 19, 1241.

[36] T. Nozaki, A. Hattori, K. Okazaki, Cat. Today 2004, 98, 607.

[37] X. Zhang, A. Zhu, X. Li, W. Gong, Cat. Today 2004, 89, 97.

[38] J.H. Lunsford, Cat. Today 2000, 63, 165.

[39] L.F. Albright, K.E. Kranz, Ind. Eng. Chem. Res. 1992, 31(2), 475.

[40] J.M. Van de Graaf, M. Zwiep, F. Kapteijn, J.A. Moulijn, Chem. Eng. Sci. 1999, 54(10), 1441.

[41] Z. Lysenko, B.R. Maughon, T. Mokhtar-Zadeh, M.L. Tulchinsky, J. Organomet. Chem. 2006, 691(24-25), 5197.

[42] T. Koerts, P.A. Leclercq, R.A. Van Santen, J. Amer. Chem. Soc. 1992, 114(18), 7272.

[43] G. Boskovic, K.J. Smith, Cat. Today 1997, 37, 25.

[44] W. Keim, Chem. Ing. Tech. 1984, 56, 850.

[45] B. Reuben, H. Wittcoff, J. Chem. Edu. 1988, 65(7), 605.

Chapter 7

Outlook and general recommendations

It is generally accepted that, in the case of Li-promoted MgO catalysts, defects sites, due to the surface substitution of Mg^{2+} ions by a Li^{+} ion in the MgO matrix, play a significant role in processes involving oxidation reactions. In principle, the impregnation of MgO supports with aqueous solutions of Li salts, as route to prepare Li-promoted MgO catalysts, would allow a homogeneous distribution of lithium on the catalyst surface. However, during the preparation procedure, the high temperature treatments (≥700°C) required to build lithium in (forming a substitutional solid solution) cause drastic sintering effect resulting in materials with low surface area and thus low catalytic activity.

An alternative route to conventional wet impregnation method, for the synthesis of Li-promoted MgO catalysts, is the sol-gel preparation. In this work, Li-promoted MgO catalysts were prepared *via* co-gelling $Mg(OCH_3)_2$ and $LiNO_3$. It is here appropriate to stress that a gel forms because of the condensation of partially hydrolyzed species into a 3 dimensional polymeric network. TGA and DSC measurements during gel studies suggested that the presence of lithium ions in the sol-gel system drastically influenced the extent of hydrolysis and condensation. It is thus likely that lithium ions are incorporated already in magnesia at the Li-Mg-gel stage facilitating formation of a substitutional solid solution. Therefore, high temperature treatments are not required and significant incorporation of lithium ions at temperatures below 600°C is observed (i.e., temperature at which Li ions are not incorporated at all in impregnated Li/MgO catalysts). Moreover, the enhanced lithium incorporation minimizes the amount of free lithium phases present. Both these effects are responsible for the higher catalyst surface area obtained after calcination. In fact, high thermal stability of Li-promoted MgO catalysts prepared using sol-gel method was also observed.

However, the sol-gel route is a versatile method in developing catalytic materials. In particular, the control of experimental variables (sol-gel parameters *i.e.*, temperature, pH, type of ligands and their concentration) can affect and tailor the final properties of sol-gel materials. In fact, the size of the alkoxy ligands can change the rates of both hydrolysis and

condensation due to steric and inductive effects. More specifically, a rapid condensation (short alkoxy ligands) may lead to a fast particle growth/densification and the resulting calcined products will have lower surface area. In contrast, the use of longer alkoxy ligands (*n*, *i*-propoxide, *n*-butoxide) may slow down the condensation reaction (compared to hydrolysis), and thus suppress rapid particle growth and densification, already at the gel stage. The resulting product, after calcinations, may possess an increased surface area and may result in more efficient catalysts. Thus, in order to increase the thermal stability of Li-promoted MgO catalysts, use of different magnesium alkoxide precursors may be recommended.

It is general knowledge that, the activity and selectivity improvements during the oxidative conversion of propane, can be explained by the promoting effect of lithium to enhance the creation of active oxygen species [O^-] caused by lithium incorporation in MgO. However, there is less consensus concerning where the active [O^-] specie are located. The most accepted proposition is that oxygen is located, respectively, (i) next to a cation defect caused by lithium in the magnesia structure, or (ii) in the lattice structure of an active crystalline lithium containing phase (i.e., Li_2O, Li_2O_2) [1, 2]. Remarkably, in this thesis TGA results of CO_2 desorption and IR spectroscopic characterization of Lewis acid sites (Mg^{2+}_{LC}) using carbon monoxide represent a valid argument for the role of substitutional lithium defects instead of a relevant particular crystalline lithium phase. Thus, participation of lithium ions in the active sites efficiently provides their stabilization in the MgO phase forming [Li^+O^-] centers. However, additional experiments using low temperature IR spectroscopy supported by *ab initio* and DFT calculations are recommended to investigate the feasibility for CO molecules to be adsorbed on incorporated Li^+ ions. More specifically, this might help to, respectively, (i) quantify the number of surface [Li^+O^-] centers, (ii) define the typical coordination number of incorporated Li^+ ions forming active sites, and (iii) investigate their migration to preferentially low coordinated cation sites.

Lunsford and coworkers established many of the now accepted concepts concerning the reaction mechanism and the properties of the active [Li^+O^-] sites during the oxidative conversion of alkanes. In particular, they suggested that [O^-] centers can activate alkanes by homolytic C-H bond splitting (heterogeneous contribution) forming hydroxyl groups [OH^-] and alkyl radicals that can be released into the gas phase where undergo radical chain reactions (homogeneous contribution). In addition, the significant role of Li-promoted MgO samples during the oxidative conversion of propane was elucidated by Leveles *et al.* comparing all the kinetic data measured with and without catalyst. They proposed that gas phase radical reactions can lead to a mixture of olefins (both from dehydrogenation and

cracking) and that the use of catalysts may allow us to have a control over the radical reactions. In fact, Li-promoted MgO can act as, respectively, (i) prominent radical initiator and (ii) efficient radical quencher. Thus, the ideal catalyst should possess active centers able to, respectively, (i) form exclusively propyl radicals which then decompose into propylene and H·, and (ii) operate at lower temperatures since C-C bond breaking selectivity was lower at lower temperatures. In the latter case, a more active catalyst is needed.

Accordingly, during the oxidative dehydrogenation/cracking of propane over Li-promoted MgO catalysts prepared using sol-gel route, a higher number of active $[Li^{+}O^{-}]$ sites per cm^3 of reactor volume was achieved compared to conventionally prepared materials and superior yields were recorded (same amounts of catalyst in the reactor). More specifically, heterogeneous H-atom abstraction from C_3H_7· radicals yielding propylene was also observed. It is appropriate to stress here that the high density of active sites is exclusively determined by the higher surface areas catalysts. Finally, a higher concentration of active $[Li^{+}O^{-}]$ sites per m^2 of catalyst will efficiently enhance the selective H-atom abstraction from C_3H_7· radicals on the catalyst surface. However, this is the challenge in the catalyst preparation.

The presence of gas phase oxygen during the oxidative dehydrogenation/cracking of propane over Li-promoted MgO catalysts is also crucial. In fact, oxygen reacts with radicals present in the gas phase and as result more reactive radicals are formed. More importantly, the second function of gas phase oxygen molecules is the regeneration of the active sites. In this respect, our observations suggest that the reaction mechanism for the deactivation/regeneration of active surface sites strongly depends on the operation temperatures. In this thesis, we demonstrated using mass spectrometry that at 550°C the catalyst deactivation implies the formation of stable $[OH^{-}]$ groups and the regeneration of the active site does not require oxygen removal from the lattice structure of MgO. In fact, as described by Sinev, a sort of ''oxidative dehydrogenation'' of hydroxyl groups occurs. In contrast, at 700°C the interaction of propane molecules with $[Li^{+}O^{-}]$ sites produces unstable surface $[OH^{-}]$ groups which implies a de-hydroxylation step involving evolution of water accompanied by the formation of oxygen vacancies. Thus, at the higher temperatures, the catalyst deactivation/regeneration goes *via* the traditional scheme of re-oxidation according to Ito and Lunsford mechanism. Moreover, we also conclude that the formation of carbon oxides species was not caused by active lattice oxygen. However, further detailed investigation at higher temperatures is recommended. In fact, at 700°C quantitative detection of CO with mass spectrometry was more difficult than at 550°C. As already discussed in this thesis, this is due to the large presence of C_2^0 and $C_2^{=}$ species (generated by the significant contribution

from homogeneous gas phase reactions at 700°C) having fragmentation pattern similar to CO. Thus, presence of CO traces can not be excluded completely.

The different operating conditions during oxidative dehydrogenation/cracking of propane showed that increasing the temperature (between 500 and 600° C) also the olefin selectivity increases. In particular, further increase of the temperature decreases propylene selectivity (dehydrogenation) and increases ethylene selectivity (cracking). Thus, the temperature can be a tool to control the ratio ethylene to propylene.

In fact, one way to tailor the final selectivity of heterogeneous-homogeneous catalytic reactions is to influence the gas-phase radical reactions network. For this purpose, the oxidative conversion of alkanes (C_1-C_3 range) was performed in a plasma micro-reactor. In this case, due to a cold plasma, hydrocarbon activation *via* homolytic C-H and C-C bond rupture (forming radicals) occurred exclusively in the gas phase at near ambient temperatures (<50°C). In contrast to the results obtained at higher temperatures (≥550°C), in all the experiments performed in a plasma micro-reactor, mainly products that require the formation of C-C bonds were observed. Indeed, C-C bond formation is an exothermic process and therefore favored at lower temperatures. However, further experiments are recommended changing the feed composition. In fact, the highly efficient coupling phenomena taking place under our conditions would suggest the direct utilization of alkanes such as C_4-C_6 hydrocarbons as feedstock for a gas to liquid (GTL) process to fuels or chemicals. Moreover, the optimization of the process is needed and therefore further developments are also recommended.

In addition, the oxidative conversion of propane in a plasma micro-reactor was also performed in presence of a thin layer of Li-promoted MgO catalyst deposited in the micro-channel where the cold plasma was ignited. Interestingly, alkyl radicals, exclusively formed by the cold plasma, can either initiate radical chain reactions in the gas phase or intensively interact with the catalyst surface due to the high surface to volume ratio, typical for micro scale reactors. Based on our results, selective interaction between catalyst surface and radical species could be recorded under our conditions. Further, the influence of the catalyst composition was investigated. In particular, secondary H-atom abstraction from propyl radicals was observed. Our proposition is that plasma enhanced the formation of selective catalytic sites on the surface of Li-promoted MgO catalyst. Therefore, a better understanding of the phenomena taking place under plasma conditions on the catalysts surface is necessary and highly recommended. The utilization of *in situ* spectroscopic techniques under plasma conditions *i.e.*, ATR and EPR on a chip would be the major breakthrough. This would allow

us to better investigate the presence of radical species (generated by cold plasma) on the catalyst surface and their interaction with surface active centers. In addition, formation of paramagnetic centers (EPR active on the surface of Li-promoted MgO catalysts) induced by the presence of a cold plasma might be established and characterized.

References

[1] H. Aritani, H. Yamada, T. Nishio, T. Shiono, S. Imamura, M. Kudo, S. Hasegawa, T. Tanaka, S. Yoshida, J. Phys. Chem. B 104 (2000) 10133.

[2] C.L. Bothe-Almquist, R.E. Ettireddy, A. Bobst, P. Smirniotis, J. Cat. 192 (2000) 174.

Publications

A. Agiral, C. Trionfetti, K. Seshan, L. Lefferts and J.G.E. (Han) Gardeniers, **Propane conversion at ambient temperatures – C-C and C-H bond activation using cold plasma in a microreactor**. *Chemical Engineering and Technology,* (accepted 2008).

C. Trionfetti, I.V. Babich, K. Seshan and L. Lefferts, **Alkali/alkaline earth oxides catalysts and oxidative/cracking of propane- Part I and Part II**. *Langmuir,* (accepted 2008).

C. Trionfetti, S. Crapanzano, I.V. Babich, K. Seshan and L. Lefferts, **A mechanistic study of active site regeneration in nano scale catalysts of Li/MgO**. *Catalysis Today,* (accepted 2008).

C. Trionfetti, A. Agiral, J.G.E. (Han) Gardeniers, L. Lefferts and K. Seshan, **Oxidative conversion of propane in a microreactor in the presence of plasma over MgO based catalysts – An experimental study**. *Journal of Physical Chemistry C,* (2008), 112(11), 4267-4274.

C. Trionfetti, A. Agiral, J.G.E. (Han) Gardeniers, L. Lefferts and K. Seshan, **Alkane activation at ambient temperatures – Unusual selectivities, C-C, C-H bond scission vs C-C bond coupling**. *ChemPhysChem,* (2008), 9(4), 533-537.

C. Trionfetti, I.V. Babich, K. Seshan and L. Lefferts, **Efficient catalyst for olefins from alkanes: Sol gel synthesis of high surface area nano scale mixed oxide clusters**. *Topics in Catalysis*, (2006), 39 (3-4), 191-198.

C. Trionfetti, I.V. Babich, K. Seshan and L. Lefferts, **Formation of high surface area Li/MgO – Efficient catalyst for the oxidative dehydrogenation of propane**. *Applied Catalysis A: General*, (2006), 310, 105-113.

E. Marcantoni, G. Roselli, L. Lucarelli, G. Renzi; A. Filippi, C. Trionfetti and M. Speranza, **Crucial role of elusive isomeric eta-complexes in gas-phase electrophilic aromatic alkylations**. *Journal of Organic Chemistry,* (2005), 70(10), 4133-41.

F. Di Pascasio, D. Gozzi, B. Panella, C. Trionfetti, **Pd/H system in H_2 plasmas**. *Journal of Applied Physics,* (2005), 97(4), 043304/1-043304/11.

F. Di Pascasio, D. Gozzi, B. Panella, C. Trionfetti, **H_2 plasma for hydrogen loading in Pd**. *Intermetallics,* (2003), 11(11-12), 1345-1354.

Acknowledgements

This thesis has been developed between September 2003 and February 2008 at the Department of Catalytic Processes and Materials, Faculty of Chemistry and Technology of Twente University in Enschede, The Netherlands.

I wish to express my gratitude to everyone who contributed to making this research work a reality. First and foremost I must single out my promoter Prof. Dr. Ir. Leon Lefferts who gave me the opportunity to embrace this project and lead it with as much entrepreneurialism as no researcher could ever wish for. Thank you for your constant attention and criticism which has allowed this work to grow solid.

Special thanks also go to Dr K. Seshan, my assistant promoter and more importantly my daily supervisor. Thank you for your time, consideration and suggestions throughout this research work. Thank you for your patience and all the time we spent together in front of your computer screen. I am grateful for your support especially during those hard times of mine.

My appreciation also goes to Prof. Dr. Ir. Han Gardeniers with whom I friendly shared interesting discussion and ideas on microreactors. The results of such a fruitful coopearation are shown in chapter 5 and 6 of this thesis.

This would have not been possible without the cooperation of Dr. Igor Babich. I will never forget our long, enjoyable and fruitful scientific discussions most of times mixed up with football. I treasure the deep friendship grown between us and the comfortable home feeling it brings. Jana, thank you for your care that time at the hospital, you do not know how much I appreciated it.

I am indebted to several researchers and staff members from who I have always benefited scientifically and personally: Dr. Barbara Mojet, Dr. Jan van Ommen (always interesting to ask for your opinion), Louise, Karin and Jeroen (the captain of our CPM football team)☺. My dear Lianne, thank you for all you have done for me and for our enjoyable conversations.

Thank you Bert, because of your precious help (you know what I mean) your constant presence and the unforgettable Friday afternoons/evenings spent drinking beer while everything around was changing.

Now a shout-out for all my colleagues from CPM and MCS and all the friends from Enschede for the informal support (outings, parties and more…) which has been indispensable. Where to start….Berta (the cherry girl), Kazu (buddy, thanks for your samurai spirit!!), Sune (my favourite ironman, our friendship will last overseas), Dejan (for sharing lost weekends and odd working hours at UT) and Iris, (the brazilian). Throughout my thesis-writing period I would have been lost without the constant presence over night of my dear Indian friends Vijay and Kumar (thanks for everything) and lately Inga, our Siberian/Mexican girl. Thanks to Hans, Patrick (I am happy we became friends) and to the funny stories from Sergio (the winner) and Son. Roald, thank you for the nice time and the detailed translation of my summary into dutch (by the way if there are mistakes please contact him ☺). I would also like to thank collectively all my ‘’co-residents’’ (read office mates), Nabeel, Khalid (the best job hunter ever), Gacia (the sol-gel girl) and the sweetie Hrudya and Marijana who nicely managed to support me during the last and crucial part of my work. I cannot thank enough some people who made my stay a great experience. Anil, I am going to miss our dinners while working until morning and planning our life at the same time. Most of our ideas, papers

and choices we made were always conceived on those evenings.☺ Davide, you are a special person to me, your arrival in Enschede changed substantially part of my life. I am just happy that you are there! Thanks to the coolest little German girl ever, Sonya and her invaluable presence. Alina, please try not to fight with me this time☺. I would also like to thank Vittorio, my flatmate of Jupiterstraat, for the nice time while living together. I cannot forget my Italian restaurant in Enschede and my friends Giorgio, Luigi e Nino. Thanks for the special food you offered me and all the evenings spent playing cards.

I now finish with Italy, where the most basic of my energy resides: my friends and my family. Their support has been unconditional all these years. I am so thankful to some very special individuals, my ''band'' from Rome, Andrea, Fabrizio, Giampaolo, Mauro, Saverio and Ugo always present like today in the second row! Thanks to Mariannina (my private fashion consultant) and Pino (my favorite sailorman). Thanks to Francesca Romana for sharing much of this experience and for showing me what ultimately life is (being strong as you are). To my grand mothers Iole and Conci and our funny daily phone calls. Thanks to my aunt (Rita) and uncle (Maurizio) who spent their summer holidays of the last 4 years in the Netherlands to visit me. Thanks to my father, mother and sister who never had any doubt I could make it. *Grazie tante, vi voglio bene!*

Cristiano

ISBN: 978-90-365-2679-1